Gersonde, R., Hodell, D.A., Blum, P., et al., 1999
Proceedings of the Ocean Drilling Program, Initial Reports Volume 177

4. Site 1089[1]

Shipboard Scientific Party[2]

BACKGROUND AND OBJECTIVES

Site 1089 (proposed site SubSAT-1B) is located in the southern Cape Basin close to the northern flank of the Agulhas Ridge at a water depth of 4620 m (see Figs. **F1,** p. 35; **F5,** p. 39; both in the "Leg 177 Summary" chapter). This area is presently located south of the Subtropical Front (STF), which bounds the Antarctic Circumpolar Current (ACC) to the north. A geophysical survey of the area near Site 1089 was conducted by *Thompson* Cruise TTN057 (Fig. **F1**). The site was selected in an area of thick sediment cover that overlies topographically irregular basement consisting of normal oceanic crust (Fig. **F2**). Site 1089 is located on a drift deposit that was formed by bottom-water currents in the southern Cape Basin. Much of the seafloor of the Cape Basin is marked by erosion above 4 km water depth (Tucholke and Embley, 1984), and some of the eroded sediment suspended by bottom-water currents may be deposited as current velocities wane in the southern Cape Basin north of the Agulhas Fracture Zone Ridge. The high sedimentation rates recorded at Site 1089 were also traced 175 km to the west (Lamont piston core V14-65), suggesting that the drift deposit is laterally continuous. Although Site 1089 is deep (4620 m) and close to the carbonate compensation depth, the high supply of terrigenous mud by currents increases bulk sedimentation rates and promotes quick burial of sediment and, thus, the preservation of calcium carbonate, which averages 35 wt% in nearby piston cores.

Previous Ocean Drilling Program (ODP) drilling of sediment drifts during Legs 162 and 172 has now shown that these high–sedimentation-rate environments provide excellent archives of past climate variability at high temporal resolution. We expected Site 1089 to represent the Southern Hemisphere analog to the drift-deposit sequences of the North Atlantic that were drilled during Legs 162 and 172. We targeted Site 1089 because of the high-resolution isotopic record of the last cli-

F1. Track line and shotpoints for the site survey of Site 1089, **p. 23.**

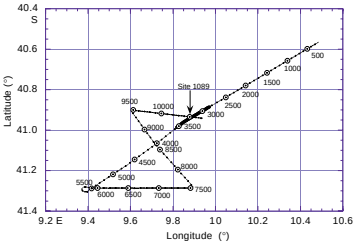

F2. Seismic line showing the location and penetration depth of Site 1089, **p. 24.**

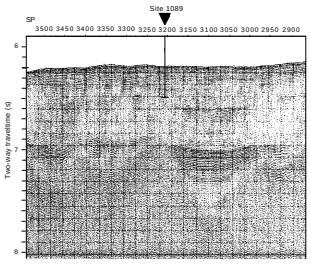

[1]**Examples of how to reference the whole or part of this volume.**
[2]**Shipboard Scientific Party addresses.**

Ms 177IR-104

matic cycle that had been obtained from nearby piston core RC11-83 (Fig. **F3;** Charles et al., 1996). Our goal was to extend this record into the early Pleistocene or late Pliocene. With few exceptions, deep-sea sedimentary sequences generally lack the resolution needed to delineate climatic variability on millennial time scales. Site 1089 is an exception because sedimentation rates average 150 m/m.y. for the late Pleistocene section.

The primary objective of Site 1089 was to recover a sediment sequence with ultra-high temporal resolution from north of the present-day Polar Front Zone that could be used to address the following problems:

1. *The response of the Southern Ocean environment to orbital forcing and the phase relationships to climate events occurring in low and high northern latitudes*. An important question in modern paleoceanography is whether climate changes recorded in sediments of the Southern Ocean lead, lag, or are in phase with climate changes in the high-latitude North Atlantic region. For example, Sowers and Bender (1995) and Bender et al. (1994) found that warming in Antarctica during the last deglaciation preceded that of Greenland by almost 2000 yr. By analysis of core RC11-83 (located near Site 1089), Charles et al. (1996) found that Northern Hemisphere climate fluctuations during the past 80 k.y. lagged those of the Southern Hemisphere by 1500 yr. Was the early response of Southern Ocean surface and deep waters relative to paleoceanographic proxies from other regions a persistent pattern during the entire late Pleistocene as suggested by Imbrie et al. (1992)?
2. *Rapid climate change on suborbital time scales in the Southern Ocean region and its relation to climate signals from polar ice cores*. The high accumulation rates at Site 1089 permit correlation of millennial-scale climate oscillations from marine-sediment records in the Southern Ocean to ice-core signals from Greenland and Antarctica. For example, the similarity between the two planktic foraminifer $\delta^{18}O$ time series in core RC11-83 and the Vostok δD_{ice} signal is striking over the past 70 k.y. (Fig. **F3;** Charles et al., 1996). With the extension of the Vostok ice-core signal over the past four climatic cycles (Petit et al., 1997), Site 1089 will be useful for detailed correlations between ice and marine-sediment cores for the past 450 k.y. and for studying the linkages between atmospheric (temperature and pCO_2) and oceanic dynamics (sea-surface temperature, productivity, and deep-water circulation).
3. *Glacial–interglacial variations in the physical and chemical properties of bottom-water masses in the South Atlantic Ocean and their relation to high-latitude climate change*. Site 1089 (4620 m) is located in lower Circumpolar Deep Water (CDW) (Fig. **F2,** p. 36, in the "Leg 177 Summary" chapter), and benthic $\delta^{13}C$ variations at this site should be sensitive to the varying flux of North Atlantic Deep Water (NADW) to the Southern Ocean. By comparing the benthic $\delta^{13}C$ record with the planktic $\delta^{18}O$ record from Site 1089, we hope to determine the phase relationship between variations in NADW and the surface-ocean response in the Southern Ocean (Charles et al., 1996). We plan to address the question whether changes in NADW flux to the Southern Ocean were an impor-

F3. Comparison of isotopic records from sediment core RC11-83 and the Vostok ice core, **p. 25.**

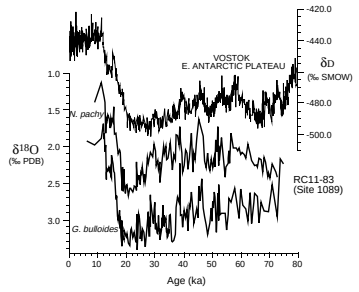

tant interhemispheric mechanism for linking climate change between the polar oceans.

4. *Glacial–interglacial variations in Southern Ocean nutrient cycling, productivity, and pCO_2 and their role in global biogeochemical cycles*. The Southern Ocean has become a region of paleoceanographic focus because of the key role it plays in global deep-water circulation and its potential significance for the global carbon cycle. For example, it has been proposed that new production (sinking flux of organic carbon) was higher and utilization of preformed nutrients in surface waters was more efficient in the glacial Southern Ocean than today, effectively lowering the glacial atmospheric CO_2 concentration. Martin (1990) proposed enhanced eolian iron fertilization from a dustier atmosphere as one potential mechanism that enhances Antarctic phytoplankton production during glaciations. The tests for such productivity changes using various tracers in Antarctic deep-sea sediments have yielded equivocal results (Boyle, 1989; Mortlock et al., 1991; Kumar et al., 1995; Frank et al., 1996, in press; Francois et al., 1998). Site 1089 should provide the northern end-member along the north-south transect of sites needed to test for glacial–interglacial changes in export production of organic carbon and biogenic silica in the South Atlantic.

OPERATIONS

Light winds and calm seas prevailed during the westward transit to Site 1089. The 166-nmi transit was made in 17.5 hr at an average speed of 9.5 kt. The vessel arrived at the Southern Cape Basin site on 19 December, and a positioning beacon was launched at 1615 hr.

Hole 1089A

The bit was run to 4628 m, and the advanced hydraulic piston corer (APC) coring assembly, fitted with an APC temperature (APCT) shoe, was deployed. After a bottom-water temperature measurement had been taken a few meters above the seafloor, Hole 1089A was spudded at 0450 hr on 20 December with a core that recovered 7.3 m of sediment and fixed the seafloor depth at 4630.2 meters below rig floor (mbrf). Core orientation began with Core 4H.

Operations at Hole 1089A were plagued by numerous problems. Cores 3H, 4H, and 6H suffered core-liner failures, with reduced recovery and disturbed core. The attempted APCT measurement with Core 4H was unsuccessful due to heave motion. Another downhole temperature was attempted with Core 7H. After a 10-min equilibration period, the overshot shearpin beneath the Tensor tool pressure case had failed, so a second run was required to retrieve the APC assembly. The APC was engaged successfully, but the coring line parted above the sinker bars. The remaining wire was reeled onto the winch, and the broken end was found ~125 m short of the ropesocket. A wireline fishing operation retrieved the broken wire and sinker bar assembly, and a pipe trip was avoided. It was discovered that the overshot shearpin had failed when the line parted and the APC was dropped, so it then became necessary to make a third wireline run to retrieve the APC.

Because of the two coring line failures in quick succession, the new forward wire was put into service. The aft wire was relegated to backup status.

When Core 7H arrived on deck, it was found to have a completely collapsed liner, and the APCT record was again degraded by vessel motion. APCT runs were discontinued at that point. Coring proceeded with liner failures of varying severity on nearly every core. About every other core had dismal recovery. Vessel heave, as noted by the driller, reached 12 ft at times. Coring conditions improved on the morning of 21 December. Core-liner failures persisted, but generally were not catastrophic and had less of a disruptive effect on the stiffer sediment.

Hole 1089A was terminated at a total depth (TD) of 216.3 meters below seafloor (mbsf), short of APC refusal, after Core 23H. The decision to abandon was primarily made to take advantage of good weather conditions for coring the upper sedimentary section in Hole 1089B. The drill string was pulled above the seafloor at 1315 hr on 21 December to begin operations at Hole 1089B.

Hole 1089B

A stratigraphic overlap was desired, so the initial APC core interval was positioned 3.5 m higher than the equivalent interval of Core 1089A-1H. The spud attempt yielded no sediment and a broken core liner. Two additional "mudline" cores were attempted from 1 m deeper than the first attempt. In both cases the core liners broke near the top and the core catchers contained plastic liner fragments and only traces of sediment. On the fourth spud attempt the bit was lowered to 4630 mbrf in an effort to recover more consolidated sediment that would not be so easily washed from the core barrel, while still maintaining an overlapping depth section. That attempt yielded a core with 4.8 m of sediment (and a broken liner). On the basis of recovery, seafloor depth was set at 4634.7 mbrf, but there is a strong possibility that some core was lost, which would make the seafloor depth too deep.

Coring success improved greatly on 22 December. Every effort was made to minimize core-liner failures by adopting measures to reduce shock and stress on the brittle liners. Those included elimination of APCT runs and core orientation, trimming down APC piston seals, closing more APC speed ports, and so forth. It is not clear, however, whether these measures were responsible for the dramatic improvements, given the circumstances of similar coring problems later in the cruise. Some liner failures persisted, but they had a minor effect on core recovery and quality. Continuous APC cores were taken to a depth of 265 mbsf. The final two cores (28H and 29H) exhibited incomplete stroke and recovery and ~40 kips overpull. A final core attempt resulted in a misrun when the APC apparently did not land and seal properly at the outer core barrel. Hole 1089B then was terminated because the scientific objectives had been achieved.

Hole 1089C

Excellent weather and minimal vessel heave conditions continued as a partial seafloor core was attempted with the core bit at 4625 mbrf. The first core recovered 2.4 m of sediment, setting the seafloor depth at 4632.1 mbrf. Core 2H was started 2 m below the bottom of Core 1H to provide stratigraphic overlap. Continuous coring then proceeded, with orientation beginning on Core 4H. Good recovery was achieved, but

core-liner failures were experienced on about 50% of the cores. Most of the failures were small implosions near the top of the liner that had little effect on the core.

Weather conditions deteriorated throughout the day with wind gusts up to 32 kt, rain showers, and a near reversal of wind direction in the afternoon. Two sets of 3-m swells arrived at nearly right angles. As a result, the vessel could not take a heading to minimize roll and heave. Rig operating limits were approached, with rolls of 9° and heaves as much as 14 ft. During the period of increasing vessel motion, double wireline trips were required for Cores 11H (did not actuate) and 13H (sheared overshot pin and mechanical actuation). Conditions improved dramatically in the late evening as the wind shifted and dropped to a light breeze. One set of swells died rapidly, and operating conditions improved just as quickly. Coring was halted at 194.4 mbsf when the scientific objectives had been reached.

Hole 1089D

A mudline core fixed the seafloor depth at 4628.5 mbrf, and continuous APC cores were taken to a TD of 118 mbsf. Again orientation began with Core 4H. Excellent core recovery and sediment conditions were achieved under good operating conditions. Only two minor core-liner failures occurred in the 13 cores recovered.

The fourth penetration at Site 1089 completed stratigraphic coverage, filling all recovery gaps in the upper portion of the section. With the scientific coring objectives for the site attained, coring ceased at 1900 hr on Christmas Eve. The drill string was tripped, and the vessel got under way at 0530 hr on 25 December.

LITHOSTRATIGRAPHY

Overview

Four holes were drilled at Site 1089 to a TD of 264.9 mbsf (280 meters composite depth [mcd]), recovering Pleistocene and upper Pliocene nannofossil ooze and diatom mud (Fig. **F4**). Nannofossil abundance varies from 0% to 90% (see **"Site 1089 Smear Slides,"** p. 84). Mud content varies from a few percent to ~80%. Foraminifer abundance ranges from 0% to 10% and is fairly constant downhole to about 220 mbsf (235 mcd) where it goes to zero. Diatoms range from a few percent to a maximum of 50% and are generally present in the 20%–30% range. The coarse sample resolution does not yield any systematic downhole trend in components (see Figs. **F4, F5;** Table **T1,** also in ASCII format in the **TABLES** directory; and **"Site 1089 Smear Slides,"** p. 84). Carbonate values range from 0 to 60 wt% (Figs. **F4, F5A;** see **"Geochemistry,"** p. 15). Variations in carbonate and nannofossil percentages agree well with the blue-band reflectance record (see **"Physical Properties,"** p. 18).

Recovery was generally good (Fig. **F4**), and in Holes 1089B and 1089C less than 3% of the recovered material was disturbed during coring (Tables **T2, T3**). A complete splice covers approximately the upper 94 m of the section (see **"Composite Depths,"** p. 8). The splice does not extend deep into the core because of several intervals of disturbed sediment. Small normal and reverse faults with offsets of as much as 8 cm were common (Fig. **F6**), but it is not clear whether they were preexisting fractures or caused by coring disturbance.

F4. Lithologic summary of Site 1089, **p. 26.**

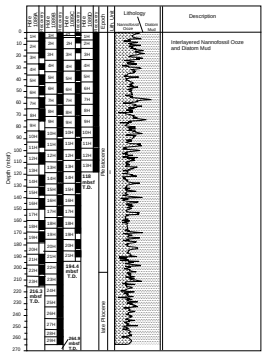

F5. Lithologic abundances, XRD measurements, and mineral ratios at Site 1089 (parts A–B), **p. 27.**

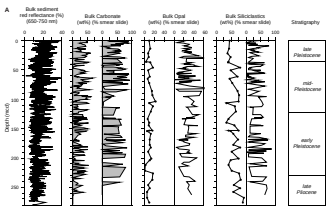

T1. X-ray diffraction data for Site 1089, **p. 57.**

T2. Summary of core disturbance at Site 1089, **p. 58.**

T3. Summary of undisturbed recovery at Site 1089, **p. 59.**

F6. Microfault cutting *Planolites* burrow with silt pod (interval 177-1089C-14H-1, 85–105 cm), **p. 29.**

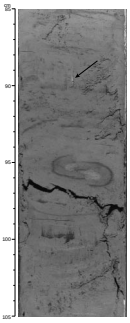

Two principal lithologies were recovered: nannofossil ooze and diatom mud. Several subordinate mixed lithologies were also recovered. Nannofossil ooze is pale to very pale gray. Rare, nearly pure nannofossil ooze (>80% nannofossils) is present only in the upper nine cores (80 mbsf). Diatom- and mud-bearing nannofossil ooze is present in Cores 177-1089B-2H (4.8 mbsf, 10.5 mcd) through 26H (240 mbsf, 255 mcd) and is absent in the lower part of the core. Diatom mud is present beginning with Core 177-1089B-3H and is common further downhole. Diatom mud is dark in color, with dark gray, dark greenish gray, dark olive, and olive green dominating. Mud-bearing diatom ooze is present but not common. It is brown, dark gray, and dark olive gray. Pure diatom ooze is present only in Core 177-1089B-18H. Nannofossil-bearing mud diatom ooze is also present. One lithostratigraphic unit was identified.

Description of Lithostratigraphic Unit

Unit I

Intervals: 177-1089A-1H through 23H (0–216.3 mbsf, 0–229.3 mcd); 177-1089B-1H through 29H (0–264.9 mbsf, 0–280 mcd); 177-1089C-1H through 21H (0–194.4 mbsf, 0–205.6 mcd); 177-1089D-1H through 13H (0–118.0 mbsf, 0–125.5 mcd)
Age: late Pliocene to Pleistocene

Unit I consists of alternating beds of nannofossil-rich and nannofossil-poor sediment, such as diatom- and mud-bearing nannofossil ooze and diatom mud. Most contacts are gradational, but when sharp contacts are observed they are equally likely to have light (nannofossil-rich) or dark (nannofossil-poor) sediment below the contact. It is not clear if the contacts represent a depositional unconformity or whether they were caused by faulting. Thin minor beds include a brown pelloidal nannofossil-bearing diatom mud in interval 177-1089A-1H, 39–41 cm, and a tan silt lamina in interval 177-1089B-16H-5, 113 cm (Fig. F7).

Bioturbation is prevalent throughout and *Planolites* ichnofossils are abundant. Thin purple bands commonly surround burrows. They give the appearance of color laminae and are probably Liesegang banding (Fig. F8). In addition to the purple Liesegang laminae, several green layers, harder than the surrounding sediment, are present (Fig. F9). These color bands may be related to a slight degree of carbonate recrystallization, with purple bands potentially reflecting rhodochrosite formation (Mn-carbonate) and green bands reflecting siderite formation (Fe-carbonate). Many of the burrows contain preserved pyrite molds and disseminated pyrite is relatively common (Fig. F6). Small (millimeters in diameter) silt pods were observed throughout and contain ~80% angular quartz with minor biosilica (sponge spicules and diatoms) (Figs. F6, F7). Macroscopically similar features have been observed in sediment cores recovered during several previous ODP legs (e.g., Leg 112), and may originate from a shelf environment or may have been carried to their present position within sponges (Martini and Locker, 1990).

Gypsum was observed in smear slides from Core 177-1089B-7H (roughly 55–60 mbsf). It may also be present as high in the hole as Core 177-1089B-5H, although the mineral was less well developed and therefore more difficult to identify. The presence of gypsum in other deep-sea sediments has been attributed to authigenic formation under reducing conditions, where calcium derived from the dissolution of biogenic

F7. Silt laminae (interval 177-1089B-16H-5, 118–133 cm), p. 30.

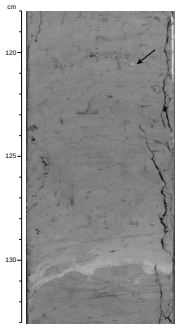

F8. Liesegang banding around Planolites burrow (interval 177-1089C-4H-4, 41–50 cm), p. 31.

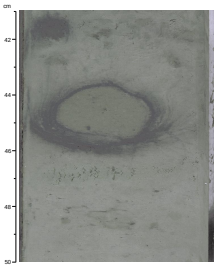

F9. Green layer above purple laminae (interval 177-1089C-3H-2, 46–56 cm), p. 32.

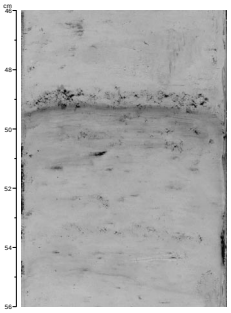

carbonate reacts with sulfate diffusing downward from seawater (e.g., Briskin and Schreiber, 1978; Siesser and Rogers, 1976). Interstitial water shows a decrease in sulfate from 24 mM at the surface to 0 at this level, and calcium reaches its lowest values (see "Geochemistry," p. 15).

Only two (>1 cm) dropstones were recorded: a 1.5-cm-long tonalite(?) in interval 177-1089A-20H-5, 20 cm, and a 1-cm-long rounded quartzite in interval 177-1089B-8H-2, 75 cm.

Soft-Sediment Deformation

Soft sediment deformation is common below 80 mbsf and as deep as 250 mbsf (Fig. F10). The deformed sediments consist of sharply dipping beds with clear color contacts (Fig. F11), and contorted beds (Fig. F12). Although microfaulting is present throughout the cores, it is most abundant in the deformed intervals. A layer exhibiting graded bedding is present at 243.3 mbsf within or at the very top of a deformed sedimentary interval (Fig. F13).

The deformed intervals are difficult to correlate between the four holes, even though the holes are separated by relatively short distances on the seafloor (a maximum of 30 m; Fig. F10B). Holes 1089A, 1089B, and 1089C can be correlated above 70 mbsf and below 160 mbsf. No further sedimentary deformation is observed down to 240 mbsf in Core 177-1089B-27H; however, Hole 1089B is the only hole to reach this depth. Between deformed intervals, the sediment succession reveals horizontal layering and appears to be undeformed. It is possible that the soft-sediment deformation is of minor extent and therefore not necessarily correlatable between holes, although the thickness of the deformed intervals (up to 15 m) and possible correlations between deformed intervals among several holes (Fig. F10A) argue for a larger scale phenomenon.

X-ray Diffraction Results

X-ray diffraction (XRD) measurements were conducted on the noncarbonate fraction of 57 samples (Fig. F5). Opal contents in the noncarbonate fraction vary between 10 and 24 wt% with some lower values, especially below 195 mbsf. Opal fluctuates independently from carbonate variations of the bulk-sediment fraction and, thus, probably cannot be related to glacial–interglacial cyclicity.

The lithogenic fraction consists of quartz, feldspar, clay minerals, and pyrite. Amphibole and clinopyroxene appear in trace amounts below significant XRD detection. All components show marked downhole variations. However, there seems to be no coherent pattern with respect to carbonate cycles or opal fluctuations, at least at this coarse resolution. Even mutual correlation among the lithogenic components is poor.

One important trend, however, is the increase of the illite/(kaolinite+chlorite) value (10 Å/7 Å) below 230 mbsf, which coincides with a change in lithology from gray carbonate-bearing sediments to predominantly greenish diatom-bearing and diatom muds and the absence of nannofossil ooze. Higher illite/(kaolinite+chlorite) values are also evident in two samples of the greenish layers that were intercalated in the overlying carbonate-bearing sediments (e.g., Fig. F8). The significance of these mineralogical changes has to be confirmed through further shore-based XRD analysis of clay minerals.

F10. Reconstruction of soft-sediment deformation at Site 1089 (parts A–B), p. 33.

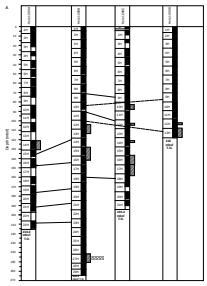

F11. Soft-sediment deformation (interval 177-1089B-27H-4, 40–75 cm), p. 35.

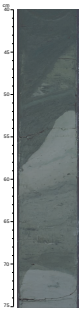

F12. Contorted beds (interval 177-1089C-10H-4, 68.5–110 cm), p. 36.

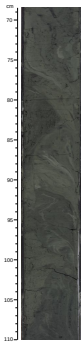

F13. Graded bed (interval 177-1089B-27H-1, 110–125), p. 37.

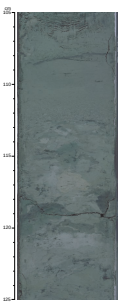

Interpretation

Site 1089 is located on a gently sloping drift deposit. The alternating dark and light beds may document variations in relative input of biogenic and terrigenous sediments in response to glacial–interglacial changes, with decreased terrigenous input and/or enhanced biogenic carbonate production and preservation during interglacial stages. These well-preserved lithologic cycles offer an excellent opportunity to examine paleoceanographic environmental changes on both Milankovitch and millennial time-scale variability. The fine grain size and scarcity of dropstones suggest that most of the terrigenous sediment is wind blown and/or derived from bottom currents. Clay-mineral and grain-size analyses will provide better clues of terrigenous sediment provenance and modes of sediment transport. Soft-sediment deformation processes, recorded in sediments below 130 mcd, were probably caused by sediment slumping that was triggered by high sedimentation rates, by undercutting bottom currents, or by a combination of both.

CHRONOSTRATIGRAPHY

Composite Depths

Multisensor track (MST) and color reflectance data (650–750 nm) collected from Holes 1089A–1089C were used to determine depth offsets in the composite section. Magnetic susceptibility, color reflectance, and gamma-ray attenuation (GRA) bulk density measurements were the primary parameters used for the core-to-core correlation at Site 1089. The data used to construct the composite section and determine core overlaps are presented on a composite depth scale in Figures **F14, F15,** and **F16,** respectively. The depth offsets that comprise the composite section for Holes 1089A–1089D are given in Table **T4** (also in ASCII format in the **TABLES** directory).

GRA bulk density and magnetic susceptibility data were collected at 2-cm intervals on all cores recovered at Site 1089. Color reflectance data were collected at 4- to 6-cm intervals on all cores from Holes 1089A and 1089B, Cores 177-1089C-1H through 9H, and Cores 177-1089D-2H, 4H, 6H, and 9H (see **"Physical Properties,"** p. 18, for details about these MST and color reflectance data).

The composite data show that the cores from Site 1089 provide a continuous overlap to a depth of 94 mcd (base of Core 177-1089C-10H). Between 94 and 156 mcd (base of Core 177-1089C-10H to Section 177-1089B-16H-5), the sedimentary section is marked by numerous highly disturbed intervals consisting of flow-in, slumping, and microfaulting. The severity and amount of disturbance in this interval makes it impossible to correlate cores between holes with any degree of certainty without further postcruise analysis. Below 154 mcd, the cores were placed into a composite depth frame, but most of the gaps between cores could not be covered by cores from other holes.

Generally, the reference core for the composite section (in this case Core 177-1089A-1H) will have a 0-mcd offset. At this site, the reference core and Cores 177-1089C-1H and 177-1089D-1H have negative offsets. The negative offset results from using the first stratigraphically intact portion of the reference core as the mudline reference. The uppermost 24 cm of Core 177-1089A-1H consists of washed-in sediment that is probably not in place. As a result, this core was shifted 24 cm up to remove this disturbed interval.

F14. Smoothed magnetic susceptibility data for Site 1089, **p. 38.**

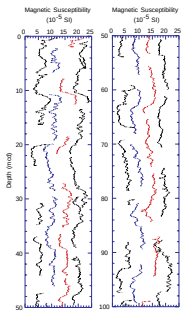

F15. Smoothed color reflectance data for Site 1089, **p. 39.**

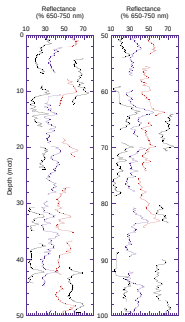

F16. Smoothed GRA bulk density data for Site 1089, **p. 40**

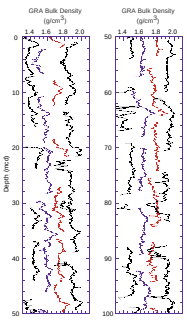

T4. Composite depths for Site 1089, **p. 60.**

Stretching and compression of sedimentary features in aligned cores indicate distortion of the cored sequence. Because much of the distortion occurred within individual cores on depth scales of <9 m, it was not possible to accurately align every feature in the MST and color reflectance records by simply adding a constant to the mbsf core depth. Within-core scale changes will require postcruise processing to align smaller sedimentary features. Only after allowing variable adjustments of peaks within each core can an accurate estimate of core gaps be made.

Following construction of the composite depth section for Site 1089, a single spliced record was assembled for the aligned cores over the upper 94 mcd primarily by using cores from Holes 1089B and 1089C. The cores were aligned relative to the mcd scale so that tie points between adjacent holes are present at exactly the same depths (mcd). Intervals having significant disturbance or distortion were avoided when possible. The Site 1089 splice (Table **T5,** also in ASCII format in the **TABLES** directory) can be used as a sampling guide to recover a single sedimentary sequence between 0 and 94 mcd. A spliced record was not constructed below 94 mcd because of the highly disturbed nature of the sediments between 94 and 156 mcd and the lack of core overlap among holes below 156 mcd. Spliced records of magnetic susceptibility, color reflectance, and GRA bulk density for the upper 94 mcd are presented in Figure **F17**.

T5. Site 1089 splice tie points, **p. 62.**

F17. Spliced magnetic susceptibility, color reflectance, and GRA bulk density at Site 1089, **p. 41.**

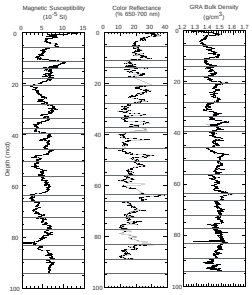

Biostratigraphy

Calcareous Nannofossils

Sediments recovered from Site 1089 provide a nearly continuous late Pliocene–Pleistocene record. Calcareous nannofossil abundances vary from abundant to barren, and moderate to poor preservation is observed in the assemblages. Dissolution is a common feature in placoliths and, in several cases, makes identification at the species level difficult. At least two samples per section were examined to establish an accurate age assignment of Holes 1089A and 1089B. Significant numbers of reworked nannofossils are recorded at certain intervals. This reworked material is mainly Pliocene in age, but lower Miocene and upper Eocene–Oligocene species have also been identified. Moreover, it is difficult to accurately establish the reworking of Pleistocene species, especially through intervals in which the biozonal events are last occurrences. To improve the Martini (1971) and Okada and Bukry (1980) standard zonations, we have considered some additional events according to Pujos (1988), Raffi et al. (1993), and Wei (1993) (see **"Explanatory Notes"** chapter).

Several events are recognized in the Pleistocene interval (Table **T6,** also in ASCII format in the **TABLES** directory; Fig. **F18**), providing a good biostratigraphic resolution and biochronology, when preservation permits. The first occurrence (FO) of *Emiliania huxleyi* at the base of Subzone NN21a is identified in Holes 1089A and 1089B between 39.56 and 40.56 mcd. However, the above-mentioned interval is affected by dissolution, and in several samples it is difficult to identify the presence of *E. huxleyi* (Table **T6**). The last occurrence (LO) of *Pseudoemiliania lacunosa* is present between 67.54 and 69.37 mcd, defining the base of Zone NN20 (Figs. **F18, F19**). Comparison of the FO of *E. huxleyi* and the LO of *P. lacunosa* with the interpreted reflectance curve (Fig. **F18**) allows us to infer that these events occurred during marine isotopic stages

T6. Main calcareous nannofossil species in Holes 1089A and 1089B, **p. 63.**

F18. Color reflectance data and related stratigraphic events at Hole 1089B, **p. 42.**

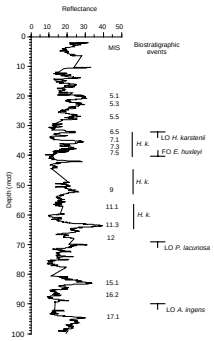

(MISs) 8 and 12, respectively[3]. The top and base of the small *Gephyrocapsa* acme are not clearly recognized, although a dominance of "very small *Gephyrocapsa*" complex is observed at the top of Zone NN19 (Table T6). The LO of *Reticulofenestra asanoi* is present at different depths in Holes 1089A and 1089B, suggesting that this event cannot be used reliably at Site 1089 (Table T6). The varying range of *R. asanoi* may have been caused by reworking, which is very intense in several intervals as noted previously. Alternatively, this species may have an extended range in the region. A quantitative study, as well as the correlation of this event at other sites, will provide a more reliable evaluation of these results.

The reentrance of medium *Gephyrocapsa* (4–5.5 µm) is present between 160.36 and 161.26 mcd. The FO of *R. asanoi* is present between 171.56 and 172.05 mcd. The LO of large *Gephyrocapsa* (>5.5 µm) is observed from 176.65 to 178.01 mcd, whereas the FO of this species is well defined between 195.56 and 197.83 mcd.

The FO of medium *Gephyrocapsa* (4–5.5 µm) is present between 223.90 and 224.80 mcd (Table T6) and marks the Pliocene/Pleistocene boundary. The LO of *Calcidiscus macintyrei* (>11 µm) is defined between 220.30 and 220.09 mcd.

The LO of *Discoaster brouweri* is identified between 236.70 and 238.53 mcd (Zone NN19). The age assigned to the lower part of Hole 1089B, below 222.5 mbsf, is younger than 2.54 Ma on the basis of the presence of *D. brouweri* (Zone NN18) (Table T6; Fig. F19). In Hole 1089B, late Pliocene species (Zones NN17 and NN18) are identified in well-preserved assemblages in some samples from resedimented clasts in Core 177-1089B-27H, below 257.11 mcd. Unfortunately, Samples 1089B-27H-CC, 28H-CC, and 29H-CC are barren, and we cannot establish whether the identified upper Pliocene assemblages are reworked (Table T6).

Planktic Foraminifers

The planktic foraminifer abundance in the four holes drilled at Site 1089 is relatively high for the Pleistocene, but it decreases significantly downhole (Table T7, also in ASCII format in the TABLES directory). The preservation of the planktic foraminifer fauna is generally moderate to poor. The degree of fragmentation is high in all studied samples. There is a distinct trend of decreasing preservation associated with the downhole decrease in abundance of planktic foraminifers. The sediments recovered from Holes 1089A–1089D span the Pliocene/Pleistocene boundary; however, as a result of the low abundance of *Globorotalia truncatulinoides* at this site, it is not possible to distinguish between the *G. truncatulinoides* and *Globorotalia inflata* Zones (Jenkins and Srinivasan, 1986). The planktic foraminifer assemblages are dominated by *Globigerina bulloides, G. quinqueloba, Globorotalia puncticuloides, Globigerinita glutinata, G. inflata,* and *Neogloboquadrina pachyderma* (sinistral). In addition, a few species (e.g., *G. truncatulinoides, Globigerina woodi, Globigerinella calida, Globigerinita uvula, Globorotalia crassaformis, G. scitula, Neogloboquadrina humerosa, N. pachyderma* [dextral], and *Orbulina universa*) make smaller contributions to the planktic foraminifer fauna at Site 1089. In the deepest hole (1089B), the studied core-catcher (CC) samples from Samples 177-1089B-19H-CC, 16–21 cm (175.33 mbsf), through 29H-CC, 62–67 cm (264.91 mbsf), are barren or contain only traces (a few broken specimens) of planktic foraminifers (Table T7).

F19. Bio- and magnetostratigraphic correlations and age designations for Site 1089, p. 43.

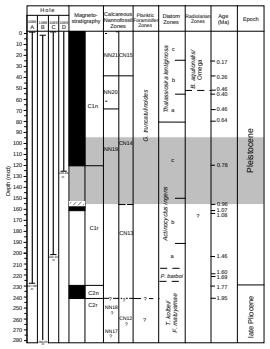

T7. Major planktic foraminifer species at Site 1089, p. 66.

[3]Note in proof: Preliminary oxygen isotopic data suggest that variations in color reflectance do not strictly reflect glacial–interglacial cycles; therefore, the MIS assignments should be viewed with caution at Site 1089.

Thus, it is possible that the faunal changes observed at Site 1089 are linked to changes in carbonate preservation.

Benthic Foraminifers

Benthic foraminifers were present in all the CC samples above 247.88 mcd at Site 1089, generally comprising between 5% and 10% of the total foraminifer fauna from the >63-µm fraction studied. Quantitative estimates of relative species abundance were made from Hole 1089A, with counts of as many as 300 specimens per sample (Table **T8,** also in ASCII format in the **TABLES** directory). Absolute foraminifer abundances, while variable, exhibit a clear trend toward higher values between ~100 and 150 mbsf, reaching a maximum of 95 specimens/cm^3 in Sample 177-1089A-16H-CC, 9–14 cm. Changes in benthic foraminifer abundance appear to reflect the general pattern of Pleistocene glacial–interglacial cyclicity at Site 1089, from generally high abundances during the glacial intervals to lower abundances during the interglacial intervals. This could be explained by the observation that sedimentation rates at Site 1089 are higher during interglacials than glacials, possibly resulting in some dilution of benthic foraminifers during interglacials. However, the low stratigraphic resolution of the CC samples studied and possible problems of flow-in associated with Hole 1089A make it difficult to determine the exact relationships that exist between benthic foraminifer abundances and the variability of the Pleistocene glacial–interglacial cycles. Preservation is generally good above 190 mcd, although there may be some variability associated with carbonate abundances through the well-developed glacial–interglacial cycles. Samples 177-1089B-26H-CC through 29H-CC are barren. Species richness is variable, with a maximum of 43 taxa recorded in Sample 177-1089A-17H-CC, 0–8 cm, and a minimum of 21 taxa recorded in Samples 177-1089A-2H-CC, 16–21 cm, and 8H-CC, 9–14 cm. Some of this variability can be accounted for by sample size as counts of 250–300 specimens are required before no correlation between the number of species and number of specimens is achieved (see **"Explanatory Notes"** chapter).

The benthic foraminifer assemblages of the Pleistocene sequence at Site 1089 (Table **T8**) are dominated by relatively few species, notably *Alabaminella weddellensis, Epistominella exigua, Oridorsalis umbonatus,* and *Pullenia quinqueloba*. These taxa, notably *E. exigua* and *A. weddellensis,* are known to respond to seasonal changes in phytodetritus supply within the flocculent layer of the ocean floor (Gooday, 1988; Mackensen et al., 1990) and may, therefore, provide a valuable tool in assessing surface-water productivity and hydrographic conditions at a very high temporal resolution through the late Pleistocene glacial–interglacial cycles. Preliminary results indicate that the glacial intervals are characterized by higher abundances of these phytodetritus species. These data, combined with benthic stable isotopic records, should provide an excellent opportunity to explore inferred changes in the nutrient status of CDW throughout the late Pleistocene at Site 1089.

Biostratigraphic differentiation of Site 1089 is limited to the LO of *Stilostomella lepidula* (e.g., Thomas, 1987) in Sample 177-1089A-10H-CC, 0–5 cm, which supports a late Pleistocene age of the sediment sequence above 103.16 mcd. The latter is in good agreement with the LO of *Actinocyclus ingens* (0.64 Ma) at a mean depth of 90.05 mcd in Holes 1089B and 1089C (see **"Diatoms,"** p. 12).

T8. Benthic foraminifers in Holes 1089A and 1089B, **p. 68.**

Diatoms

Holes 1089A–1089D recovered a continuous late Pliocene to Pleistocene record at high sedimentation rates ranging between 84 and 128 m/m.y. (Fig. F20; Table T9, also in ASCII format in the TABLES directory). This allows the application and testing of the revised biostratigraphic zonation recently proposed by Gersonde and Bárcena (1998) for the northern area of the Southern Ocean. The latter provides biostratigraphic age control at a resolution of ~0.2 m.y. Improved temporal resolution can be achieved particularly for the last 700 k.y. by the combination of color reflectance logs, which reflect glacial–interglacial variability in carbonate content, and the abundance pattern of selected diatom taxa, which allow the identification of specific MISs. In addition to the CC samples obtained from all holes, we have examined smear slides from Hole 1089B (Tables T10, T11; both also in ASCII format in the TABLES directory). All diatom stratigraphic information from the four holes is combined and converted to the mcd scale. This is crucial because significant disturbance of the sedimentary record by slumping is present in all holes between 100 and 150 mbsf (see "Lithostratigraphy," p. 5), resulting in strong offsets of isochronous intervals in the different holes (see "Composite Depths," p. 8). However, the slumping did not result in disturbance of the stratigraphic sequence.

Diatoms are common to abundant in most samples and are generally moderately preserved. Diatoms are most abundant in the upper 120 mcd, representing the last 800 k.y. (Fig. F21). In addition to planktic marine taxa, a few benthic marine taxa and *Paralia sulcata,* a taxon that preferentially dwells in near-shore marine environments, are also recorded. These diatoms most likely originated from the shallow waters off the African continent. The consistent presence of near-shore and shallow-water diatoms throughout the entire sedimentary record indicates a near-continuous input of sediment particles derived from African near-shore environments by deep- and/or bottom-water advection. More detailed, shore-based studies may determine if this input is controlled by glacial–interglacial sea-level variations. Lateral advection of reworked sediments by bottom currents is also documented by sparse diatoms stratigraphically older than the sedimentary record.

The biostratigraphic analyses of the diatom assemblages indicate that the base of the *Thalassiosira lentiginosa* Subzone c, defined by the LO of *Hemidiscus karstenii,* can be placed around 30 mcd (Fig. F21). The presence of this datum within MIS 6.5 is corroborated by the interpretation of the color reflectance record (Fig. F18). The presence of *H. karstenii* in the *T. lentiginosa* Subzone b, displaying abundance peaks in MISs 11, 9, and 7 (Burckle, 1982) (Fig. F18), permits recognition of these stages as reflected in the color reflectance record. MIS 11.3 is marked by the first abundant reentry of *H. karstenii* that has its FO in the late Miocene (see Gersonde and Bárcena, 1998). Assemblages from MIS 11 are typically characterized by abundant occurrences of *Azpeitia tabularis* (Fig. F21), a pattern that has also been observed in other cores from the Atlantic sector of the Southern Ocean (R. Gersonde, unpubl. data). The LO of *Actinocyclus ingens*, which marks the top of the *A. ingens* Subzone c within the lower and warmer portion of MIS 16, is recognized at 90 mcd. This event, which occurred at 0.64 Ma, supports the identification of MISs 17, 16, and 15 in the color reflectance record (Fig. F18). Within the *A. ingens* Subzone c, the LOs of *Thalassiosira elliptipora* and *T. fasciculata* are encountered at 120 and 110 mcd, respectively, at or close to the

F20. Age-depth plot of control points at Site 1089, p. 44.

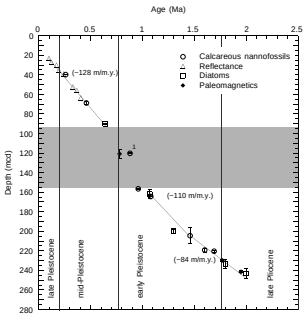

T9. Control points used to calculate sedimentation rates at Site 1089, p. 70.

T10. Diatom, silicoflagellate, ebridian, *Actiniscus*, sponge spicule, and phytolith occurrence, Site 1089, p. 71.

T11. Biostratigraphic age assignments at Site 1089, p. 80.

F21. Diatom abundance and preservation at Site 1089, p. 45.

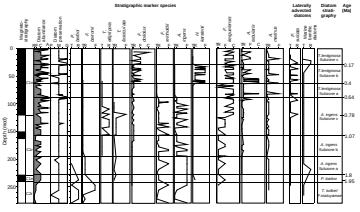

Brunhes/Matuyama boundary (Fig. F21), as reported by Gersonde and Bárcena (1998).

The base of the *A. ingens* Subzone c, marked by the first abundant appearance datum of *T. elliptipora* and correlated to the lower boundary of the Jaramillo Subchron (C1r.1n) in the Matuyama Chron at ~1.1 Ma, is present at ~162 mcd (Table T9). The base of the *A. ingens* Subzone b is marked by the LO of *Fragilariopsis barronii*. This datum was found around 200 mcd. However, reworking and rare occurrences of this taxon might indicate that the depth assignments of this datum are not reliable at Site 1089. The nominate taxon of the *Proboscia barboi* Zone, which nearly coincides with the Olduvai Subchron (C2n), was found below ~233 mcd (Table T9). The low number of samples studied in this sedimentary interval hinders the exact identification of the lower and upper boundaries of this zone. This datum is corroborated, however, by the recognition of the Olduvai Subchron between 230 and 242 mcd (Table T9). Below 247 mcd, we found *Fragilariopsis matuyamae,* a taxon that is characteristic of the *Thalassiosira kolbei/F. matuyamae* Zone, in the lower reversed portion of Subchron C2r of the Matuyama Chron. *T. kolbei,* however, was only encountered in trace to rare amounts.

The correlation of diatom ranges with the magnetostratigraphic record at Site 1089 indicates that the biostratigraphic zonation proposed by Gersonde and Bárcena (1998) is well adapted to sediments of the northern area of the Southern Ocean. In addition, an acme of *A. ingens* reported by Gersonde and Bárcena (1998) from the middle to lower portion of the Matuyama Chron is present at Site 1089. The biostratigraphic study of Site 1089 also allows preliminary definition of the ranges of warm-water taxa such as *Fragilariopsis reinholdii* and *F. doliolus* for further biostratigraphic use in the northern realm of the Southern Ocean. The LO of *F. reinholdii* at Site 1089 is apparently synchronous with its LO reported from low latitudes (Barron, 1992). It occurred around 0.65 Ma, close to or synchronous with the LO of *A. ingens*. The FO of *F. doliolus,* at ~1.8 Ma in the equatorial Pacific (Barron, 1992), was encountered in trace numbers near the Olduvai Subchron at Site 1089. However, the first consistent occurrences were found only in the late *A. ingens* Subzone b around 1.1 Ma (Fig. F21). *Fragilariopsis kerguelensis,* a taxon which dominates surface sediment assemblages in the Southern Ocean (Zielinski and Gersonde, 1997), displays high numbers during the last ~800 k.y. It is, thus, prominent in sediments deposited during the late Pleistocene when climatic variability was marked by 100-k.y. cycles. The first significant occurrence of this taxon is found at Site 1089 in the *P. barboi* Zone (Fig. F21). *Alveolus marinus,* a warm-water dwelling taxon, is encountered throughout most of the sedimentary record at rare or trace amounts. This taxon does, however, display prominent abundance peaks in mid- and late Pleistocene warm stages such as MISs 15, 11, 9, and 5 (Fig. F21).

Silicoflagellates of the genera *Distephanus* and *Dictyocha* are only found in small numbers.

Radiolarians

Radiolarian biostratigraphy at Site 1089 is based on examination of 31 CC samples (Table T12, also in ASCII format in the TABLES directory). All samples yielded well-preserved, highly diverse radiolarian assemblages. Co-occurrences of warm-water species (e.g., *Dictyocoryne truncatum* and *Spongaster tetras*) and Antarctic species (e.g., *Antarctissa*

T12. Main components of the radiolarian assemblage at Site 1089, p. 83.

spp. and *Saccospyris antarctica*) are recognized in many samples, which is probably a result of the proximity of Site 1089 to the STF.

All samples contain small numbers of *Cycladophora pliocenica* and *Saturnalis circularis,* which are characteristic below the Psi Zone. Further indication of reworking comes from the presence of the Cretaceous *Dictyomitrella* sp. and Miocene *Actinomma golownini* in Samples 177-1089C-19H-CC and 177-1089D-1H-CC, respectively. This impedes biostratigraphic zonation based on radiolarian occurrences at Site 1089. An exception is the LO of *Stylatractus universus,* which marks the base of the Omega Zone at 0.46 Ma that was found in Samples 177-1089A-7H-CC, 177-1089B-7H-CC, 177-1089C-6H-CC, and 177-1089D-7H-CC, consistently around 60 mcd (Tables **T11, T12**).

Only one specimen of *Cycladophora davisiana,* which is abundant to common in most samples, was present on a strewn slide in Sample 177-1089B-29H-CC. This may suggest that this horizon (279.65 mcd) is very close to the first appearance datum of *C. davisiana* at 2.61 Ma.

Paleomagnetism

Archive halves of APC cores recovered at Site 1089 were measured using the shipboard pass-through magnetometer. Measurements were made at 5-cm intervals. Sections obviously affected by drilling disturbance were not measured, although intervals affected by slumping from the base of the Brunhes Chron to the top of the Jaramillo Subchron were measured (see **"Lithostratigraphy,"** p. 5). All cores from Holes 1089A and 1089B, Cores 177-1089C-1H through 8H and 11H through 21H, and Cores 177-1089D-11H through 12H were measured after alternating-field (AF) demagnetization at peak fields of 0 (natural remanent magnetization [NRM]), 5, 10, 15, and 20 mT. Cores 177-1089D-1H through 10H and Cores 177-1089C-9H through 10H were measured after AF demagnetization at peak fields of 0, 10, and 20 mT.

NRM intensities are ~1×10^{-2} A/m at the top of each hole, decrease through the upper 50 m to ~1×10^{-3} A/m, and then remain fairly uniform throughout the cored interval. After AF demagnetization at peak fields of 20 mT, intensities generally decreased to ~3.5×10^{-4} A/m. NRM inclinations are typically steep down as a result of a magnetic overprint that has been attributed to the drill string. The drill-string magnetization is generally removed by peak demagnetization fields of 10 mT. At demagnetization fields above this value, the resulting characteristic inclination values are consistent with those expected for the site location (60°) (Fig. **F22**). Declinations are consistent within core sections and within individual cores. The Tensor orientation tool was used below the third core at all holes except Hole 1089B, where weather conditions were deemed unsuitable for its deployment.

Unfortunately, only the record from Hole 1089B approaches completeness (Fig. **F22**). At Hole 1089A, recovery was particularly poor and the quality of the recovered core was compromised by the failure of core liners. The Brunhes/Matuyama boundary is present in the interval from 105 to 114 mbsf in Hole 1089B (Fig. **F22;** Table **T13**); it is not well preserved, however, because of slumping that affects an interval from the earliest Brunhes Chron to the top of the Jaramillo Subchron. Sharper polarity transitions are found for the lower boundary of what is interpreted as the Jaramillo Subchron and at the upper and lower boundaries of the Olduvai Subchron (Table **T13**).

F22. Inclination of the remanent magnetization after AF demagnetization at Site 1089, **p. 46.**

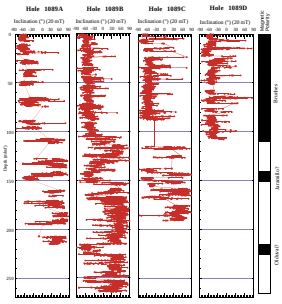

T13. Preliminary positions of polarity chron boundaries at Site 1089, **p. 86.**

Stratigraphic Summary

A 264.9-m-thick sedimentary section spanning the interval from the Holocene through the late Pliocene was recovered at Site 1089. The basal age was estimated to be ~2 Ma. Holes 1089A–1089D were cored with the APC to 216.30, 264.9, 194.4, and 118.0 mbsf, respectively. A continuous sedimentary section could be documented to 94 mcd. Between 94 and 156 mcd (base of Core 177-1089C-10H to Section 177-1089B-16H-5), the sedimentary section is marked by numerous highly disturbed intervals that made it impossible to correlate between holes. Below 156 mcd, the cores were placed into a composite, albeit incomplete, depth framework.

Age assignment and calculation of sedimentation rates for Site 1089 are based on calcareous nannofossil and diatom biostratigraphies, as well as measurements of geomagnetic polarity changes (Table T9). Because of reworking and difficulties in the identification of stratigraphically useful species, only one stratigraphic data point was established using radiolarian biostratigraphy. Despite apparent disturbance of some cored intervals, reworking of stratigraphically older species, and bottom-water advection of microfossils, the different stratigraphic marker groups and polarity reversal stratigraphy that were obtained allow the establishment of a consistent age assignment for Site 1089 (Fig. F19). In the upper 100 m of the recovered section, MISs were identified based on fluctuations of color reflectance combined with stratigraphically useful diatom and calcareous nannofossil occurrences. Biostratigraphic events resulted in the establishment of age control points separated by ~100 k.y. or less between 0 and 0.5 Ma (Fig. F20). In the older section of Site 1089, the age-depth points are separated by intervals spanning ~200 k.y. Of the 25 datum levels, 23 were chosen as control points (Table T9) to establish an age-depth model and estimate sedimentation rates. Depth uncertainty of the calcareous nannofossil datums corresponds to 0.7 m, or one-half core section. Depth uncertainties in the assignment of geomagnetic polarity changes and diatom datums are indicated by vertical error bars in Figure F20.

The resulting age-depth relationship shows a rather continuous sedimentation (Fig. F20). Calculated sedimentation rates average ~128 m/m.y. in the upper 94 mcd (~0.7 Ma). Below the disturbed section, the sedimentation rates are slightly lower (between 84 and 11 m/m.y.). The interval of relatively high sedimentation corresponds to the disturbed section between 95 and 154 mcd. Within the upper 60 m of the cored interval, corresponding to approximately the last 400 k.y., there is a tendency for increased sedimentation during interglacial intervals and relatively lower sedimentation during glacial intervals (Table T9). On the basis of the age model derived from the control points, the Pliocene/Pleistocene boundary can be placed at ~229 mcd.

GEOCHEMISTRY

Volatile Hydrocarbons

As part of the shipboard safety and pollution program, volatile hydrocarbons (methane, ethane, and propane) were measured in the sediments of Site 1089 from every core using the standard ODP headspace sampling techniques. Results are presented in Table T14 and Figure F23. Headspace methane (C_1) concentrations increase rapidly from

T14. Concentrations of methane, ethane, and propane at Site 1089, p. 87.

F23. Concentration of methane and sulfate vs. depth at Site 1089, p. 47.

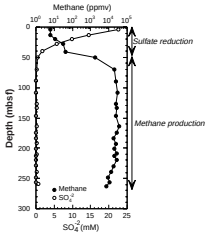

30 to 19,000 parts per million by volume (ppmv) between 40 and 70 mbsf (Fig. F23). Below this depth, methane concentrations are generally higher and relatively constant. Low concentrations (1 ppmv) of headspace ethane (C_2) were detected between 164 and 239 mbsf. The C_1/C_2 values are extremely high, suggesting that the methane is largely of microbial origin. Higher molecular weight hydrocarbon gases (C_4–C_6) are not observed. Methanogenesis begins at around 50 mbsf, as clearly shown by the sharp increase in methane concentrations and the contemporaneous sharp disappearance of sulfate in interstitial water (Fig. F23). This inverse correlation strongly suggests that the methane results from methanogenic bacterial activity.

Interstitial Water Chemistry

Shipboard chemical analyses of the interstitial water from sediments at Site 1089 included measurements of salinity, pH, alkalinity, chlorinity, calcium, magnesium, sulfate, silica, phosphate, ammonium, strontium, iron, manganese, and lithium (see "Explanatory Notes" chapter for more details on methods). The results from the shipboard analyses are presented in Table T15 and Figure F24. The results represent 17 interstitial water samples from Hole 1089A to a depth of 213 mbsf and eight samples from Hole 1089B from 201 to 259 mbsf; the total of 25 samples is considered to represent a single continuous profile.

Salinity decreases moderately downhole from 34.5 to a single low value of 33 at 259 mbsf. Chlorinity increases by about 0.9% in the uppermost 30 mbsf and then remains relatively constant throughout the rest of the section. The initial increase is significant relative to the precision of the measurement (0.2%) and likely results from downward diffusion of higher salinity waters associated with glaciations (McDuff, 1985). This increase is not observed in salinity because of the poor resolution in the refractometer measurements.

Site 1089 is characterized by reducing sediments, as indicated by the disappearance of sulfate by 50 mbsf, and high methane concentrations deeper in the section (Figs. F23, F24). Hydrogen sulfide was not apparent by smell, but gas bubbles, presumably methane, were often observed during the squeezing process in samples below 50 mbsf.

Sulfate decreases rapidly from 23 mM at 4 mbsf to near zero at 50 mbsf. The reducing conditions associated with sulfate reduction in the upper 50 m of the section exert strong control over the interstitial water profiles of several species measured during shipboard analyses, including alkalinity, Ca^{+2}, Fe^{+2}, PO_4^{-3}, NH_4^+, and to a lesser degree, Sr^{+2} and Li^+. Alkalinity increases from 10 to 42 mM, ammonium increases from 670 to 2500 µM, and phosphate increases from 67 to 190 µM. Fe^{+2} concentrations average ~6 µM in the sulfate reduction zone, but then rise sharply to concentrations averaging ~17 µM in the methanogenic zone (below 50 mbsf). The Fe^{+2} values should be interpreted with caution because it is not possible to collect, clean, and squeeze sediment samples for interstitial water analysis under oxygen-free conditions while maintaining timely processing of samples through the shipboard laboratory. Nevertheless, the iron values reported here are probably at least qualitative reflections of in situ interstitial water levels. The rapid increases in alkalinity, ammonium, and phosphate are direct consequences of organic-matter diagenesis associated with sulfate reduction. The presence of measurable Fe^{+2}, together with the absence of dissolved sulfides, suggests that sedimentation rates at this site are rapid relative to sulfate reduction rates. Therefore, at least some of the reactive iron

T15. Interstitial water chemistry at Site 1089, p. 88

F24. Interstitial water chemistry profiles vs. depth at Site 1089, p. 48.

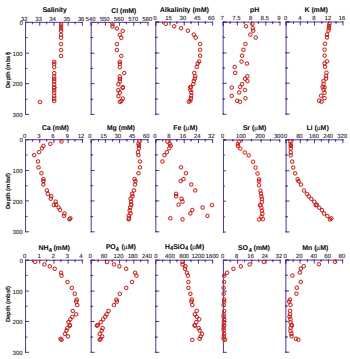

(oxy)hydroxides are buried throughout the primary iron reduction zone (not sampled here, i.e., between 0 and 4 mbsf) and also through the sulfate reduction zone. The presence of relatively high dissolved Mn^{+2} levels of as much as 69 µM in the sulfate reduction zone lends support to the interpretation that burial rates of iron (and manganese) oxides exceed microbial reduction of these metals.

Ca^{+2} shows a dramatic decrease in the sulfate reduction zone from 7.9 mM at 4 mbsf (bottom-water $Ca^{+2} \approx 10.5$ mM) to 1.9 mM at 50 mbsf. We suggest two possible reasons for this rapid decrease in Ca^{+2} in the sulfate reduction zone: (1) calcite precipitation caused by the rapid increase in alkalinity resulting from sulfate reduction (Kastner et al., 1990), and (2) authigenic gypsum formation, which is commonly associated with reducing conditions (Criddle, 1974; Siesser and Rogers, 1976; Briskin and Schrieber, 1978; Schnitker et al., 1980; all as cited in Rothwell, 1989). Mg^{+2} remains relatively constant over the uppermost 90 m at concentrations of ~50 mM, a value not much below the bottom-water Mg^{+2} concentrations of ~54 mM. This behavior creates abnormally high Mg/Ca values in the interstitial water (the maximum ratio at 50 mbsf is nearly 30; for comparison, typical Mg/Ca values in Sites 1088 and 1090 reach a maximum of ~5). These high values are atypical of carbonate precipitation, even in sabkha environments where elevated Mg/Ca values (of ~10) are commonly observed. However, Ca^{+2} loss through gypsum formation in the upper 50 m is consistent with the continued small increase in alkalinity below 50 mbsf without corresponding increases in phosphate. Careful reinspection of the smear slides from Hole 1089B did, in fact, identify the presence of gypsum in Cores 177-1089B-6H and 7H (see **"Lithostratigraphy,"** p. 5).

Sr^{+2} shows complex behavior in the sulfate reduction zone, with Sr^{+2} concentrations of ~75 to 80 µM over the uppermost 30 m, slightly below bottom-water concentrations of ~87 µM. Sr^{+2} increases rapidly from 30 to 60 mbsf, and more gradually downhole. The Ca^{+2}, Mg^{+2}, and Sr^{+2} concentrations below 100 m are consistent with dissolution of biogenic calcite and interaction with basalt. The behavior of Sr^{+2} in the uppermost 30 m is more complex, suggesting multiple competing reactions controlling Sr^{+2} concentrations in the sulfate reduction zone.

Li^{+} concentrations are constant at 24 µM in the uppermost 50 m, somewhat below bottom-water concentrations of ~27 µM; below 50 mbsf, Li^{+} increases with depth to concentrations of 230 µM at 259 mbsf. The curvature in the profile and the fact that Li^{+} concentrations are less than bottom-water concentrations in the upper 50 m suggest that Li^{+} is consumed in the upper 100 to 150 m of the sediments; clearly there is a deep source, perhaps interaction with basement or alteration of volcanic materials.

T16. Concentrations of IC, $CaCO_3$, TC, TOC, TN, TS, and TOC/TN at Site 1089, **p. 90.**

F25. $CaCO_3$, TOC, TN, TS, and TOC/TN vs. depth at Site 1089, **p. 49.**

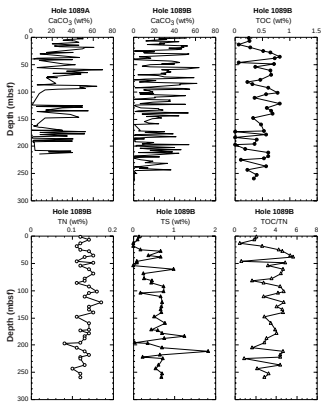

Solid Phase Analysis

The shipboard solid phase analysis at Site 1089 consisted of measurements of inorganic carbon, total nitrogen (TN), total carbon, and total sulfur (TS) (see **"Explanatory Notes"** chapter for methods). The results from Holes 1089A and 1089B are presented in Table **T16** and Figure **F25**. Calcium carbonate ($CaCO_3$) contents in Hole 1089A range from 0.6 to 69.3 wt%, with an average value of 27.0 wt%. Those in Hole 1089B (the more complete hole) also fluctuate between 0.4 and 64.1 wt%, with an average value of 20.7 wt%. These high-amplitude fluctuations in $CaCO_3$ contents correspond to alternating intervals of light nannofossil ooze and nannofossil-poor terrigenous sediment (see

"Lithostratigraphy," p. 5). The results suggest that the variations of $CaCO_3$ delineate glacial–interglacial cycles in carbonate deposition and preservation since the late Pliocene. $CaCO_3$ contents are slightly higher above 150 mbsf than deeper in the section. This trend may be related to a gradual increase in sedimentation rates in the upper part of the record.

Total organic carbon (TOC) contents vary between 0 and 0.82 wt%, with an average value of 0.43 wt%. Somewhat higher TOC values (>0.5 wt%) are present above 140 mbsf, in the upper part of Hole 1089B. TN contents are generally low (0.0–0.17 wt%). TS values vary between 0 and 1.82 wt%. TOC/TN values vary between 0.5 and 5.7, indicating a predominance of marine organic material.

PHYSICAL PROPERTIES

GRA bulk density, magnetic susceptibility, natural gamma-ray (NGR) emission, and *P*-wave velocity were measured with the MST on whole-core sections recovered from Site 1089 (Table T17). Color reflectance and resistivity were measured on the working half of all split APC cores using the Oregon State University Split Core Analysis Track (OSU-SCAT) (see "Explanatory Notes" chapter). Color reflectance was also measured with the Minolta CM-2002 spectrophotometer on cores from Hole 1089B (Table T17). Other physical properties measurements conducted on discrete samples included moisture, density, and *P*-wave velocity. Measured parameters were initial wet bulk mass (M_b), dry mass (M_d), and dry volume (V_d). Velocity was measured on split-core sections using the *P*-wave velocity sensor 3 (PWS3).

T17. Physical properties measurements conducted at Site 1089, p. 94.

Multisensor Track and Density

P-wave velocity, GRA bulk density, magnetic susceptibility, and NGR were determined every 2 cm for Holes 1089A and 1089B (down to Core 177-1089B-15H). Sampling time was 4 s at every point. Time constraints were such that only magnetic susceptibility and GRA density were recorded on the other holes and cores, except Section 177-1089C-18H-3 where the *P*-wave logger (PWL) was turned on again. There is considerable cyclicity in the GRA bulk density record, with an overall increasing trend downhole as a result of compaction. There is also a step to greater values around 140 mbsf that is particularly apparent in Holes 1089B and 1089C. The agreement is good between discrete-sample densities (determined using the moisture and density [MAD] method) and GRA densities (Figs. F26, F27). On average, one sample was taken per core section for MAD determination in Holes 1089B and 1089C. Volume magnetic susceptibility shows considerable cyclicity with values ranging between 2×10^{-5} and 15×10^{-5} SI units. Both the frequency of the cyclicity (periods of 120–40 k.y.) and average values show an overall increasing trend downhole (Fig. F26). NGR variations generally correspond to the variations in magnetic susceptibility (Fig. F26). The downhole increase that is apparent in GRA density and magnetic susceptibility, however, is not apparent in the NGR record.

F26. Site 1089 porosity, resistivity, *P*-wave velocity, bulk density, magnetic susceptibility, and NGR, p. 50.

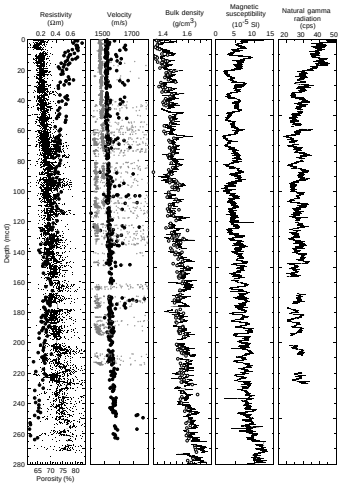

F27. Relationship between GRA and MAD bulk density at Site 1089, p. 51.

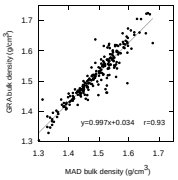

P-wave Velocity

P-wave velocities measured with the PWS3 velocimeter were slightly greater on average than those logged by the PWL of the MST. (Fig. F26).

PWS3 velocities increased slightly downhole from an average of ~1510 at the top to 1545 m/s at the bottom. There is also an overall increase downhole in the PWL data between 0 and 70 mcd. A bimodal distribution develops between 70 and 120 mcd, where measured values shift between 1425 and 1475 m/s. This is not apparent in the PWS3 data. Below 120 mcd, the PWL velocities appear to continue the trend of the lower distribution that developed between 70 and 120 mcd, resulting in a net increase in the difference between PWL and PWS3 velocities. The reason for this is uncertain, but it is probably an artifact of the quality of the contact between the core liner and the sediment or a wrong threshold setting (see "Explanatory Notes" chapter). This may result in a lower signal level and the second rather than first wavelet being autopicked by the PWL, which leads to longer traveltimes and lower velocities being recorded.

Resistivity and Porosity

Porosity determined gravimetrically on discrete samples (by the MAD method) ranged from 82% at the top of the hole to 62% at the bottom of the hole (Fig. F26). Resistivity measurements at Site 1089 are lowest at the top and gradually increase downhole, and values range from 0.1 to ~0.8 Ωm, with discrete spikes exceeding 1.0 Ωm (Fig. F26). The formation factor was calculated for the resistivity measurements (see "Explanatory Notes" chapter) and was plotted against porosity determined from discrete samples from the same depth (Fig. F28A). A power-curve fit to this plot yields the a and m parameters in the modified Archie equation

$$F = a\Phi^{-m},$$

where F is the formation factor, Φ is the porosity fraction, a is a proportionality constant, and m is a constant that is a function of the particular lithology. The equation of the curve fit can then be used to estimate porosity from the high-resolution resistivity measurements provided by the OSU-SCAT. The ability of this estimate to reproduce the measured porosities is shown in Figure F28B, where the resistivity measurements that were used to determine a and m are used to calculate porosity. There is, in general, good agreement with a mean difference of 3% between measured and estimated porosity values. The agreement could be further improved by considering each major lithologic unit separately.

Diffuse Spectral Reflectance

Closely spaced (4 to 6 cm) measurements of diffuse spectral reflectance at Site 1089 exhibit rhythmic variations with a tendency toward lower maximum reflectance values below 100–150 mcd (Fig. F29). Values in the red reflectance band (650–750 nm) range from ~10% to ~45%. Minimum reflectance values in the red and near-infrared (nIR) bands exhibit little trend below 40 mcd but increase up section above that depth. This change is not observed in the blue reflectance band and is possibly related to the oxidation of shallow, surface sediments relative to those below. As at Site 1088, reflectance in the blue, red, and nIR bands is highly correlated. Likewise, reflectance values are well correlated with GRA density (see "Chronostratigraphy," p. 8).

Color reflectance measurements were obtained with the Minolta CM-2002 spectrophotometer on Cores 177-1089B-7H through 11H for

F28. Porosity and formation factor calculations at Site 1089, p. 52.

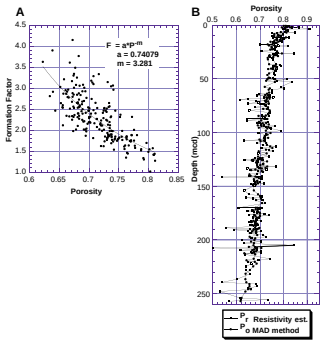

F29. Site 1089 diffuse spectral reflectance variations, p. 53.

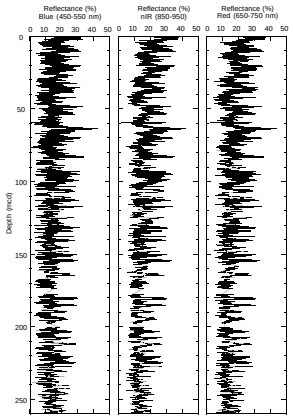

comparison with data obtained with the OSU-SCAT reflectance instrument. CM-2002 measurements were made at 5-cm spacing through the "granular material cover-set" on cores covered with Glad plastic wrap. Although the cover-set may alter the shape of the observed reflectance spectra, this compromise seemed reasonable to prevent the possibility of contaminating the instrument's integrating sphere or of scratching the glass lens of the cover-set. Care was taken to ensure that the CM-2002 was calibrated between cores to ensure minimal core-to-core offsets.

Blue (450–550 nm) and red (650–750 nm OSU-SCAT; 650–700 nm Minolta) reflectance measurements generated by the instruments are, to first order, similar (Fig. F30). More detailed comparison of the full reflectance measurements from the two instruments will be conducted postcruise.

Heat Flow

A total of 99 thermal conductivity measurements on core sections from Site 1089 ranged from 0.79 to 1.05 W/(m·K) (Table T18, also in ASCII format in the TABLES directory). The average value is 0.92 W/(m·K), and the distribution of the values is shown in Figure F31. There is a reasonably good linear correlation between bulk density and thermal conductivity measurements (interpolated values) in the uppermost 100 mbsf, but deeper intervals do not show any significant correlation.

Three temperature measurement attempts were made at Site 1089, one in bottom water about 20 m above the seafloor, and two in sediment with Cores 177-1089-4H and 7H (Fig. F32; Table T19). The seafloor measurement yielded a bottom-water temperature of 1.1°± 0.1°C. The sediment data were too noisy to be interpreted as a result of considerable heave that created random frictional heat when the probe was stationed in the hole. Heat flow could therefore not be determined at this site.

F30. OSU-SCAT and Minolta spectral reflectance at Hole 1089B, p. 54.

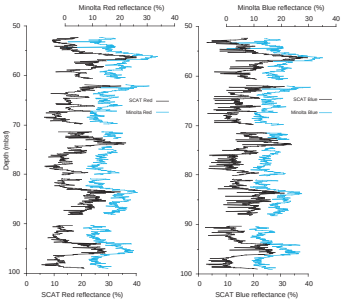

T18. Thermal conductivity measurements at Site 1089, p. 95.

F31. Thermal conductivity measurements at Site 1089, p. 55.

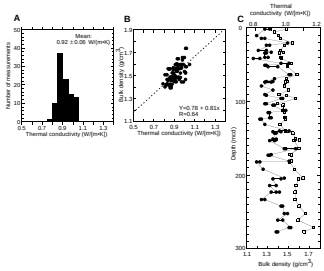

F32. Downhole temperature measurements at Site 1089, p. 56.

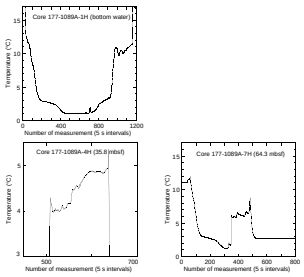

T19. Temperature measurement attempts at Site 1089, p. 97.

REFERENCES

Barron, J.A., 1992. Neogene diatom datum levels in the equatorial and North Pacific. *In* Ishizaki, K., and Saito, T. (Eds.), *The Centenary of Japanese Micropaleontology:* Tokyo (Terra Sci. Publ.), 413–425.

Bender, M., Sowers, T., Dickson, M., Orchardo, J., Grootes, P., Mayewski, P., and Messe, D., 1994. Climate teleconnections between Greenland and Antarctica throughout the last 100,000 years. *Nature*, 372:663–666.

Boyle, E.A., 1989. Effect of high latitude processes on glacial chemical profiles and atmospheric CO_2. *Eos*, 70:1143.

Briskin, M., and Schreiber, B.C., 1978. Authigenic gypsum in marine sediments. *Mar. Geol.,* 28:37–49.

Burckle, L.H., 1982. First appearance datum of *Hemidiscus karstenii* in late Pleistocene of the subantarctic region. *Antarctic J. U.S.,* 175:142–143.

Charles, C.D., Lynch-Stieglitz, J., Ninnemann, U.S., and Fairbanks, R.G., 1996. Climate connections between the hemispheres revealed by deep sea sediment core/ice core correlations. *Earth Planet. Sci. Lett.*, 142:19–27.

Criddle, A.J., 1974. A preliminary description of microcrystalline pyrite from nannoplankton ooze at site 251, Southwest Indian Ocean. *In* Davies, T.A., Luyendyk, B.P., et al., *Init. Repts. DSDP,* 26: Washington (U.S. Govt. Printing Office), 603–611.

Francois, R., Altabet, M.A., Ein-Fen, Y., Sigman, D.M., Bacon, M.P., Frank, M., Bohrmann, G., Bareille, G., and Labeyrie, L.D., 1998. Contribution of Southern Ocean surface-water stratification to low atmospheric CO_2 concentrations during the last glacial period. *Nature*, 389:929–935.

Frank, M., Gersonde, R., and Mangini, A., in press. Quantification of lateral sediment redistribution applying 230Thex: implications for the reconstruction of particle flux and export paleoproductivity from marine sediments. *In* Wefer, G. and Fischer, G. (Eds.), *Proxies in Paleoceanography.*

Frank, M., Gersonde, R., Rutgers van der Loeff, M., Kuhn, G., and Mangini, A., 1996. Late Quaternary sediment dating and quantification of lateral sediment redistribution applying 230Thex: a study from the eastern Atlantic sector of the Southern Ocean. *Geol. Rundsch.,* 85:554–566.

Gersonde, R., and Bárcena, M.A., 1998. Revision of the late Pliocene–Pleistocene diatom biostratigraphy for the northern belt of the Southern Ocean. *Micropaleontology*, 44:1–15.

Gooday, A.J., 1988. A response by benthic foraminifera to the deposition of phytodetritus in the deep sea. *Nature,* 332:70–73.

Imbrie, J., Boyle, E.A., Clemens, S.C., Duffy, A., Howard, W.R., Kukla, G., Kutzbach, J., Martinson, D.G., McIntyre, A., Mix, A.C., Molfino, B., Morley, J.J., Peterson, L.C., Pisias, N.G., Prell, W.L., Raymo, M.E., Shackleton, N.J., and Toggweiler, J.R., 1992. On the structure and origin of major glaciation cycles, 1. Linear responses to Milankovitch forcing. *Paleoceanography,* 7:701–738.

Jenkins, D.G., and Srinivasan, M.S., 1986. Cenozoic planktonic foraminifers from the equator to the sub-antarctic of the southwest Pacific. *In* Kennett, J.P., von der Borch, C.C., et al., *Init. Repts. DSDP,* 90: Washington (U.S. Govt. Printing Office), 795–834.

Kastner, M., Elderfield, H., Martin, J.B., Suess, E., Kvenvolden, K.A., and Garrison, R.E., 1990. Diagenesis and interstitial-water chemistry at the Peruvian continental margin—major constituents and strontium isotopes. *In* Suess, E., von Huene, R., et al., *Proc. ODP, Sci. Results,* 112: College Station, TX (Ocean Drilling Program), 413–440.

Kumar, K., Anderson, R.F., Mortlock, R.A., Froelich, P.N., Kubik, P., Dittrich-Hannen, B., and Suter, M., 1995. Increased biological productivity and export production in the glacial Southern Ocean. *Nature*, 378:675–680.

Mackensen, A., Grobe, H., Kuhn, G., and Fütterer, D.K., 1990. Benthic foraminiferal assemblages from the eastern Weddell Sea between 68° and 73° S: distribution, ecology and fossilization potential. *Mar. Micropaleontol.*, 16:241–283.

Martin, J.H., 1990. Glacial-interglacial CO_2 change: the iron hypothesis. *Paleoceanography,* 5:1–13.

Martini, E., 1971. Standard Tertiary and Quaternary calcareous nannoplankton zonation. *In* Farinacci, A. (Ed.), *Proc. 2nd Int. Conf. Planktonic Microfossils Roma:* Rome (Ed. Tecnosci.), 2:739–785.

Martini, E., and Locker, S., 1990. Clusters of sponge spicules from Quaternary sediments at Sites 685 and 688 off Peru. *In* Suess, E., von Huene, R., et al., *Proc. ODP, Sci. Results,* 112: College Station, TX (Ocean Drilling Program), 175–180.

McDuff, R.E., 1985. The chemistry of interstitial waters, Deep Sea Drilling Project Leg 86. *In* Heath, G.R., Burckle, L.H., et al., *Init. Repts. DSDP,* 86: Washington (U.S. Govt. Printing Office), 675–687.

Mortlock, R.A., Charles, C.D., Froelich, P.N., Zibello, M.A., Saltzman, J., Hays, J.D., and Burckle, L.H., 1991. Evidence for lower productivity in the Antarctic Ocean during the last glaciation. *Nature*, 351:220–223.

Okada, H., and Bukry, D., 1980. Supplementary modification and introduction of code numbers to the low-latitude coccolith biostratigraphic zonation (Bukry, 1973; 1975). *Mar. Micropaleontol.,* 5:321–325.

Petit, J.R., Basile, I., Leruyuet, A., Raynaud, D., Lorius, C., Jouzel, J., Stievenard, M., Lipenkov, V.Y., Barkov, N.I., Kudryashov, B.-B., Davis, M., Saltzman, E., and Kotlyakov, V., 1997. Four climatic cycles in Vostok ice core. *Nature*, 387:121–164.

Pujos, A., 1988. Spatio-temporal distribution of some Quaternary coccoliths. *Oceanol. Acta*, 11:65–77.

Raffi, I., Backman, J., Rio, D., and Shackleton, N.J., 1993. Plio-Pleistocene nannofossil biostratigraphy and calibration to oxygen isotopes stratigraphies from Deep Sea Drilling Project Site 607 and Ocean Drilling Program Site 677. *Paleoceanography,* 8:387–408.

Rothwell, R.G., 1989. *Minerals and Mineraloids in Marine Sediments: An Optical Identification Guide:* Basking, UK (Elsevier Appl. Sci. Publ.).

Schnitker, D., Mayer, L.M., and Norton, S., 1980. Loss of calcareous microfossils from sediments through gypsum formation. *Mar. Geol.*, 36:M35–M44.

Siesser, W.G., and Rogers, J., 1976. Authigenic pyrite and gypsum in South West African continental slope sediments. *Sedimentology*, 23:567–577.

Sowers, T., and Bender, M., 1995. Climate records covering the last deglaciation. *Science*, 269:210–214.

Thomas, E., 1987. Late Oligocene to Recent foraminifers from Deep Sea Drilling Project Sites 608 and 610, northeastern North Atlantic. *In* Ruddimann, W.F., Kidd, R.B., Thomas, E., et al., *Init. Repts. DSDP,* 94: Washington (U.S. Govt. Printing Office), 997–1031.

Tucholke, B.E., and Embley, R.W., 1984. Cenozoic regional erosion of the abyssal seafloor off South Africa. *In* Schlee, J.S. (Ed.), *Interregional Unconformities and Hydrocarbon Accumulation.* AAPG Mem., 36:145–164.

Wei, W., 1993. Calibration of Upper Pliocene-Lower Pleistocene nannofossil events with oxygen isotope stratigraphy. *Paleoceanography,* 8:85–99.

Zielinski, U., and Gersonde, R., 1997. Diatom distribution in Southern Ocean surface sediments: implications for paleoenvironmental reconstructions. *Palaeogeogr., Palaeoclimatol., Palaeoecol.*, 129:213–250.

Figure F1. Track line and shotpoints for the site survey of Site 1089 conducted during *Thompson* Cruise TTN057. The bold portion of the track line corresponds to the segment of the seismic profile displayed in Figure F2, p. 24.

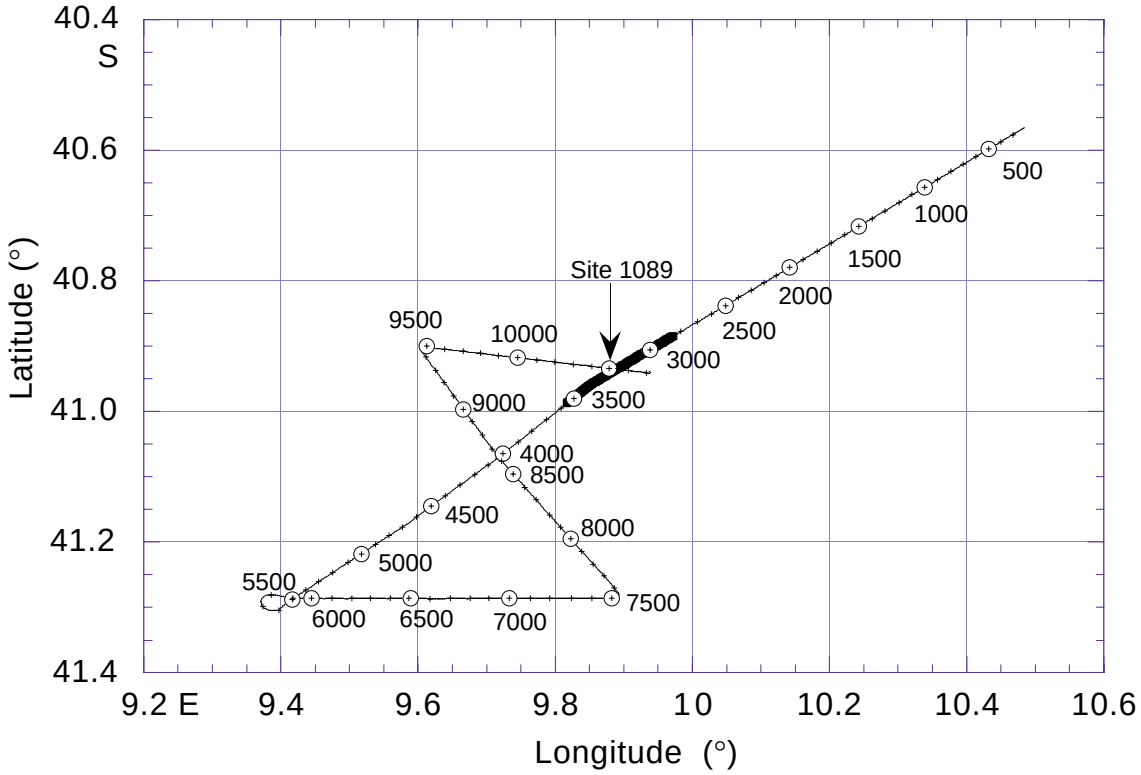

Figure F2. Single-channel seismic line collected during site-survey *Thompson* Cruise TTN057 showing the location and penetration depth of Site 1089. SP = shotpoint.

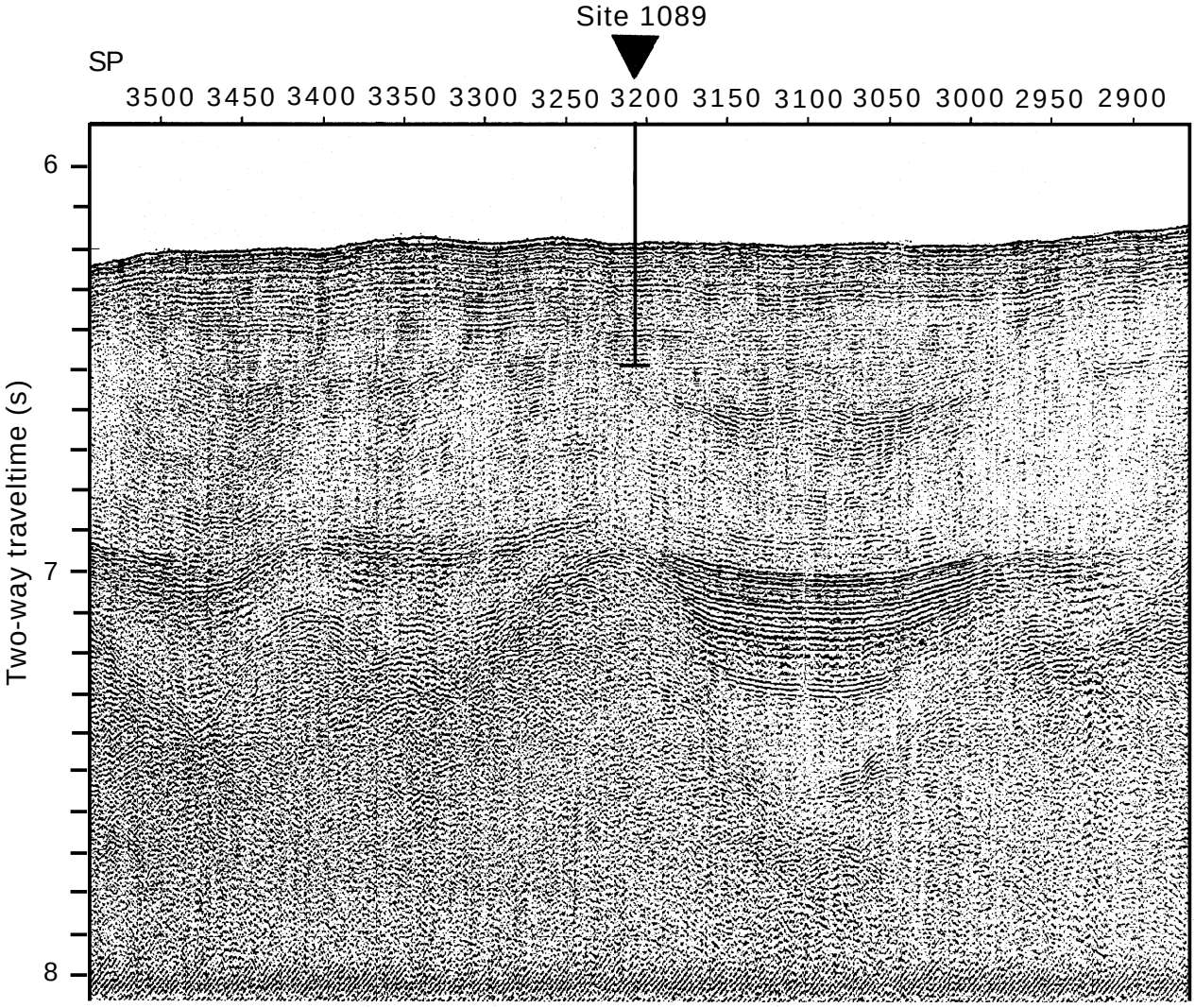

Figure F3. Oxygen isotopic record of Core RC11-83 (located near Site 1089) compared with a hydrogen isotopic record from the Vostok ice core (Charles et al., 1996). PDB = Peedee belemnite, SMOW = standard mean ocean water.

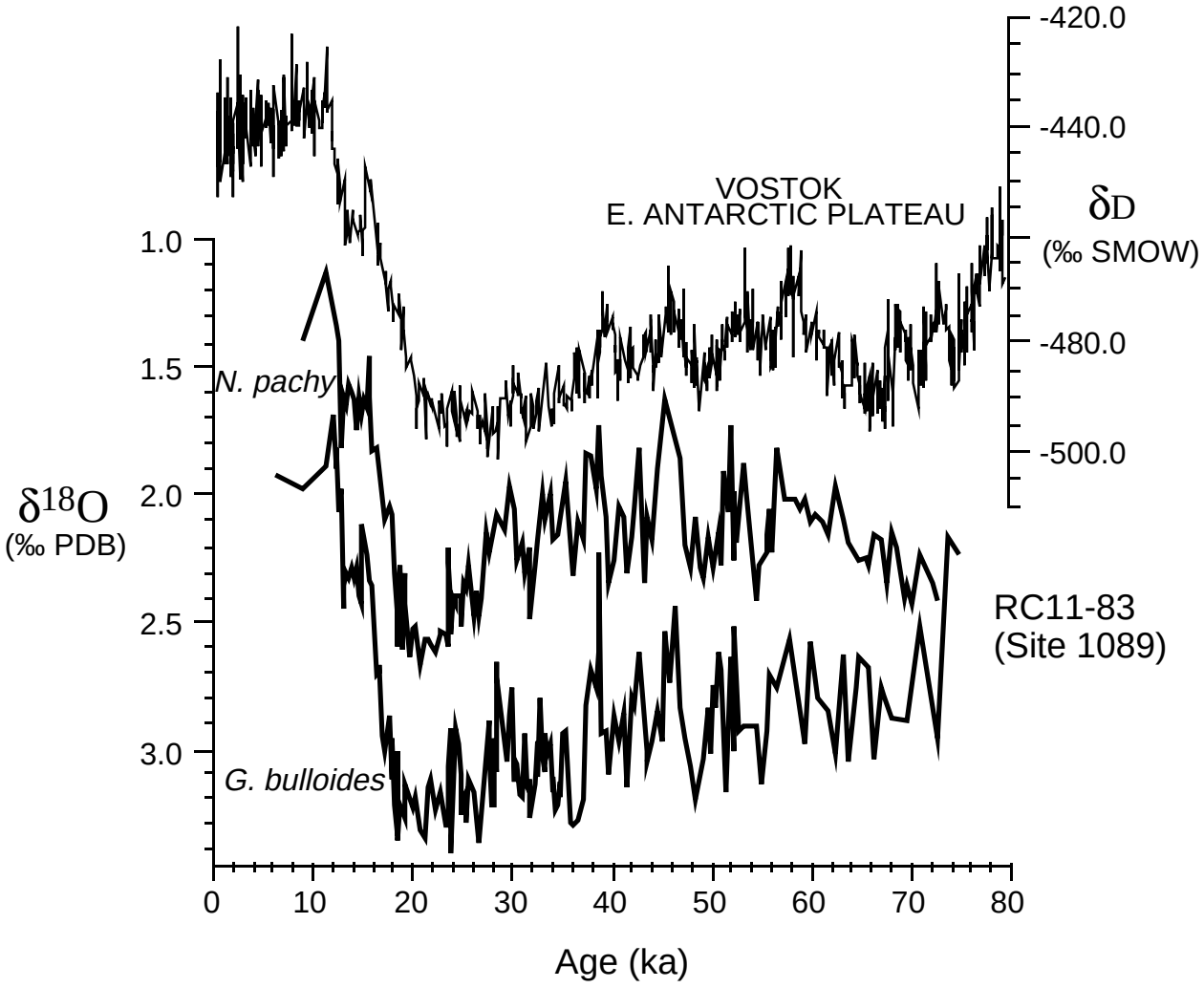

Figure F4. Lithologic summary of Site 1089 showing core recovery and a schematic representation of the variation between the two main lithologies. The lithologic variation was estimated using a 50-cm running average of the blue reflectance record. T.D. = total depth.

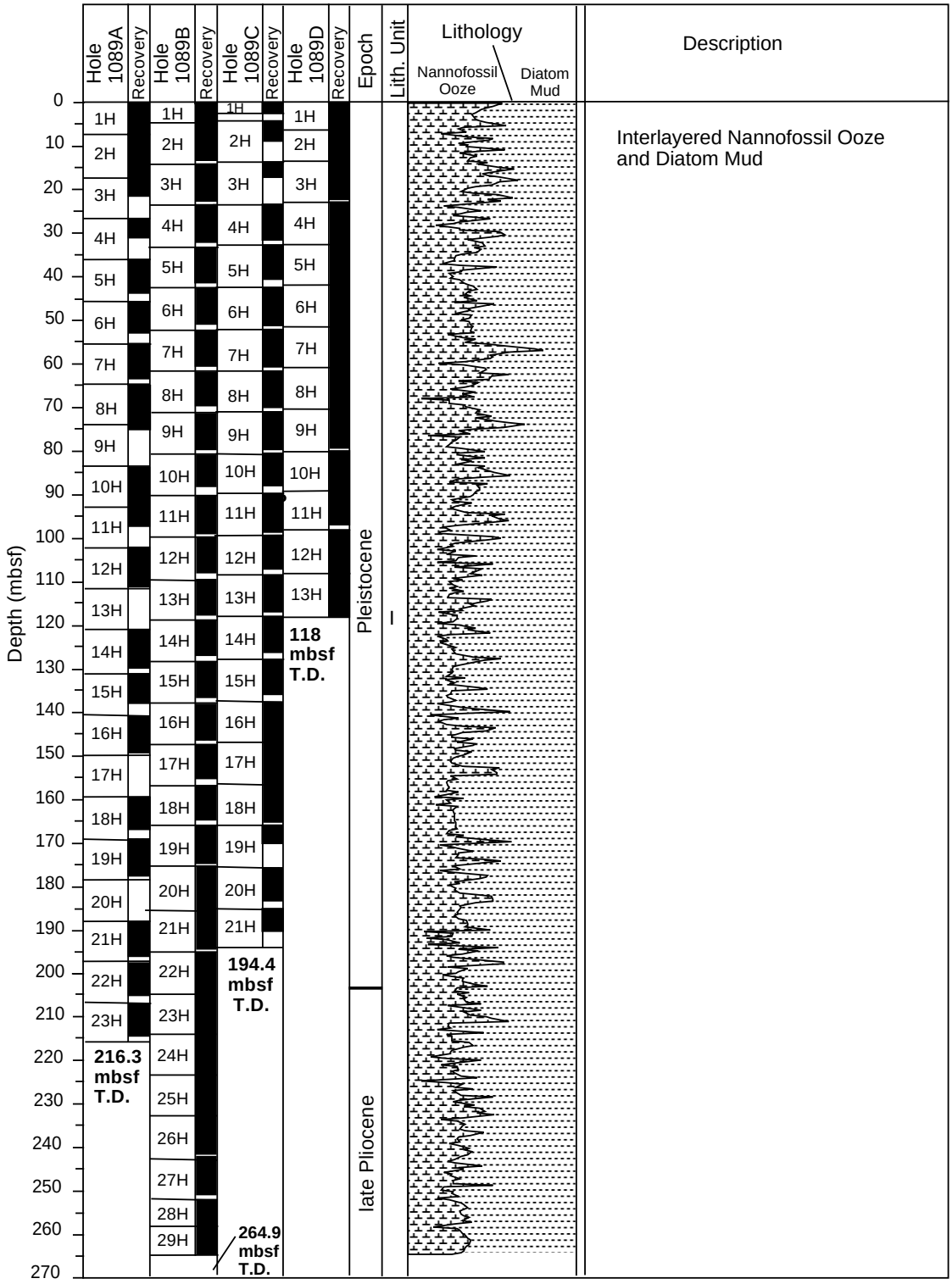

Figure F5. A. Comparison of downhole compositional variations at Site 1089 based on smear-slide (percent area), OSU-SCAT (red reflectance), coulometry (carbonate), and XRD (opal) estimates. Frames from left to right: red reflectance (650–750 nm), coulometric, and smear-slide estimates of carbonate abundance (nannofossils + foraminifers on smear slides); opal and diatom abundance; mud and terrigenous sediment; and chronostratigraphy. (Continued on next page.)

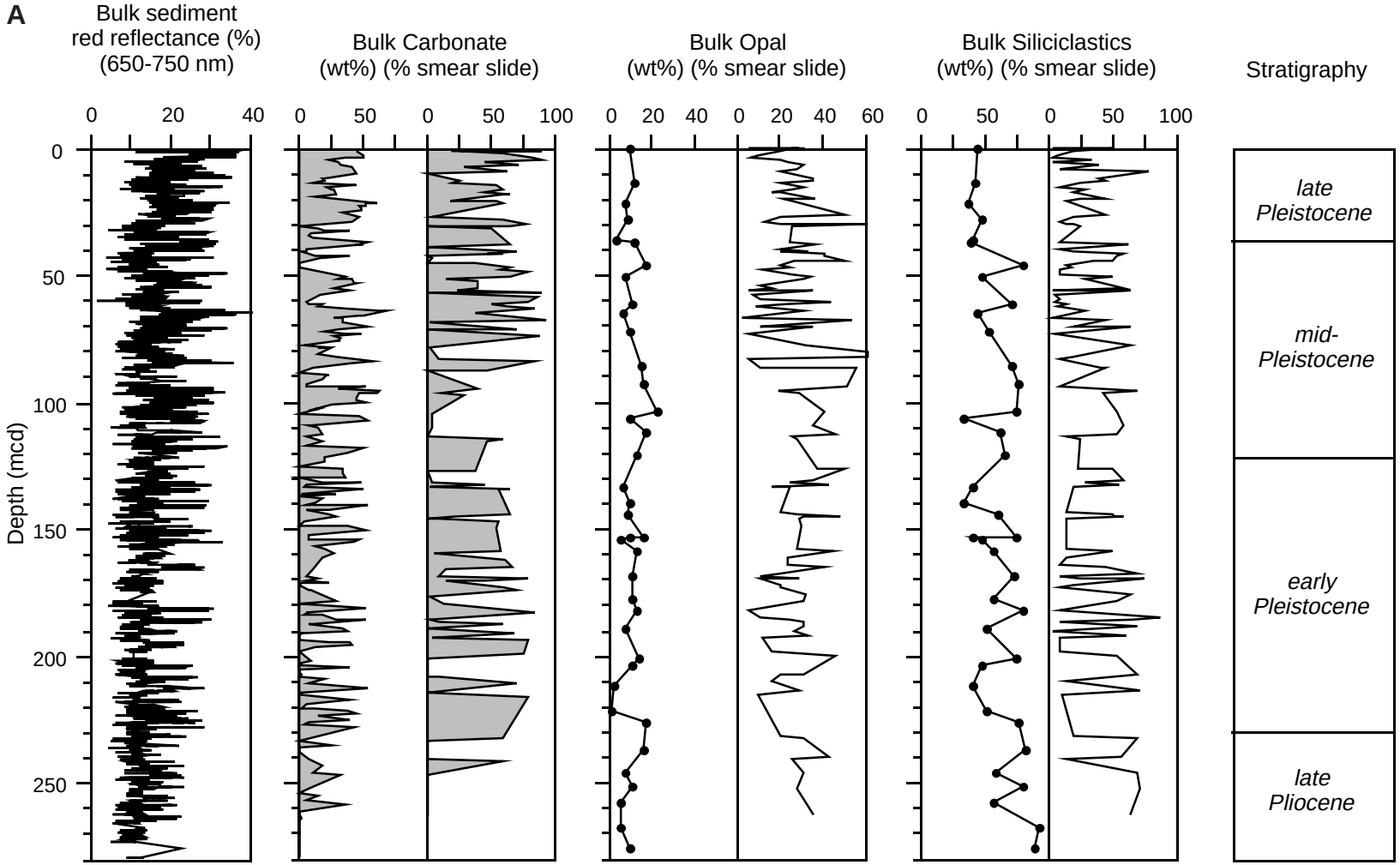

Figure F5 (continued). B. Downhole mineralogical variations inferred from XRD measurements of carbonate-free sediment from Site 1089. Qz = quartz, Fsp = feldspar, CM = clay minerals, Kao = kaolinite, Chl = chlorite.

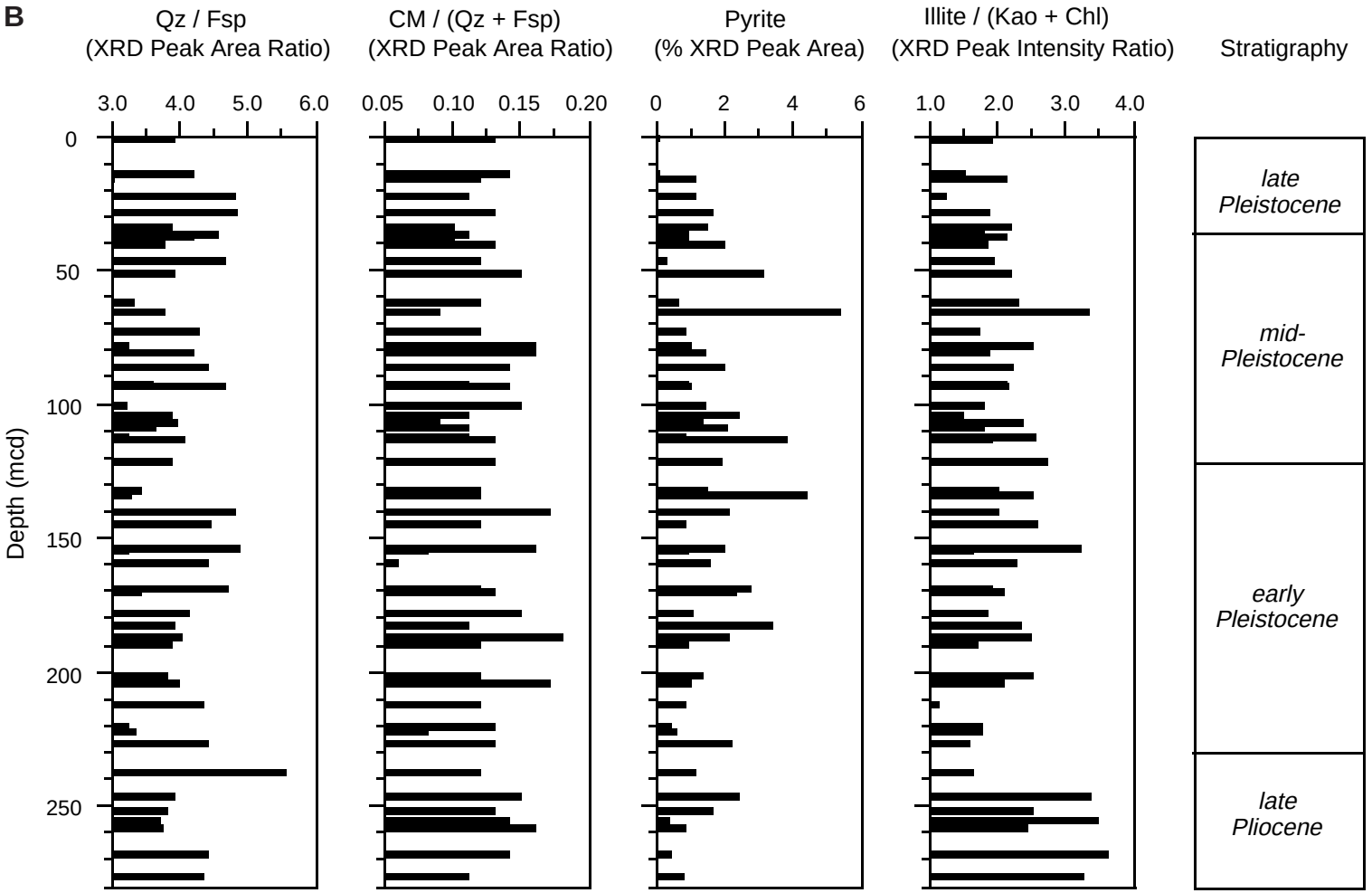

Figure F6. Microfault cutting *Planolites* burrow at 95 cm (interval 177-1089C-14H-1, 85–105 cm). Note small silt pod at 90 cm (arrow).

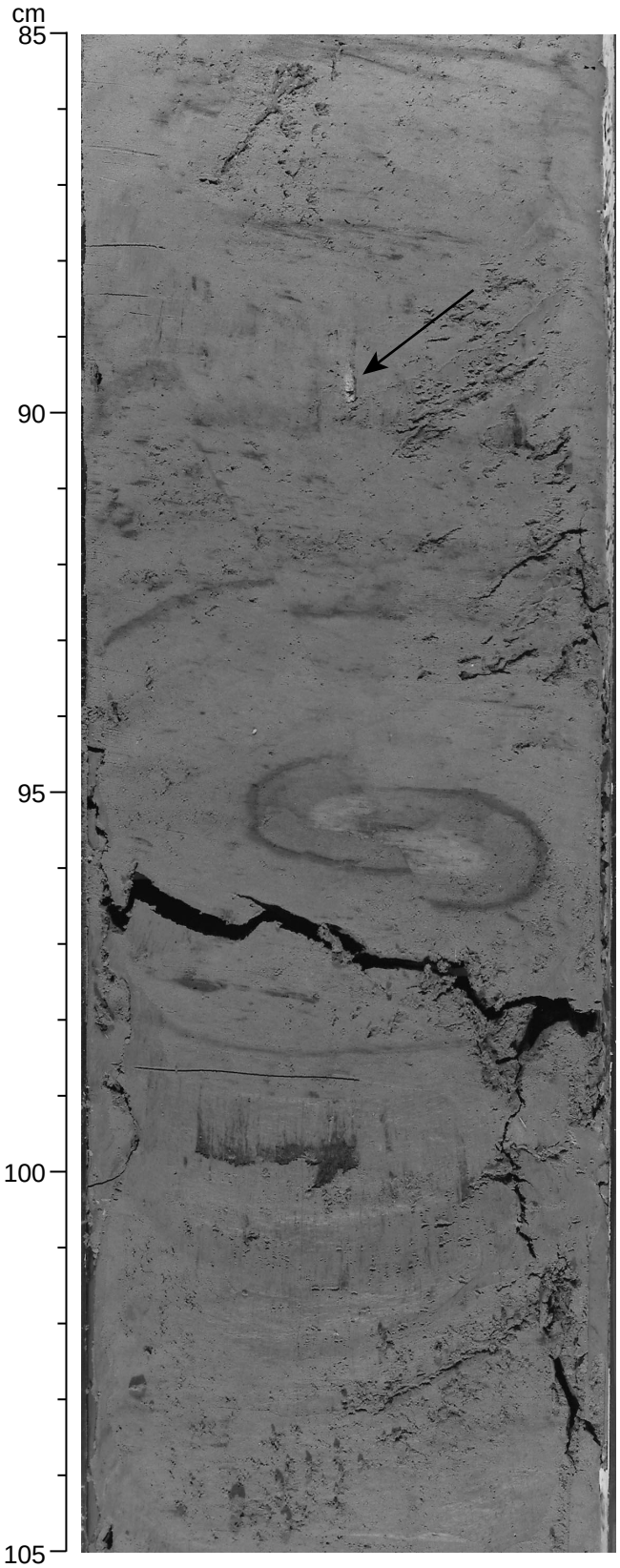

Figure F7. Tan silt laminae at 131 cm in a nannofossil- and diatom-bearing mud with bioturbation and a small silt pod at 121 cm (arrow) (interval 177-1089B-16H-5, 118–133 cm).

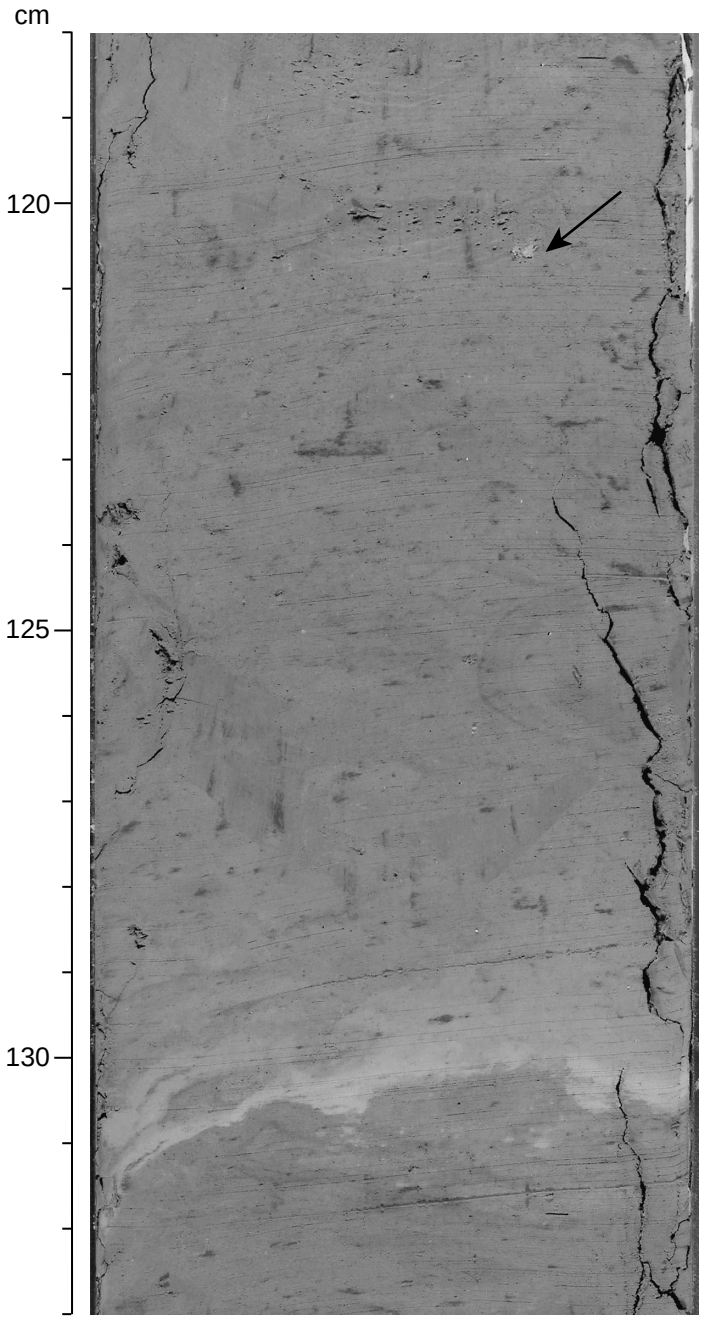

Figure F8. Purple Liesegang banding around *Planolites* burrow at 45 cm (interval 177-1089C-4H-4, 41–50 cm).

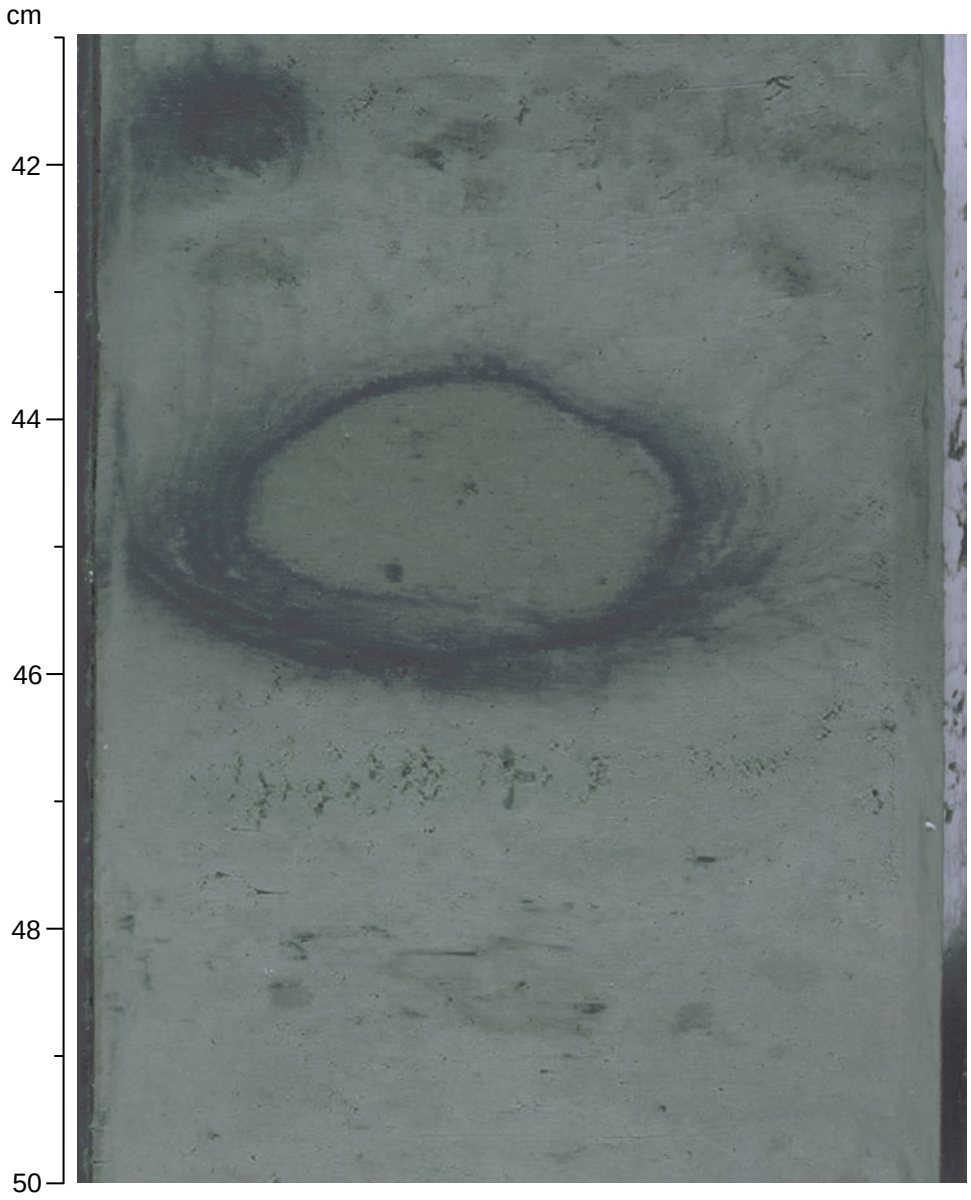

Figure F9. Green layer at 49 cm above purple laminae (interval 177-1089C-3H-2, 46–56 cm). Green layer is harder than the surrounding sediment.

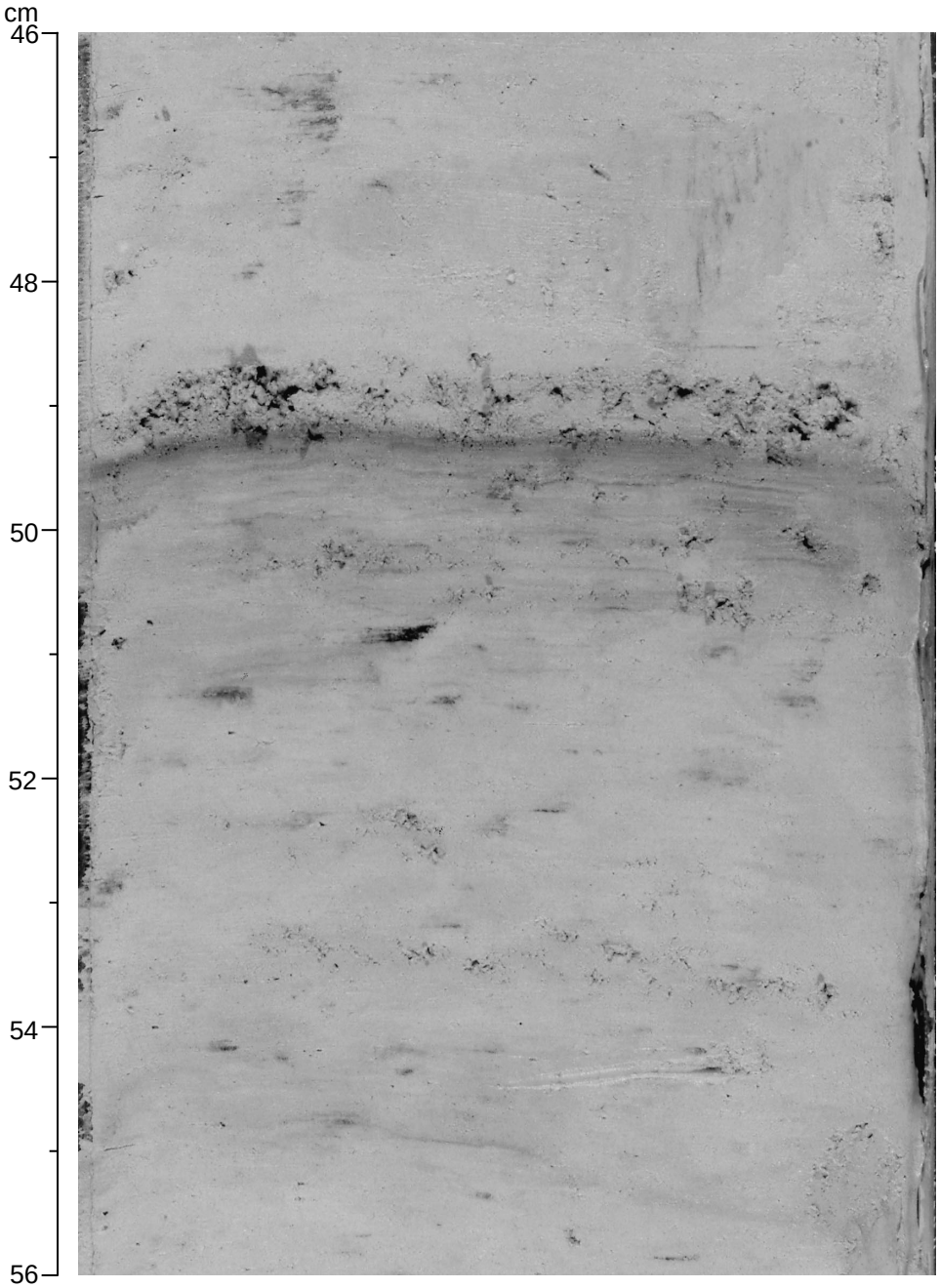

Figure F10. A. Reconstruction of soft-sediment deformation with correlation lines. Hatched boxes indicate deformed intervals. Small squares point to a deformed interval that included rip-up clasts and a graded layer. T.D. = total depth. (Continued on next page.)

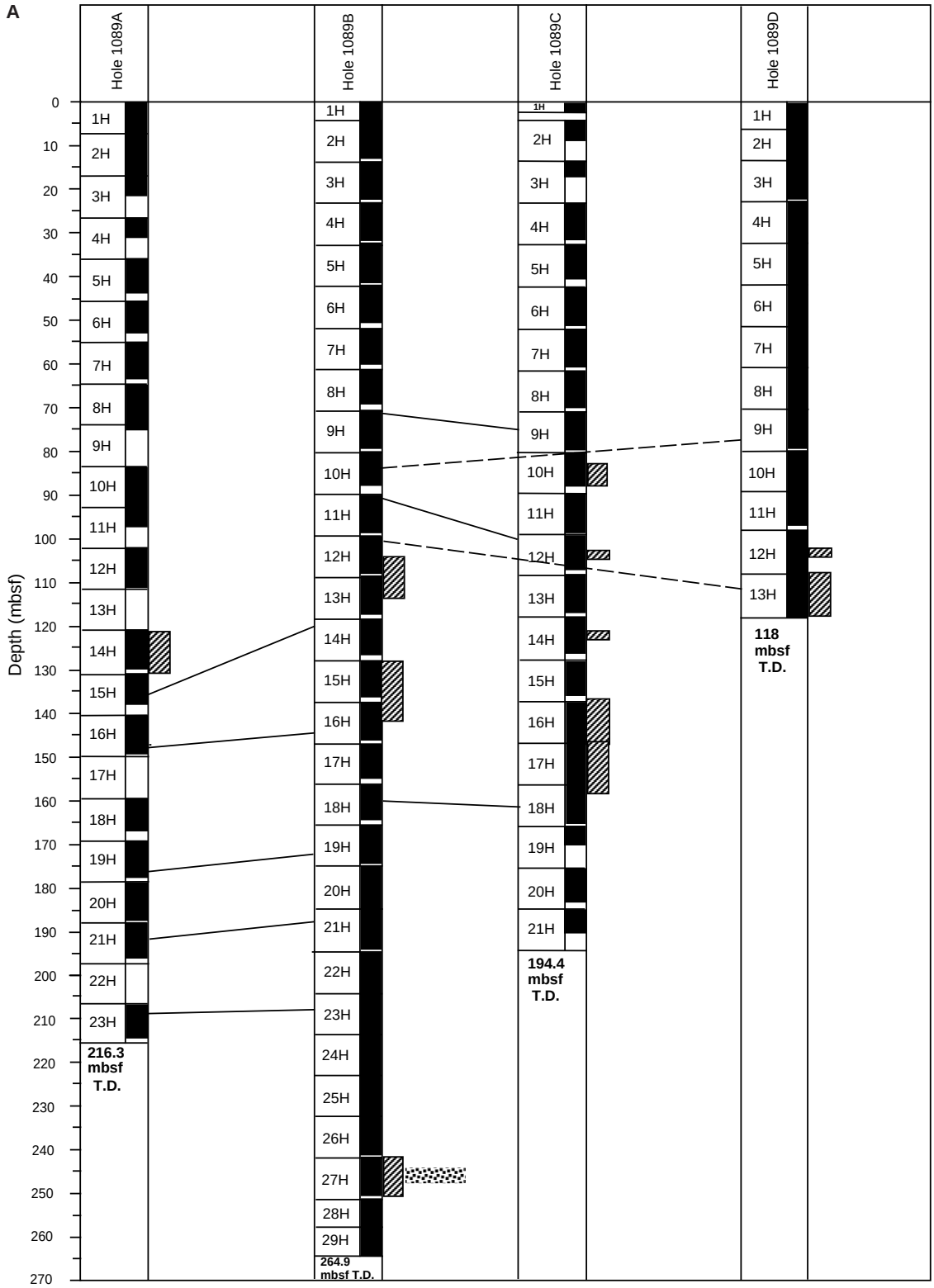

Figure F10 (continued). B. Relative location of the four holes drilled at Site 1089.

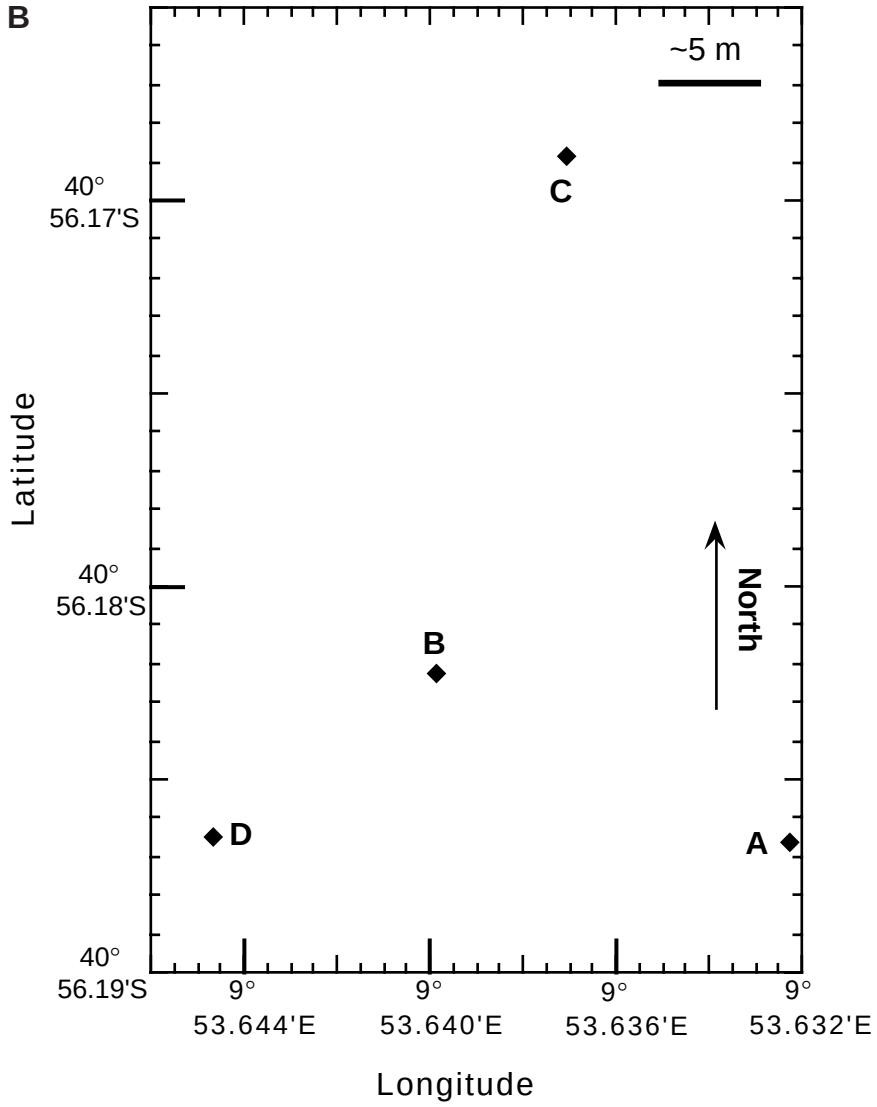

Figure F11. Soft-sediment deformation interval showing sharp color and lithologic contacts. Small microfaults with offset beds are present at 70 cm (interval 177-1089B-27H-4, 40–75 cm).

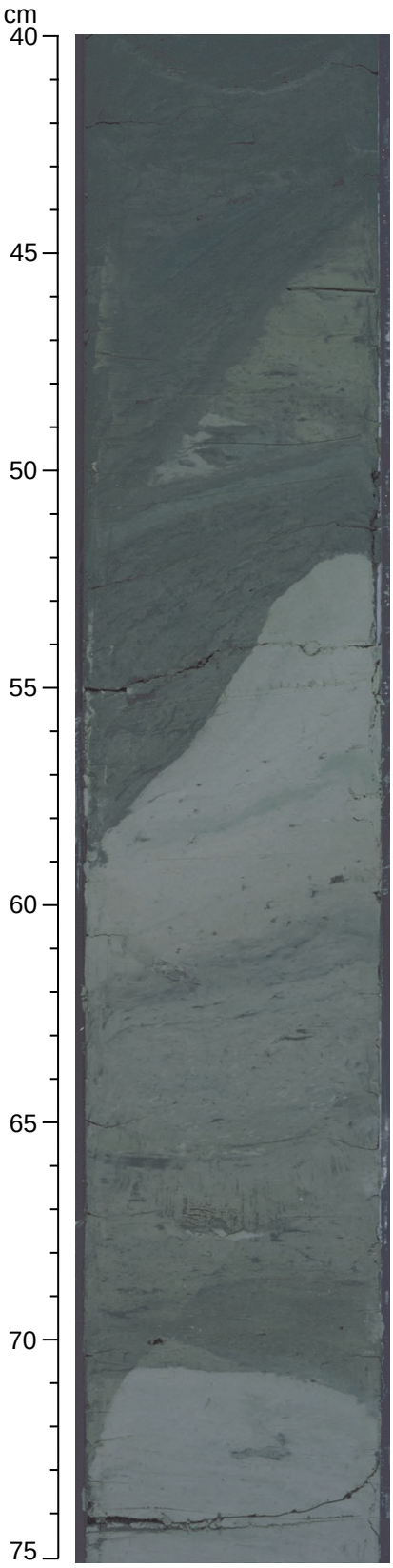

Figure F12. Contorted beds in soft-sediment deformation interval. Note microfault at 70 cm (interval 177-1089C-10H-4, 68.5–110 cm).

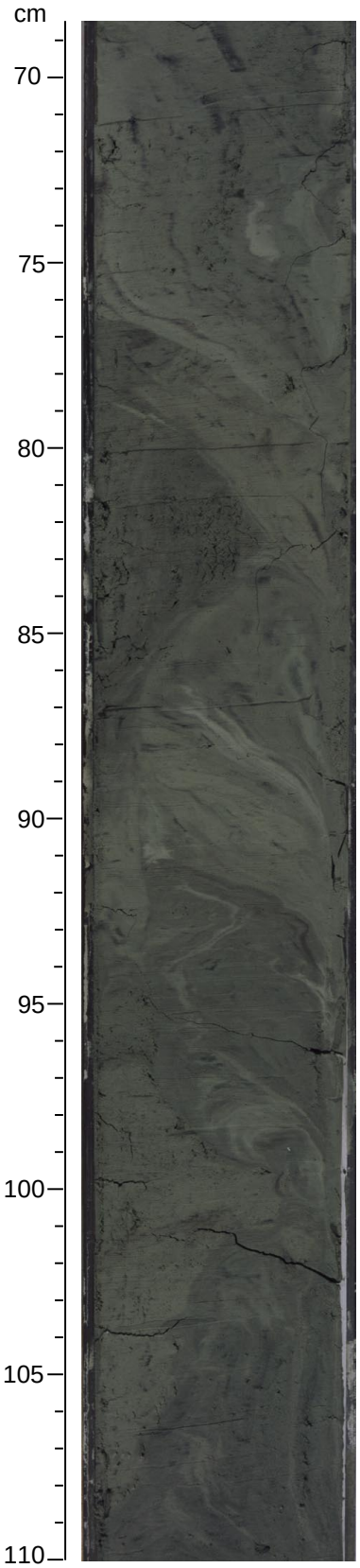

Figure F13. Graded bed (109–113 cm) within or just above the very top of a deformed sediment interval. Note rip-up mud clasts at the base of the graded bed (113–115 cm) (interval 177-1089B-27H-1, 105–125 cm).

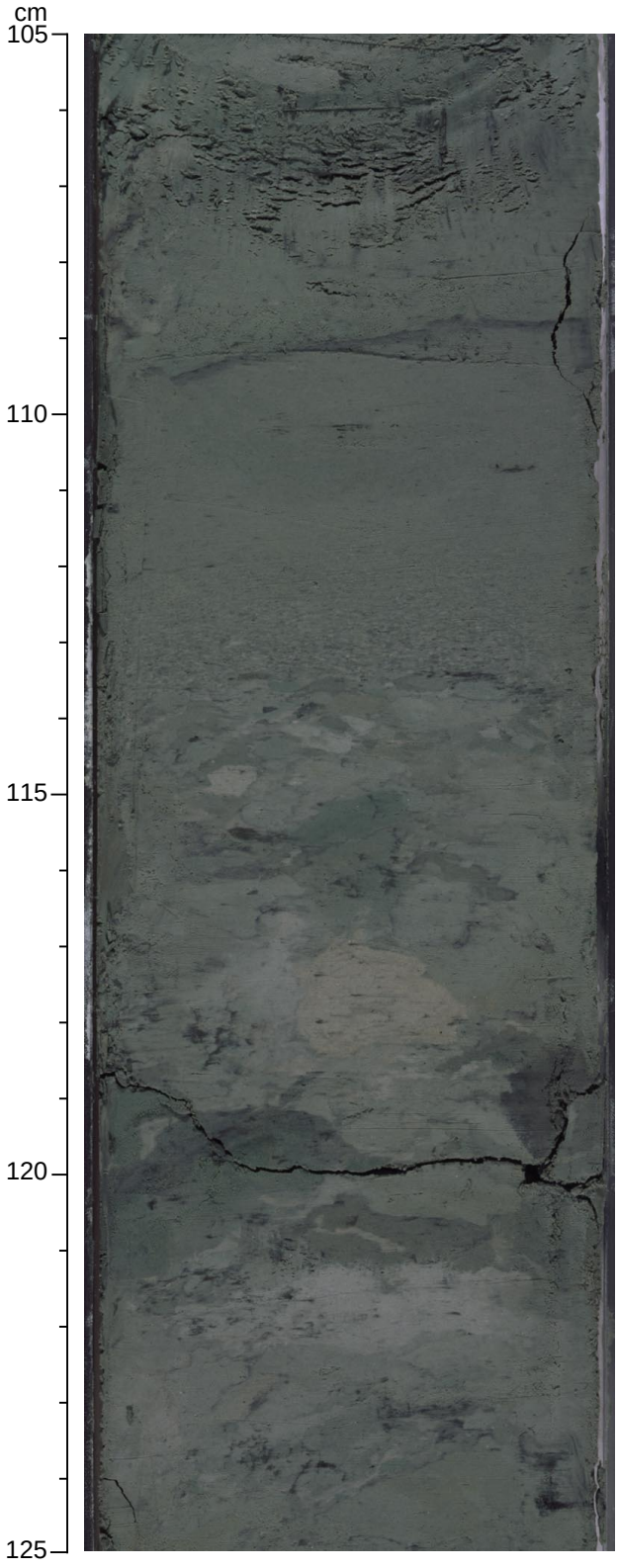

Figure F14. Smoothed (5-point average) magnetic susceptibility data for Site 1089. Holes 1089A (left curve), 1089B (second from left curve), 1089C (second from right curve), and 1089D (right curve) are horizontally offset from each other by a constant (2.0 × 10^{-5} SI units). Data from the top 5 cm of each section have been removed, as well as magnetic susceptibility values <–6.3 and >1.9 (× 10^{-5} SI units).

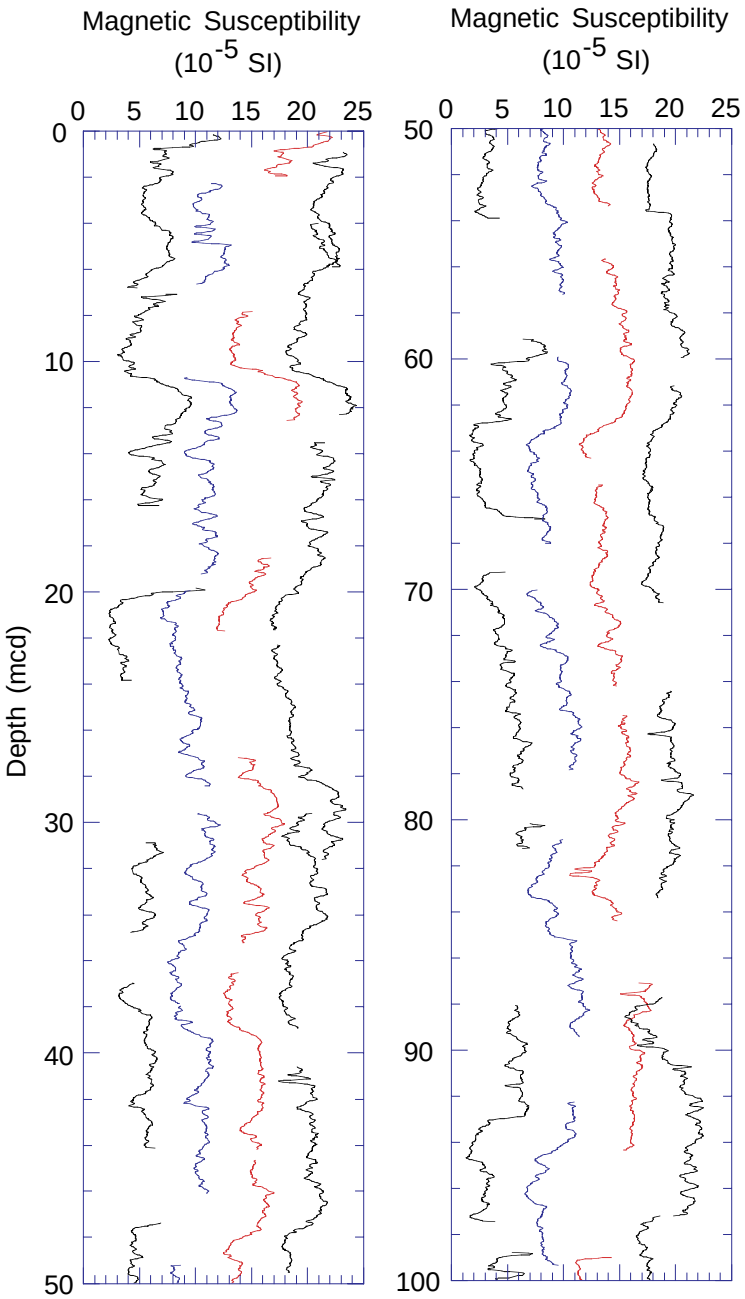

Figure F15. Smoothed (5-point average) color reflectance data (650–750 nm) for Site 1089. Holes 1089A (left curve), 1089B (second from left curve), 1089C (second from right curve), and 1089D (right curve) are horizontally offset from each other by a constant (15%). Data from the top 5 cm of each core have been removed.

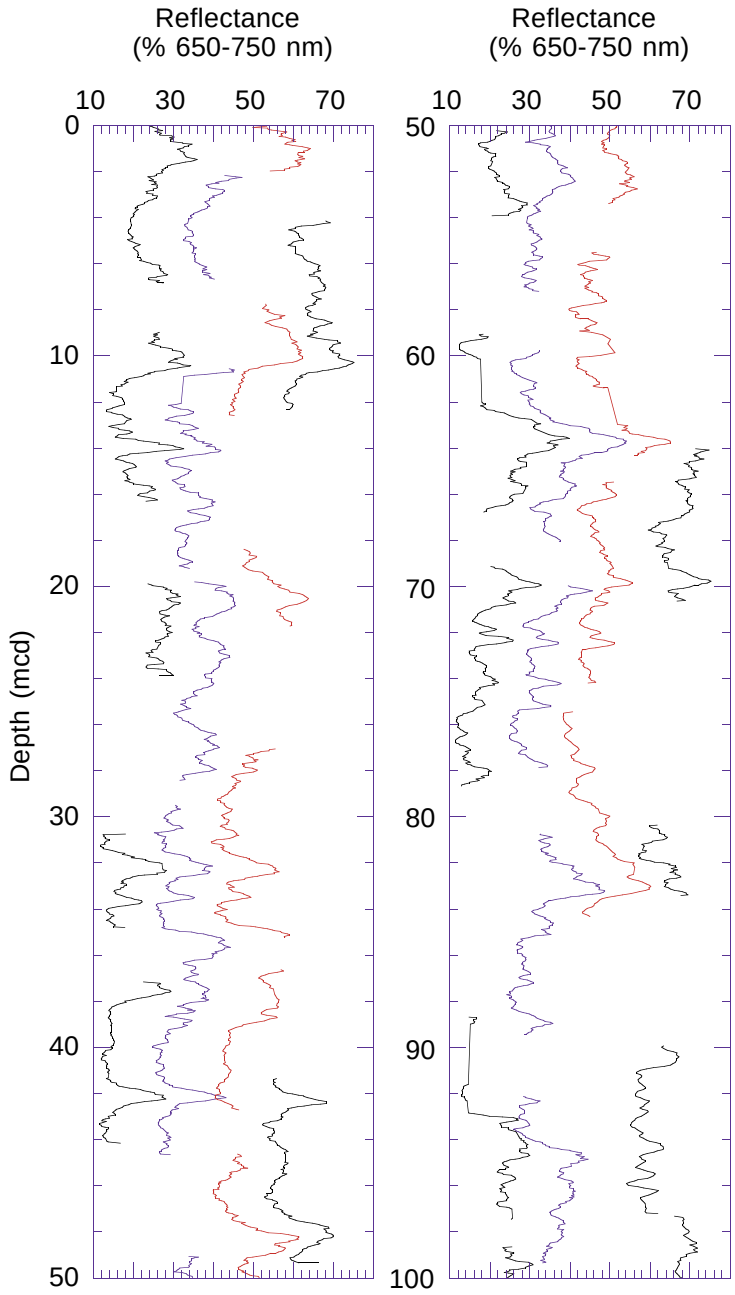

Figure F16. Smoothed (5-point average) GRA bulk density data for Site 1089. Holes 1089A (left curve), 1089B (second from left curve), 1089C (second from right curve), and 1080D (right curve) are horizontally offset from each other by a constant (0.15 g/cm³). Data from the top 5 cm of each core have been removed, as well as bulk density values <1 g/cm³ and >2.8 g/cm³.

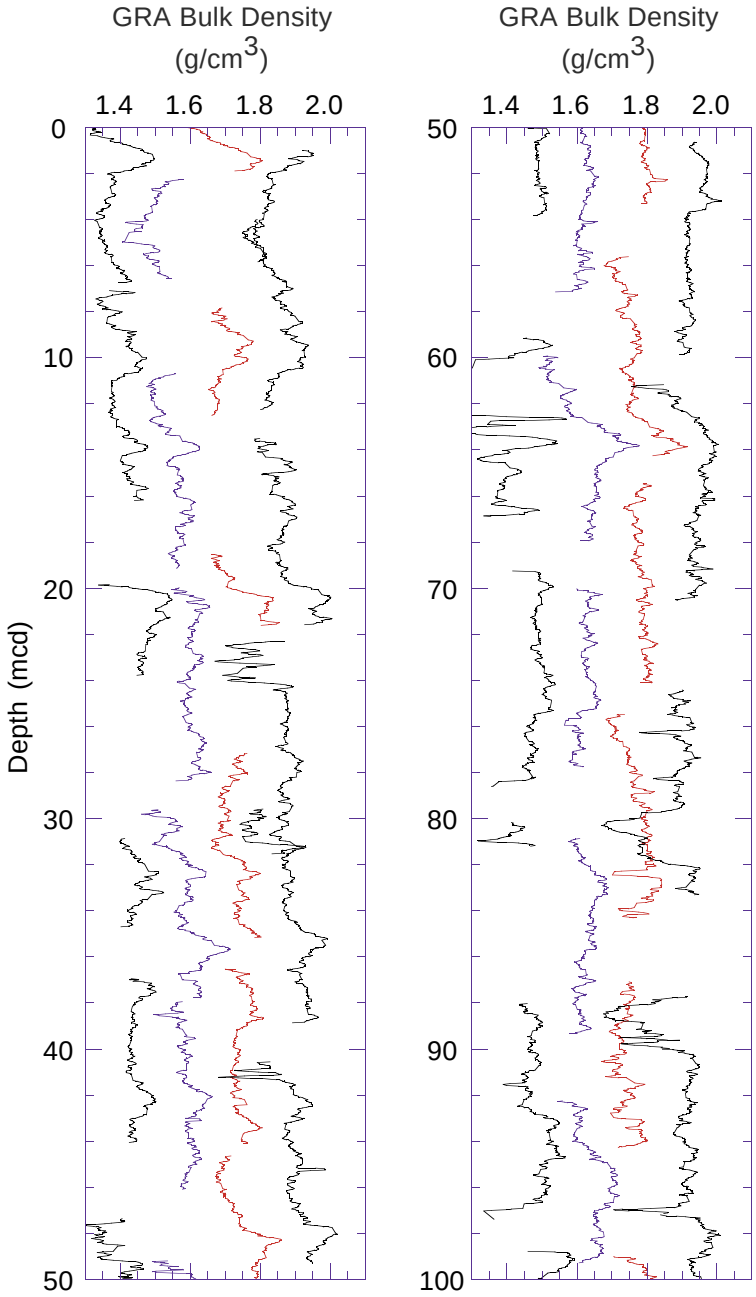

Figure F17. Spliced records of magnetic susceptibility, color reflectance, and GRA bulk density for the upper 100 mcd of Site 1089. All three data sets were smoothed with a 5-point running mean. The horizontal lines in each plot identify the splice tie points. Note that the color reflectance data are not continuous as color data were not collected on all cores used for the sampling splice.

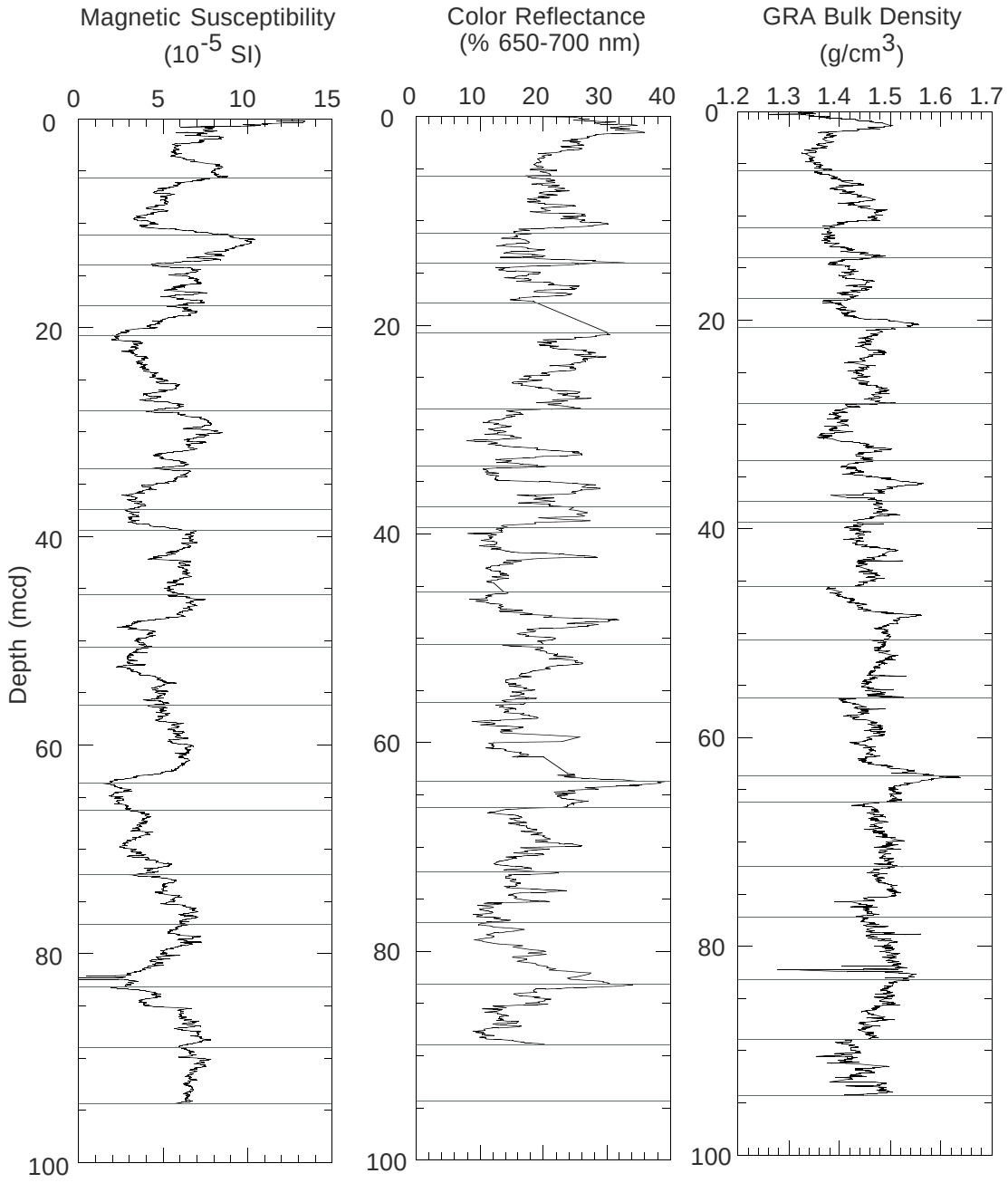

Figure F18. Color reflectance (5-point smoothed) data of the top 100 m of Hole 1089B and related calcareous nannofossil and diatom stratigraphic events used for the identification of marine isotopic stages (MIS) (see note 3). LO = last occurrence, FO = first occurrence, *H. k.* = *H. karstenii*.

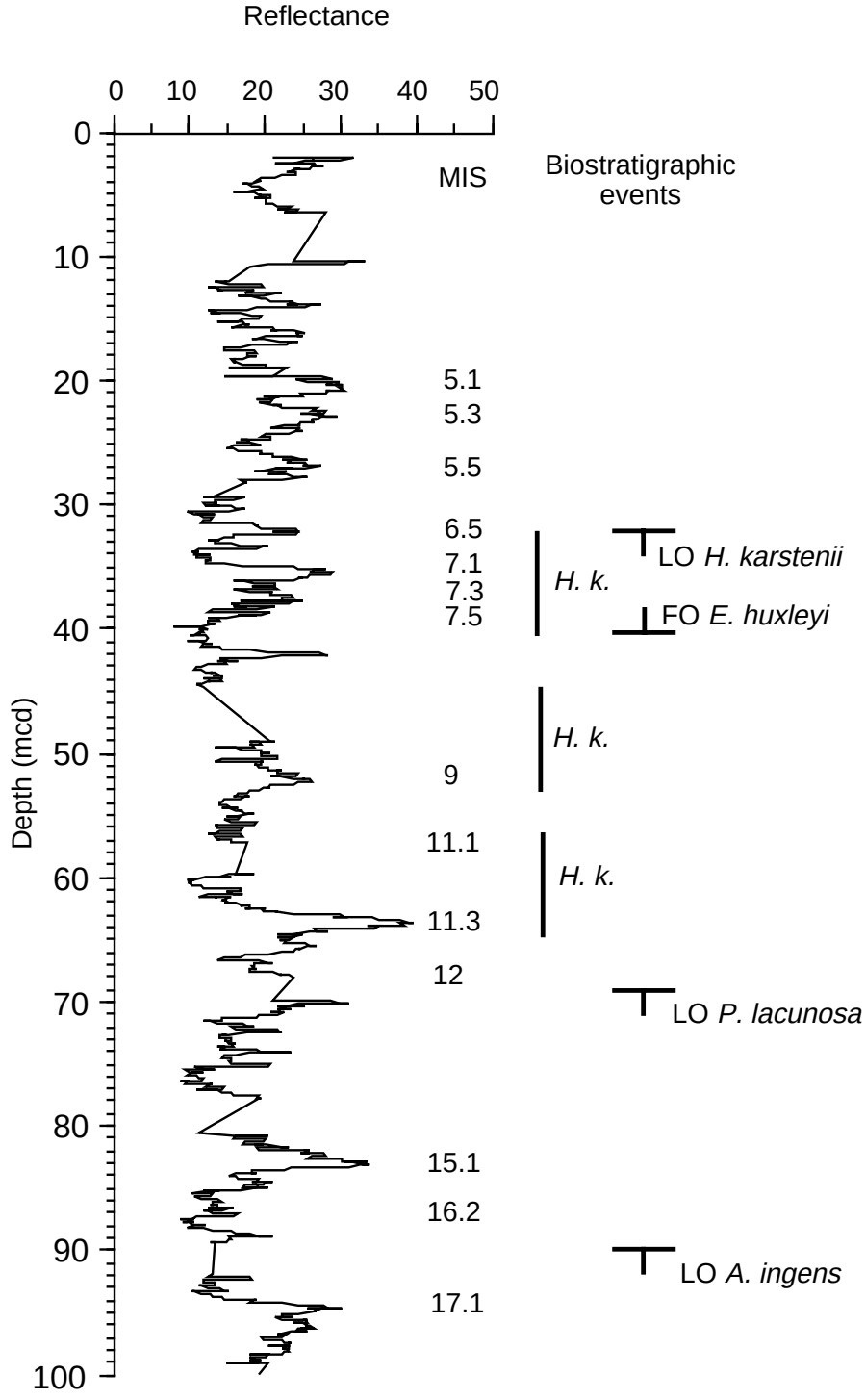

Figure F19. Biostratigraphic and magnetostratigraphic correlation chart for Site 1089, and selected absolute age designations. Shaded area indicates disturbed interval.

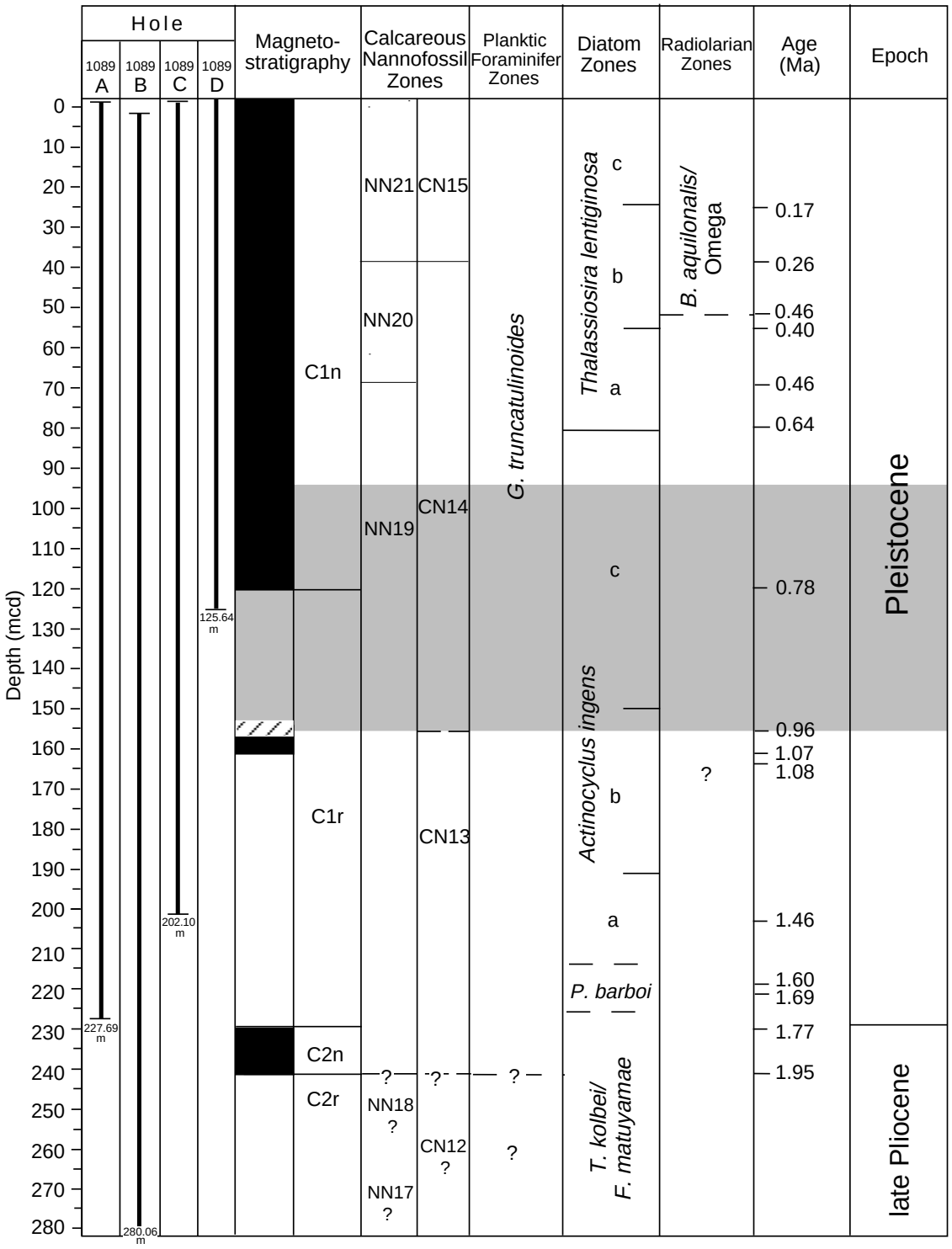

Figure F20. Age-depth plot of control points at Site 1089, integrating biostratigraphy, geomagnetic polarity, and color reflectance data from Holes 1089A–1089C. Plotted are the mean sample composite depths. The dark shading indicates the depth range of the disturbed sedimentary section between 94 and 156 mcd. Vertical error bars indicate approximate depth uncertainty in the geomagnetic polarity and diatom datums. The solid line represents a visual best fit through the control points (Table T9, p. 70). Corresponding sedimentation rate averages are given in parentheses. 1 = LO of *R. asanoi*.

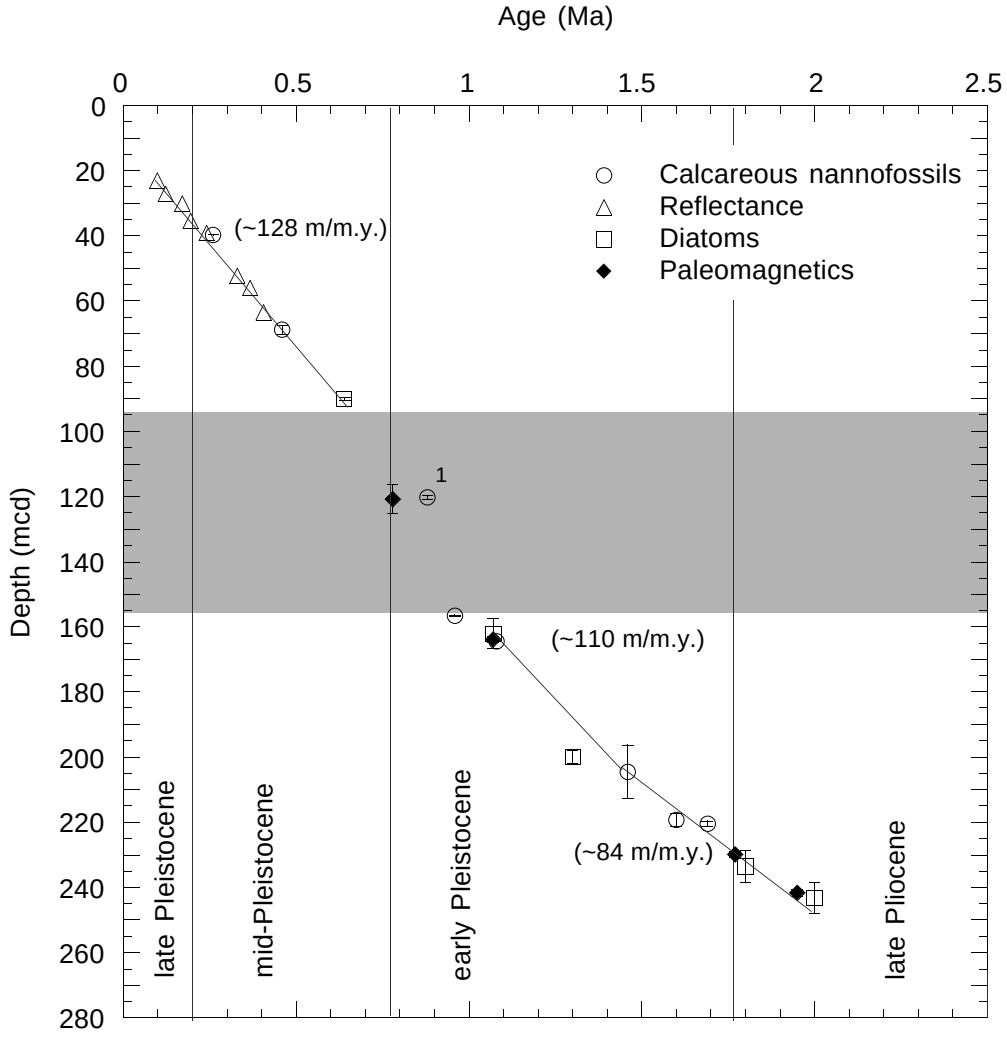

Figure F21. Diatom abundance and preservation and abundance pattern of selected biostratigraphic and paleoenvironmental significant diatom taxa at Site 1089, correlated with the magnetostratigraphic and diatom biostratigraphic record. Abundance abbreviations: A = abundant, C = common, F = few, R = rare, T = trace; preservation abbreviations: G = good, M = moderate, P = poor. Magnetostratigraphy shading: black = normal, white = reversed.

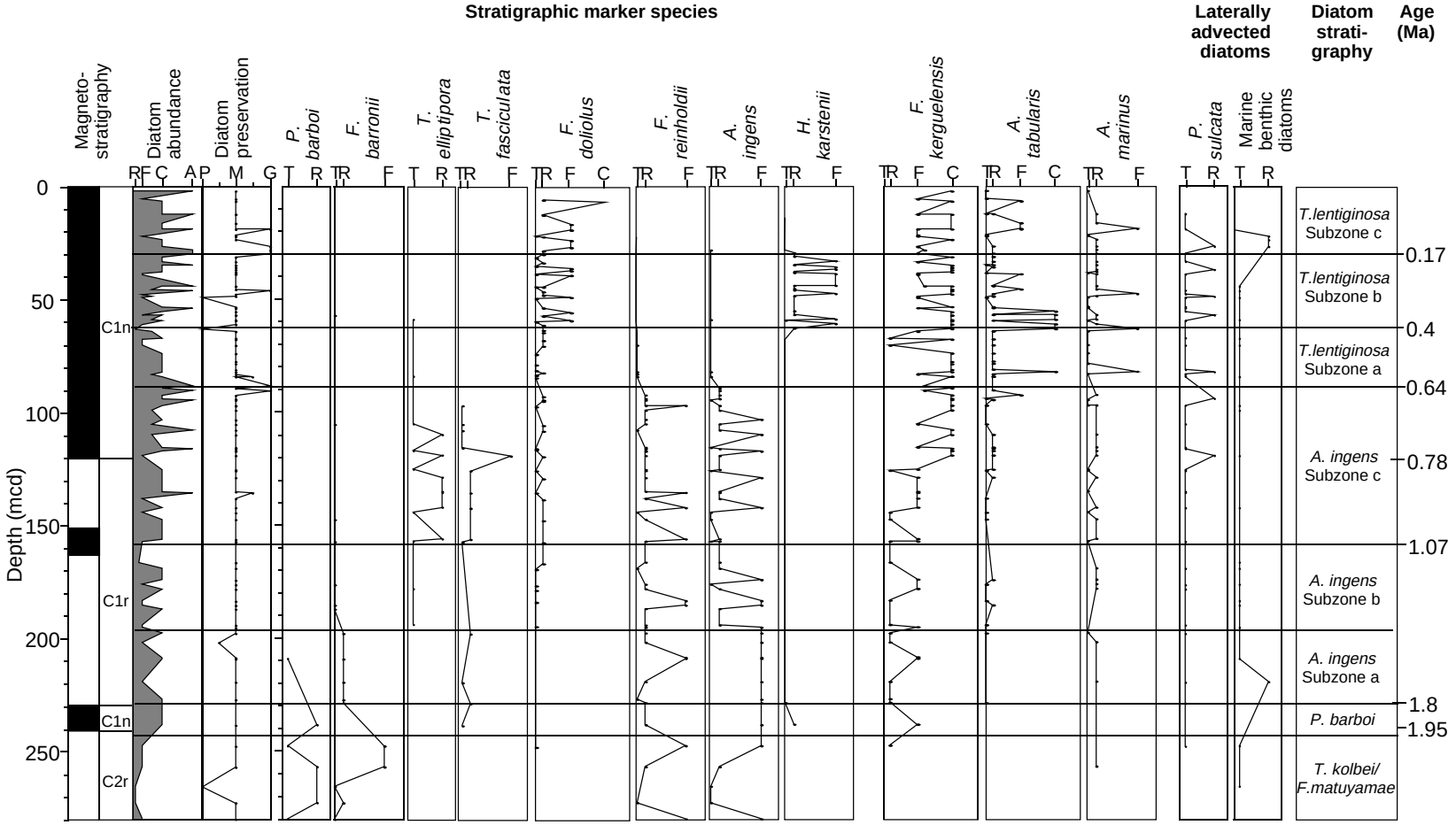

Figure F22. Inclination of the remanent magnetization after alternating-field demagnetization at peak fields of 20 mT for Site 1089. The Brunhes Chron and the Jaramillo and Olduvai Subchrons are tentatively identified. Magnetic polarity shading: black = normal, white = reversed.

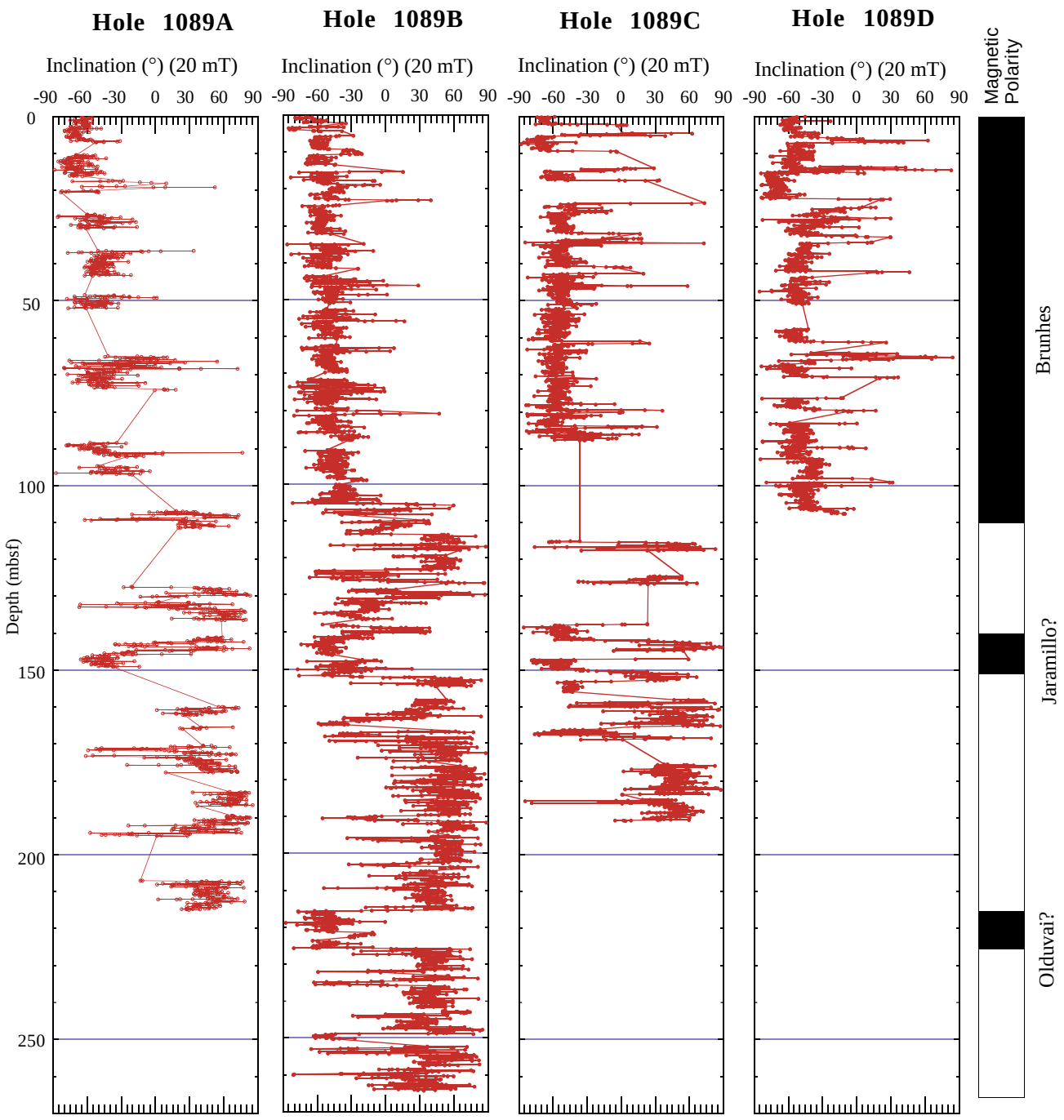

Figure F23. Concentration of methane in sediments and sulfate in interstitial water vs. depth at Site 1089; the data are reported in Tables **T14,** p. 87, and **T15,** p. 88.

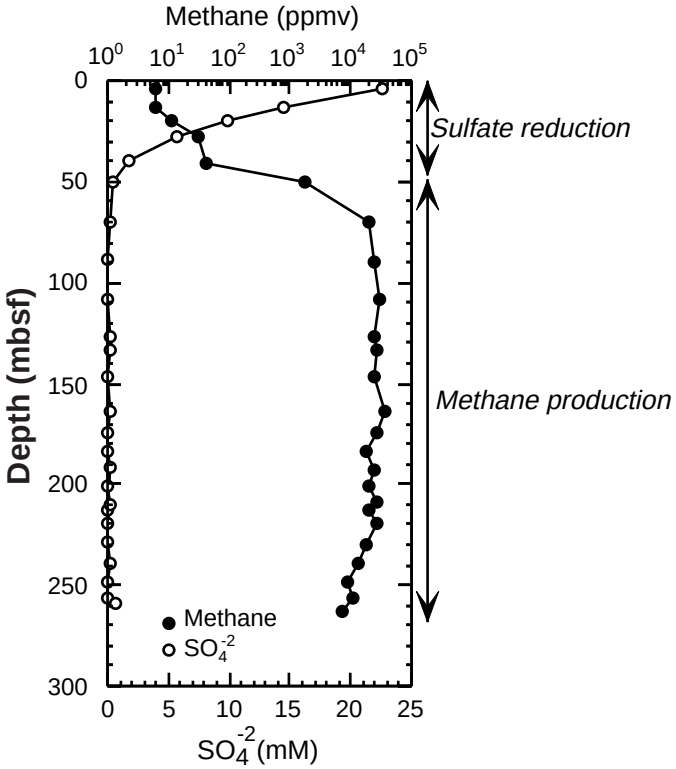

Figure F24. Interstitial water chemistry profiles vs. depth for salinity, chlorinity, alkalinity, pH, potassium, calcium, magnesium, strontium, lithium, ammonium, phosphate, silica, sulfate, and manganese at Site 1089; the data are reported in Table **T15,** p. 88.

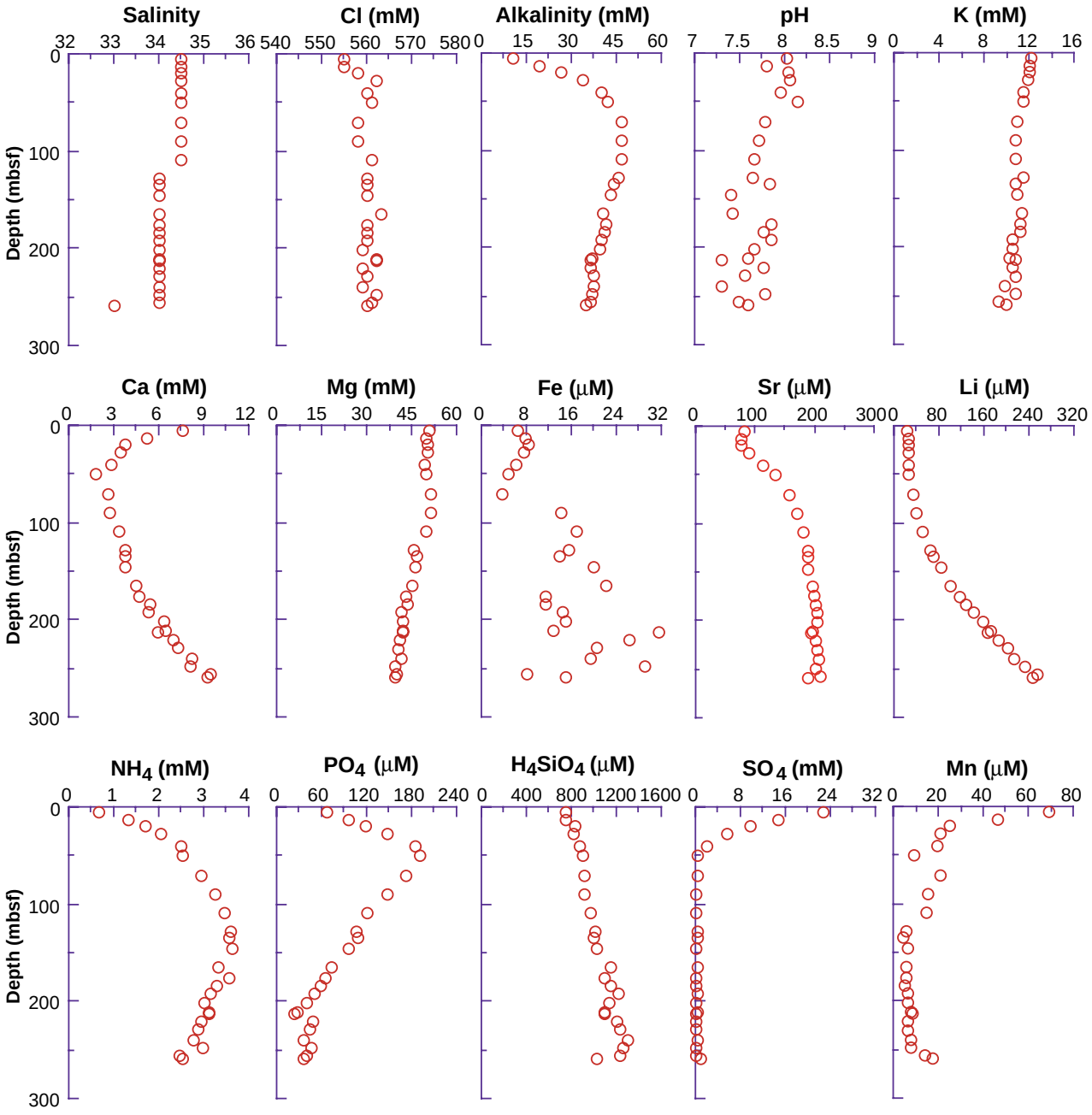

Figure F25. Concentration of calcium carbonate ($CaCO_3$), total organic carbon (TOC), total nitrogen (TN), total sulfur (TS), and TOC/TN vs. depth at Site 1089; the data are reported in Table **T16,** p. 90.

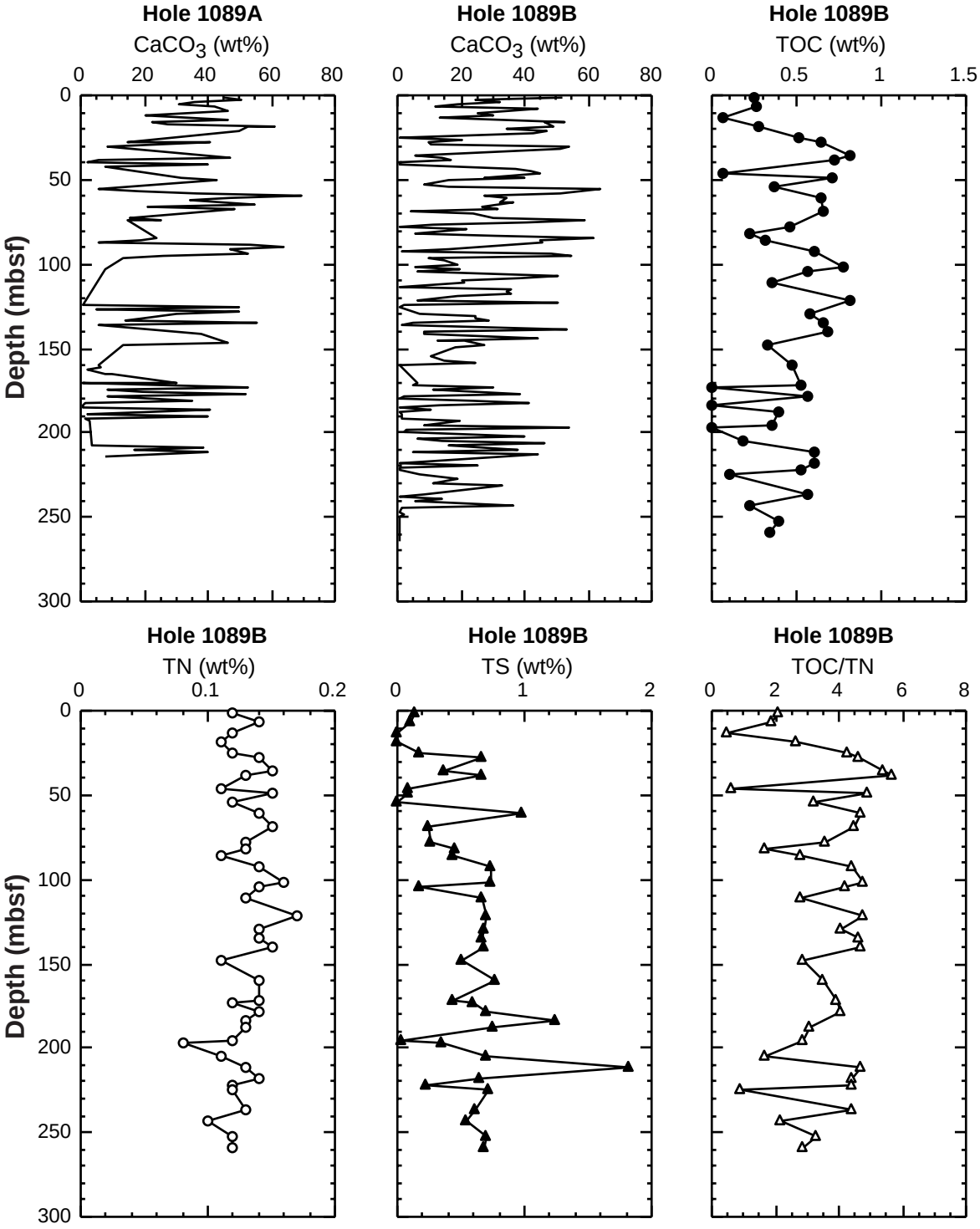

Figure F26. Site 1089 downhole variations of porosity (solid circles = MAD method) and OSU-SCAT resistivity (dots; line = smoothed values), *P*-wave velocities (dots = PWL, solid circles = PWS3), GRA bulk density (solid line = smoothed data) and MAD bulk density (open circles), volume-specific magnetic susceptibility, and NGR (smoothed data).

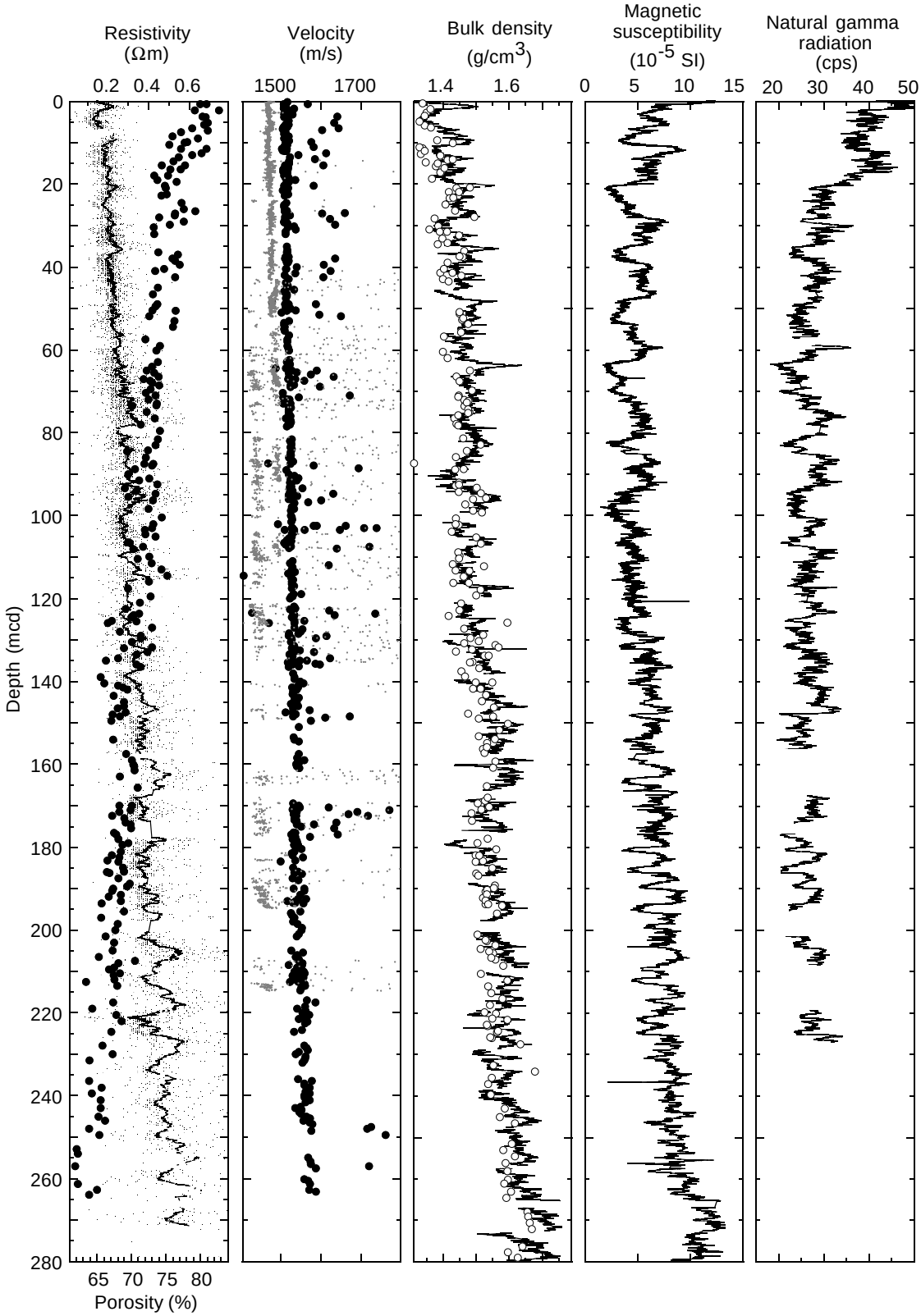

Figure F27. Relationship between GRA bulk density and gravimetric (MAD) bulk density at Site 1089.

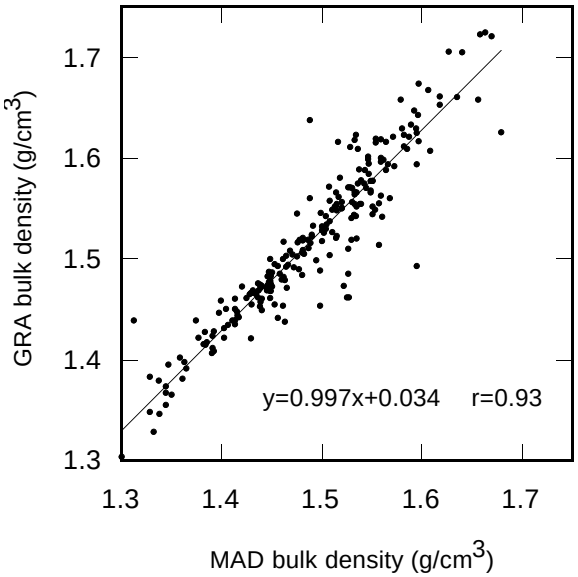

Figure F28. Site 1089 **(A)** best exponential fit between porosity (MAD method) and formation factor calculated from OSU-SCAT resistivity, and **(B)** comparison between porosity calculated from the MAD method (P_o) and from calibrated resistivity measurements (P_r).

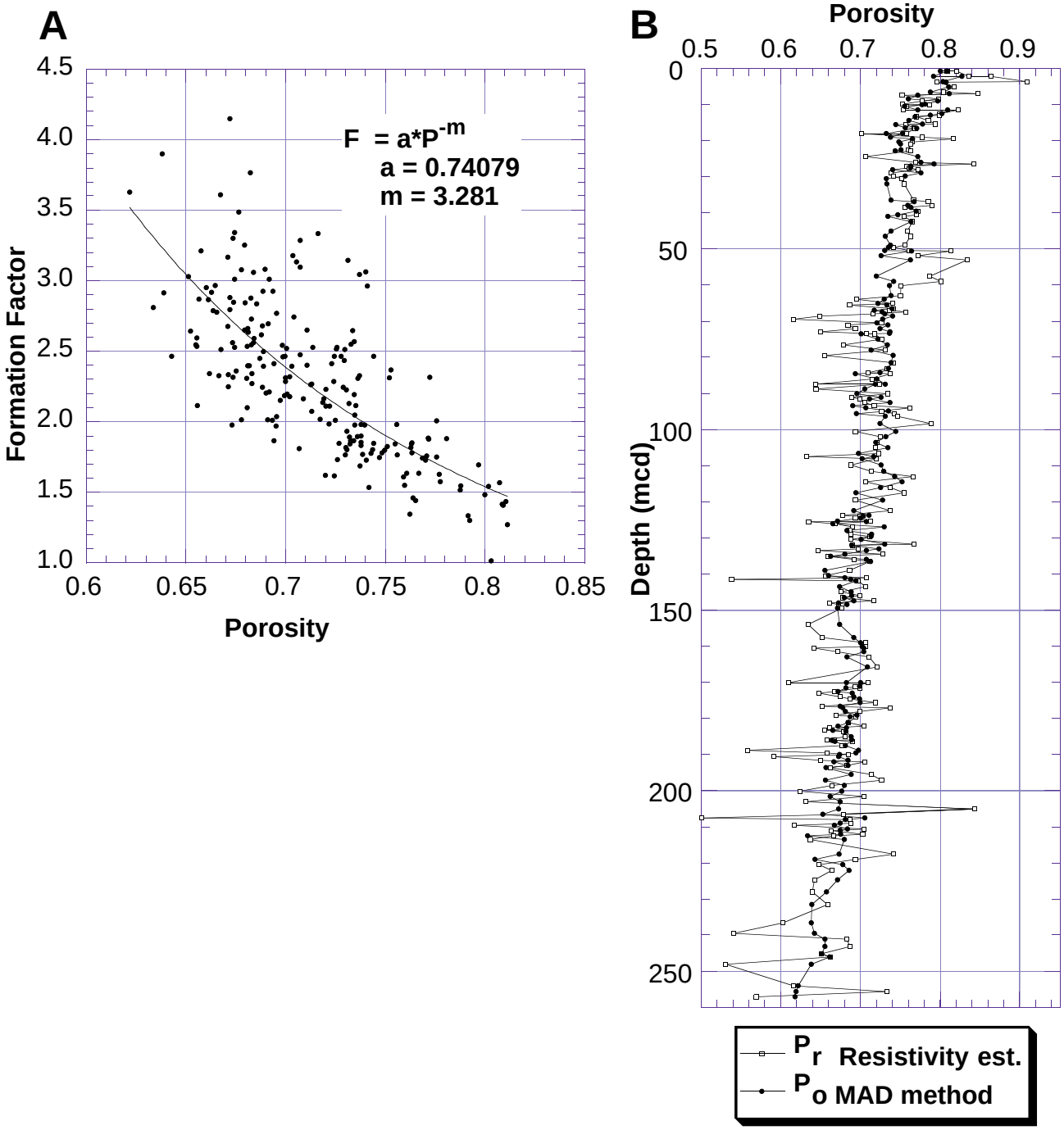

Figure F29. Site 1089 downhole diffuse spectral reflectance variations presented for the blue, near infrared (nIR), and red bands.

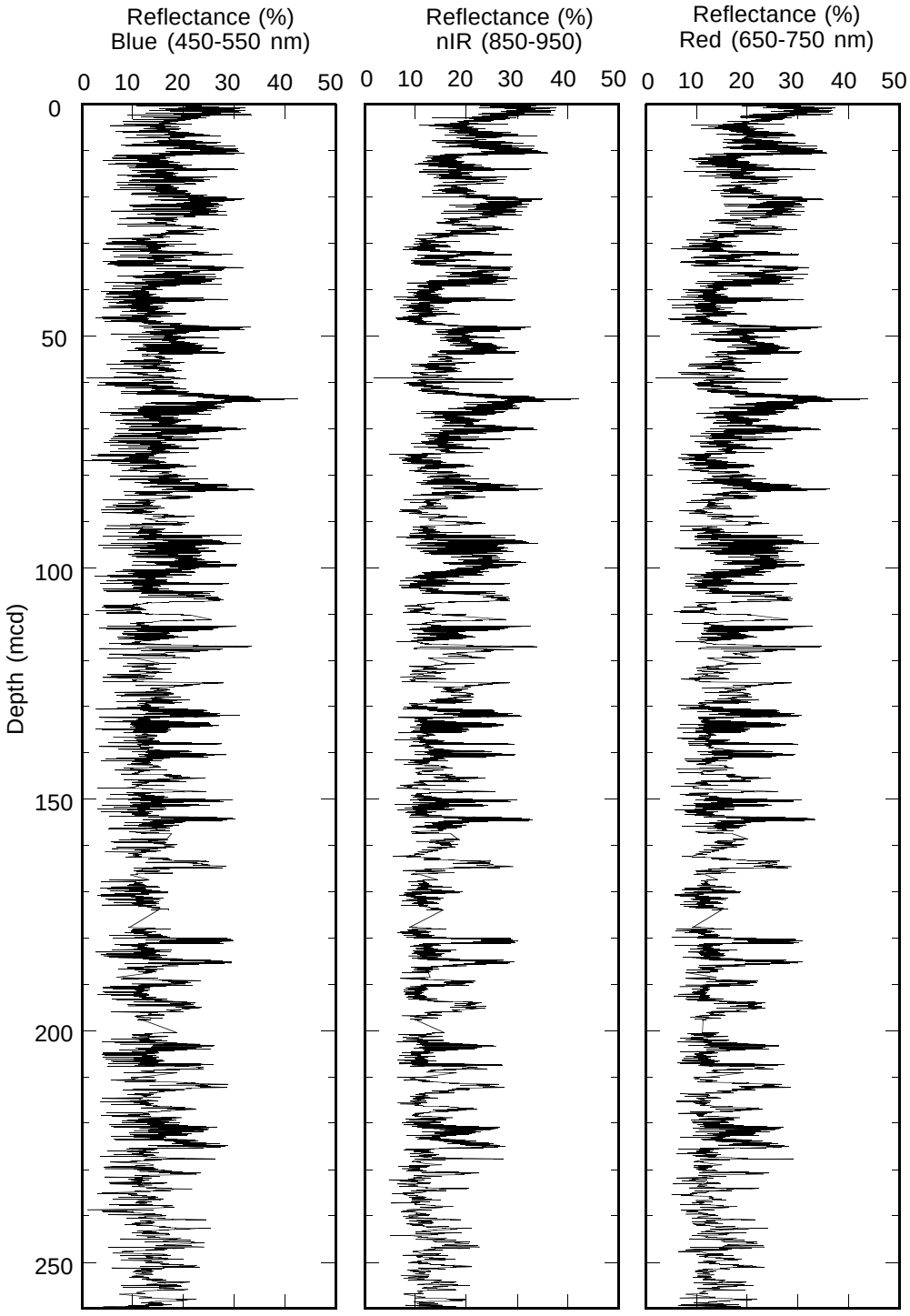

Figure F30. Comparison between OSU-SCAT and Minolta CM-2002 spectral reflectance at Hole 1089B.

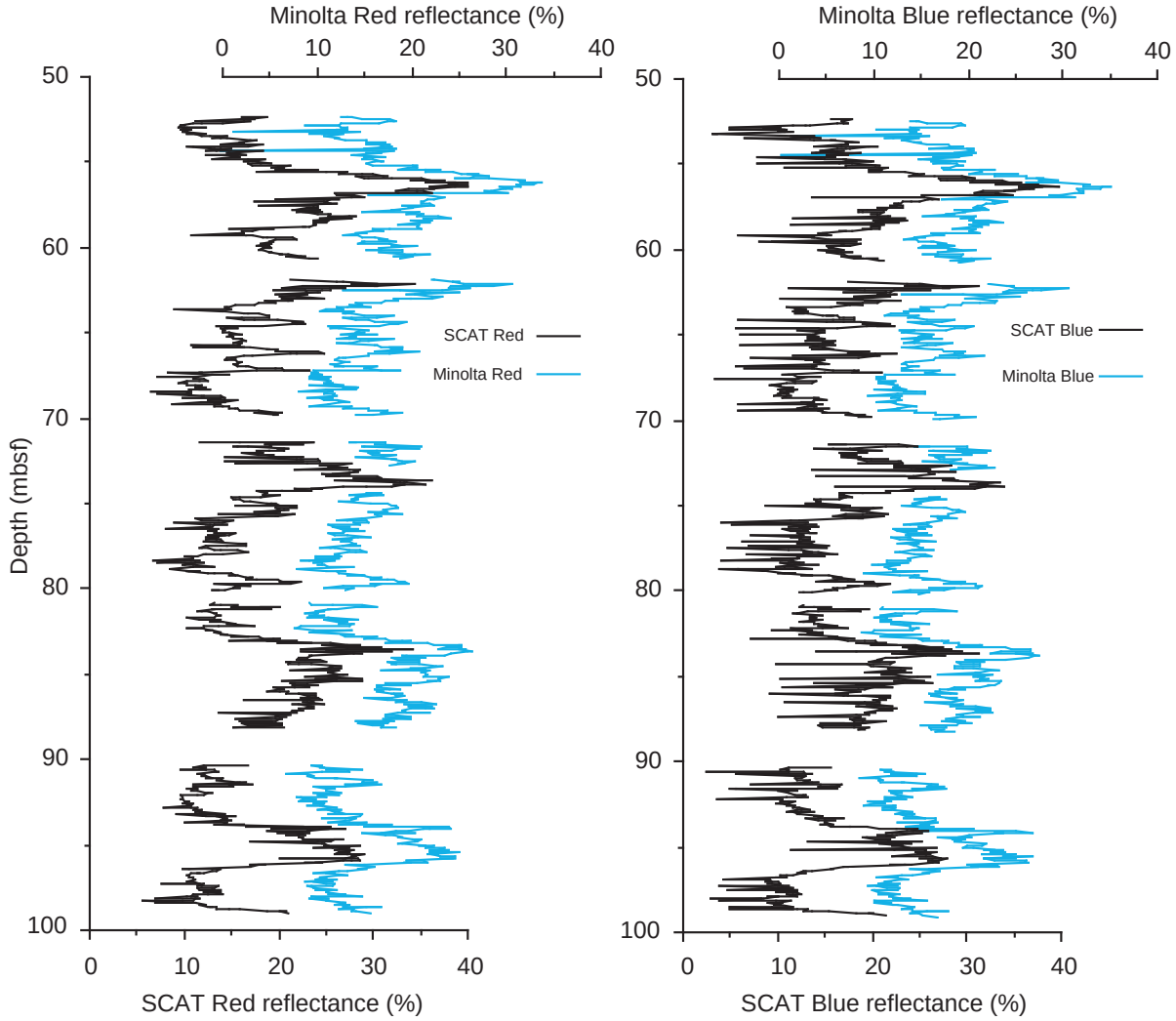

Figure F31. Thermal conductivity measurements of sediment cores at Site 1089. **A.** Frequency distribution of measured values. **B.** Correlation of measured values with interpolated GRA bulk density values. **C.** Thermal conductivity (solid circles) compared to interpolated GRA bulk density (open squares).

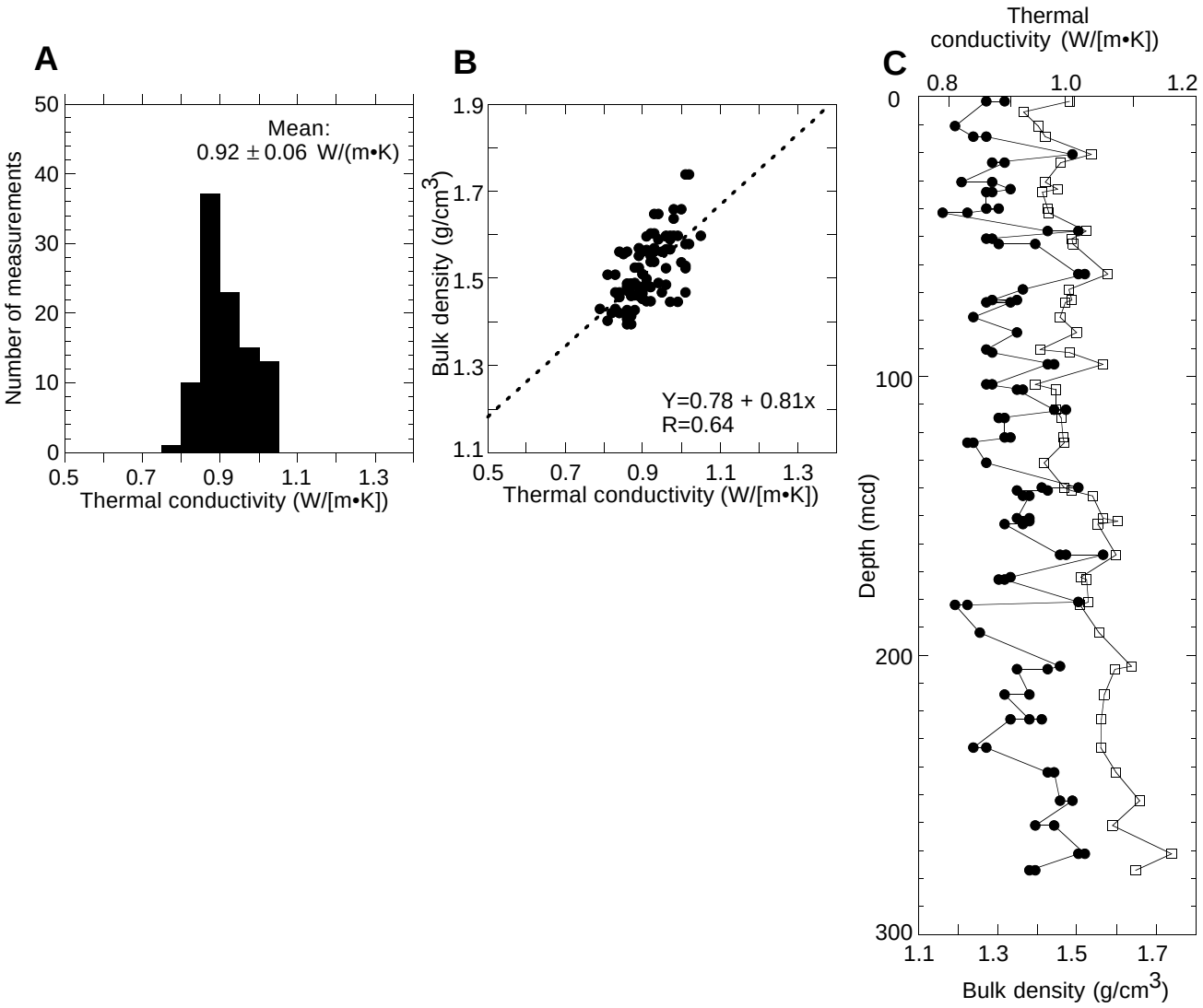

Figure F32. Downhole temperature measurements at Site 1089. The time-temperature record shown in each panel is ~1 hr. A bottom-water measurement was taken with the barrel of Core 177-1089A-1H before the core was shot. Sediment measurements were taken after the corresponding cores were shot.

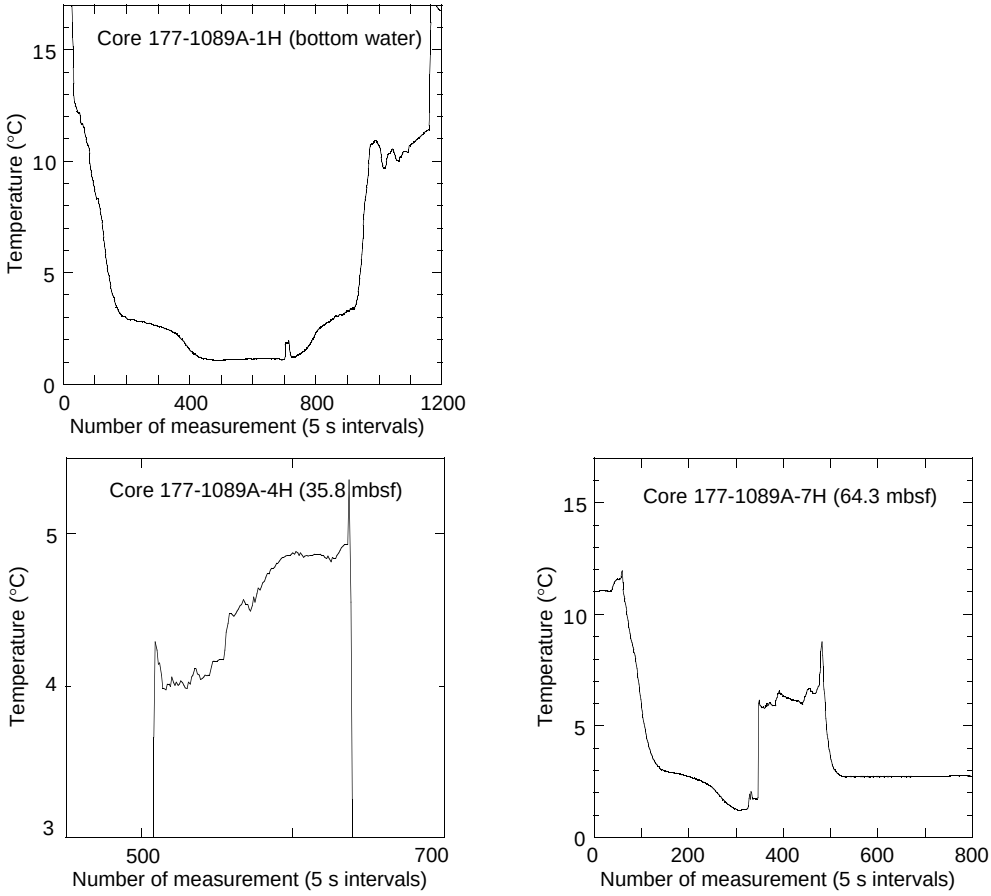

Table T1. X-ray diffraction data for Site 1089.

Core, section, interval (cm)	Depth (mbsf)	Depth (mcd)	Bulk carbonate fraction (wt%; coulometry)	Opal noncarbonate fraction (wt%; XRD intensity)	Bulk opal (wt%)	Siliciclastics (wt%)	Pyrite (%; XRD peak area)	Quartz/ feldspar (XRD peak area ratio)	Clay/(quartz + feldspar) (XRD peak area ratio)	10 Å/7 Å (XRD peak intensity ratio)
177-1089A-										
1H-1, 77-79	0.78	0.54	45.2	18	9.864	44.936	0	3.9	0.13	1.89
2H-7, 24-26	16.55	16.13					1.08	2.94	0.12	2.11
3H-2, 73-74	19.04	21.88	52.9	18	8.478	38.622	1.06	4.79	0.11	1.24
4H-3, 72-73	29.78	34.16					1.48	3.87	0.1	2.18
5H-1, 68-69	36.49	37.45	47.3	23	12.121	40.579	0.85	4.19	0.1	2.1
5H-3, 70-72	39.51	40.47					1.94	3.76	0.13	1.84
6H-3, 72-73	49.03	50.91					3.04	3.07	0.15	2.19
7H-5, 61-63	61.18	65.32	46.8	13	6.916	46.284	5.3	3.76	0.09	3.3
8H-6, 119-120	73.00	77.77					0.94	3.22	0.16	2.5
9H-1, 61-62	74.42	80.6					1.38	4.19	0.16	1.85
10H-3, 118-119	87.49	92.02					0.9	3.57	0.11	2.1
11H-2, 71-73	94.78	100.57					1.4	3.2	0.15	1.79
12H-1, 74-75	103.05	108.84					1.99	3.6	0.11	1.79
12H-4, 75-76	107.56	113.35		22			3.81	4.04	0.13	1.89
14H-4, 22-23	126.03	131.82		22			1.48	3.42	0.12	2
15H-3, 70-71	134.51	140.3	55.3	23	10.281	34.419	2.08	4.77	0.17	2
16H-5, 22-23	146.53	153.95	46.6	20	10.68	42.72	0.64	4.84	0.16	3.19
18H-2, 69-70	161.50	169.46					2.28	3.42	0.13	2.07
19H-1, 121-122	170.02	178.03	30.2	16	11.168	58.632	1.04	4.12	0.15	1.84
20H-1, 73-74	179.04	186.86					1.43	4	0.18	2.26
20H-1, 107-108	179.38	187.2					2.08	3.55	0.15	2.46
21H-2, 72-73	190.03	203.65	39.8	18	10.836	49.364	0.93	3.96	0.17	2.07
23H-1, 76-77	207.57	219.87					0.37	3.22	0.13	1.75
177-1089B-										
2H-3, 72-73	8.53	14.23	44	22	12.32	43.68	0.04	4.19	0.14	1.5
3H-6, 71-72	22.52	27.96	42.5	16	9.2	48.3	1.6	4.8	0.13	1.88
4H-5, 71-72	30.52	36.12	54	8	3.68	42.32	0.88	4.52	0.11	1.8
5H-6, 72-73	41.53	45.99	0.5	18	17.91	81.59	0.25	4.65	0.12	1.92
6H-2, 76-77	45.07	51.27	42.2	14	8.092	49.708	2.97	3.9	0.11	1.76
7H-2, 72-73	54.53	61.95	16	14	11.76	72.24	0.61	3.3	0.12	2.28
8H-2, 73-74	64.04	72.09	36.2	16	10.208	53.592	0.82	4.26	0.12	1.72
9H-4, 72-73	76.53	85.9	11.3	18	15.966	72.734	1.94	4.39	0.14	2.23
10H-1, 72-73	81.53	92.79	5.7	18	16.974	77.326	0.95	4.63	0.14	2.13
11H-2, 74-75	92.55	103.81	1.5	23	22.655	75.845	2.34	3.88	0.11	1.48
11H-4, 70-71	95.51	106.77	54.5	23	10.465	35.035	1.29	3.95	0.09	2.35
12H-1, 72-73	100.53	111.79	19.2	22	17.776	63.024	0.79	3.24	0.11	2.53
13H-1, 60-61	109.91	121.17	20.3	17	13.549	66.151	1.86	3.86	0.13	2.71
14H-3, 77-78	122.58	133.84	50.4	14	6.944	42.656	4.33	3.26	0.12	2.5
15H-4, 72-73	133.53	144.79	28.8	13	9.256	61.944	0.79	4.44	0.12	2.57
16H-3, 119-120	142.00	153.26	8.3	18	16.506	75.194	1.97	4.59	0.13	2.32
16H-4, 119-120	143.50	154.76	44.2	11	6.138	49.662	0.86	3.22	0.08	1.6
17H-1, 72-73	148.03	159.29	27.3	19	13.813	58.887	1.54	4.38	0.06	2.25
18H-1, 72-73	157.53	168.79	14.9	13	11.063	74.037	2.74	4.68	0.12	1.9
19H-3, 72-73	170.03	181.87	6.3	14	13.118	80.582	3.33	3.89	0.11	2.33
20H-1, 72-73	176.53	189.21	38.9	14	8.554	52.546	0.91	3.85	0.12	1.7
21H-1, 72-73	186.03	201.13	10.2	16	14.368	75.432	1.3	3.81	0.12	2.5
22H-2, 72-73	197.03	212.13	54.2	7	3.206	42.594	0.81	4.33	0.12	1.11
23H-2, 74-75	206.55	221.65	46.1	2	1.078	52.822	0.51	3.33	0.08	1.77
23H-5, 68-69	4.34	0.11	3.25							

Notes: XRD = X-ray diffraction. This table is also available in ASCII format in the **TABLES** directory.

Table T2. Summary of core disturbance at Site 1089.

Core, section, interval top (cm)	Interval top (mbsf)	Core, section, interval bottom (cm)	Interval bottom (mbsf)	Thickness of disturbed interval (m)
177-1089A-		177-1089A-		
2H-1, 0	7.30	2H-2, 120	10.00	2.70
6H-1, 0	45.30	6H-2, 140	48.20	2.90
7H-1, 0	54.80	7H-1, 75	55.55	0.75
7H-1, 123	56.03	7H-2, 110	57.40	1.37
7H-3, 70	58.50	7H-3, 123	59.03	0.53
9H-1, 100	74.80	9H-1, 133	75.13	0.33
10H-1, 0	83.30	10H-4, 55	88.35	5.05
12H-2, 135	105.15	12H-3, 115	106.45	1.30
14H-1, 0	121.30	14H-1, 95	122.25	0.95
15H-1, 0	130.80	15H-1, 65	131.45	0.65
16H-1, 0	140.30	16H-1, 57	140.87	0.57
18H-3, 120	163.50	18H-4, 90	164.70	1.20
19H-1, 0	168.80	19H-1, 85	169.65	0.85
20H-1, 20	178.50	20H-2, 123	181.03	2.53
177-1089B-		177-1089B-		
1H-1, 0	0.00	1H-1, 35	0.35	0.35
2H-1, 0	4.80	2H-1, 37	5.17	0.37
3H-1, 0	14.30	3H-1, 97	15.27	0.97
4H-1, 0	23.80	4H-1, 50	24.30	0.50
5H-1, 0	33.30	5H-1, 145	34.75	1.45
6H-1, 0	42.80	6H-1, 70	43.50	0.70
13H-1, 0	109.30	13H-1, 33	109.63	0.33
177-1089C-		177-1089C-		
2H-1, 0	4.40	2H-1, 45	4.85	0.45
3H-1, 0	13.90	3H-1, 55	14.45	0.55
4H-1, 0	23.40	4H-1, 47	23.87	0.47
5H-1, 0	32.90	5H-1, 40	33.30	0.40
13H-2, 145	111.85	13H-3, 57	112.47	0.62
15H-3, 0	130.90	15H-3, 45	131.35	0.45
18H-1, 0	156.40	18H-1, 85	157.25	0.85
177-1089D-		177-1089D-		
2H-1, 0	6.70	2H-1, 65	7.35	0.65
3H-1, 0	13.50	3H-2, 47	14.87	1.37
4H-1, 0	23.00	4H-3, 0	26.00	3.00
5H-1, 0	32.50	5H-2, 25	34.25	1.75
6H-1, 0	42.00	6H-1, 60	42.60	0.60
7H-1, 0	51.50	7H-5, 10	57.60	6.10
8H-1, 0	61.00	8H-3, 35	64.35	3.35
9H-1, 0	70.50	9H-5, 30	76.45	5.95
10H-1, 0	80.00	10H-2, 90	82.40	2.40
Total:				55.31

Table T3. Summary of undisturbed recovery at Site 1089.

Hole	Length cored (m)	Length recovered (m)	Recovery (%)	Disturbed thickness (m)	Undisturbed recovery (%)
1089A	216.3	149.64	69.18	21.68	86
1089B	264.9	246.62	93.10	4.67	98
1089C	192.4	160.29	83.31	2.94	98
1089D	118	119.36	101.15	26.02	78
Total:	791.6	675.91		55.31	

Table T4. Composite depths for Site 1089. (See table note. Continued on next page.)

Core, section	Depth (mbsf)	Offset (m)	Depth (mcd)
177-1089A-			
1H-1	0	-0.24	-0.24
2H-1	7.3	-0.42	6.88
3H-1	16.8	2.84	19.64
4H-1	26.8	4.38	31.18
5H-1	35.8	0.96	36.76
6H-1	45.3	1.88	47.18
7H-1	54.8	4.14	58.94
8H-1	64.3	4.77	69.07
9H-1	73.8	6.18	79.98
10H-1	83.3	4.53	87.83
11H-1	92.8	5.79	98.59
12H-1	102.3	5.79	108.09
14H-1	121.3	5.79	127.09
15H-1	130.8	5.79	136.59
16H-1	140.3	7.42	147.72
18H-1	159.3	7.96	167.26
19H-1	168.8	8.01	176.81
20H-1	178.3	7.82	186.12
21H-1	187.8	13.62	201.42
23H-1	206.8	12.3	219.1
177-1089B-			
1H-1	0	2.04	2.04
2H-1	4.8	5.7	10.5
3H-1	14.3	5.44	19.74
4H-1	23.8	5.6	29.4
5H-1	33.3	4.46	37.76
6H-1	42.8	6.2	49.0
7H-1	52.3	7.42	59.72
8H-1	61.8	8.05	69.85
9H-1	71.3	9.37	80.67
10H-1	80	11.26	92.06
11H-1	90.3	11.26	101.56
12H-1	99.8	11.26	111.06
13H-1	109.3	11.26	120.56
14H-1	118.8	11.26	130.06
15H-1	128.3	11.26	139.56
16H-1	137.8	11.26	149.06
17H-1	147.3	11.26	158.56
18H-1	156.8	11.26	168.06
19H-1	166.3	11.84	178.14
20H-1	175.8	12.68	188.48
21H-1	185.3	15.1	200.4
22H-1	194.8	15.1	209.9
23H-1	204.3	15.1	219.4
24H-1	213.8	15.1	228.9
25H-1	223.3	15.1	238.4
26H-1	232.8	15.1	247.9
27H-1	242.3	15.1	257.4
28H-1	251.8	15.1	266.9
29H-1	257.9	15.1	273.0
177-1079C-			
1H-1	0	-0.3	-0.3
2H-1	4.4	3.24	7.64
3H-1	13.9	4.42	18.32
4H-1	23.4	3.58	26.98
5H-1	32.9	3.42	36.32
6H-1	42.4	2.06	44.46
7H-1	51.9	3.52	55.42
8H-1	61.4	3.87	65.27
9H-1	70.9	4.38	75.28
10H-1	80.4	6.49	86.89
11H-1	89.9	8.89	98.79
12H-1	99.4	8.89	108.29
13H-1	108.9	8.89	117.79
14H-1	118.4	8.89	127.29
15H-1	127.9	8.89	136.79
16H-1	137.4	10.65	148.05
17H-1	146.9	13.11	160.01
18H-1	156.4	13.11	169.51
19H-1	165.9	13.99	179.89
20H-1	175.4	10.59	185.99
21H-1	184.9	11.21	196.11
177-1089D-			
1H-1	0	-0.64	-0.64
2H-1	6.7	-2.88	3.82

Table T4 (continued).

Core, section	Depth (mbsf)	Offset (m)	Depth (mcd)
3H-1	13.5	-0.18	13.32
4H-1	23	-0.9	22.1
5H-1	32.5	-3.1	29.4
6H-1	42	-1.62	40.38
7H-1	51.5	-1.06	50.44
8H-1	61	-0.03	60.97
9H-1	70.5	3.73	74.23
10H-1	80.5	7.52	88.02
11H-1	89.5	7.52	97.02
12H-1	99	7.52	106.52
13H-1	108.5	7.52	116.02

Note: This table is also available in ASCII format in the **TABLES** directory.

Table T5. Site 1089 splice tie points.

Core, section, interval (cm)	Depth (mbsf)	Depth (mcd)		Core, section, interval (cm)	Depth (mbsf)	Depth (mcd)
177-				177-		
1089A-1H-4, 140	5.90	5.66	tie to	1089D-2H-2, 34	8.54	5.66
1089D-2H-5, 136	14.06	11.18	tie to	1089A-2H-3, 130	11.60	11.18
1089A-2H-5, 112	14.42	14.00	tie to	1089B-2H-3, 50	8.30	14.00
1089B-2H-5, 140	12.20	17.90	tie to	1089D-3H-4, 72	18.08	17.90
1089D-3H-6, 54	20.90	20.72	tie to	1089B-3H-1, 98	15.28	20.72
1089B-3H-6, 76	22.56	28.00	tie to	1089C-4H-1, 102	24.42	28.00
1089C-4H-5, 52	29.92	33.50	tie to	1089B-4H-3, 110	27.90	33.50
1089B-4H-6, 52	31.82	37.42	tie to	1089C-5H-1, 110	34.00	37.42
1089C-5H-3, 8	35.98	39.40	tie to	1089B-5H-2, 14	34.94	39.40
1089B-5H-6, 30	41.10	45.56	tie to	1089C-6H-1, 110	43.50	45.56
1089C-6H-5, 18	48.58	50.64	tie to	1089B-6H-2, 14	44.44	50.64
1089B-6H-5, 122	50.02	56.22	tie to	1089C-7H-1, 80	52.70	56.22
1089C-7H-6, 78	60.18	63.70	tie to	1089B-7H-3, 98	56.28	63.70
1089B-7H-5, 54	58.84	66.26	tie to	1089C-8H-1, 98.5	62.39	66.26
1089C-8H-5, 114	68.54	72.41	tie to	1089B-8H-2, 106	64.36	72.41
1089B-8H-5, 138	69.18	77.23	tie to	1089C-9H-2, 44.5	72.85	77.23
1089C-9H-6, 38	78.78	83.16	tie to	1089B-9H-2, 98.5	73.79	83.16
1089B-9H-6, 76	79.56	88.93	tie to	1089C-10H-2, 54	82.44	88.93
1089C-10H-5, 146	87.86	94.35				

Note: This table is also available in ASCII format in the **TABLES** directory.

Table T6. Distribution of main calcareous nannofossil species in Holes 1089A and 1089B. (**See table note.** Continued on next two pages.)

Core, section, interval (cm)	Depth (mbsf)	Depth (mcd)	Abundance	Preservation	*Discoaster brouweri*	*Gephyrocapsa caribbeanica*	*Calcidiscus macintyrei*	*Gephyrocapsa* small	*Gephyrocapsa* medium (4-5.5 µm)	*Gephyrocapsa* large (>5.5 µm)	*Gephyrocapsa* sp. 3	*Reticulofenestra asanoi*	*Pseudoemiliania lacunosa*	*Emiliania huxleyi*	Comments
177-1089A-															
1H-CC, 17-22	7.27	7.03	A	G				D						C	
2H-CC, 16-21	16.90	16.48	A	M				A	C					A	
3H-CC, 13-18	21.18	24.02	A	M				D						C	
4H-CC, 22-27	30.66	35.04	C	M										F	
5H-2, 70-70	38.00	38.96	A	M										F	
5H-2, 100-100	38.30	39.26	A	M										F	
5H-2, 130-130	38.60	39.56	F	M										F	
5H-2, 149-149	38.79	39.75	C	M											
5H-CC, 14-19	43.36	44.32	C												Disturbed
6H-CC, 18-23	52.25	54.13	A	M					C						
7H-1, 130-130	56.10	60.24	A	M		A		A	R						
7H-1, 120-120	56.00	60.14	C	P		A		A	R						
7H-2, 30-30	56.60	60.74	C	M				D							
7H-2, 120-120	57.50	61.64	C	M				D							
7H-3, 30-30	58.10	62.24	A	G				D							
7H-CC, 51-56	63.40	67.54	A	G		A			C				?		
8H-1, 30-30	64.60	69.37	C	M									R		
8H-1, 120-120	65.50	70.27	A	M									R		
8H-2, 30-30	66.10	70.87	A	G		D			C				R		
8H-2, 120-120	67.00	71.77	A	M		D			F				F		
8H-3, 30-30	67.60	72.37	A	M		D		D	F				F		
8H-3, 120-120	68.50	73.27	C	P					C				C		
8H-4, 30-30	69.10	73.87	A	P									C		
8H-4, 120-120	70.00	74.77	C	M		C			F		F		C		
8H-5, 30-30	70.60	75.37	A	M									A		
8H-5, 120-120	71.50	76.27	F	P				C	R						
8H-6, 30-30	72.10	76.87	C	M									F		
8H-6, 120-120	73.00	77.77	C	M		D									
8H-7, 10-10	73.40	78.17	A	P		D							R		
8H-7, 60-60	73.90	78.67	A	M									C		
8H-CC, 9-14	74.03	78.80	A	M				A					C		
9H-CC, 10-15	75.24	81.42	A	G				D	F		F		C		
10H-CC, 0-15	92.97	97.50	A	M				A	C		A	R	C		
11H-CC, 53-58	97.90	103.69	A	M				A			A	R	C		
12H-3, 30-30	105.60	111.39	C	M								R	C		
12H-4, 120-120	108.00	113.79	A	M									F		
12H-6, 30-30	110.10	115.89	C	M								F	C		
12H-7, 30-30	111.50	117.29	F	M								F			
12H-CC, 0-5	111.59	117.38	A	M				D			C	F	F		
13H-CC, 0-5	111.80	111.80	A	M				D			C	F	C		
14H-CC, 11-16	130.07	135.86	A	G				D			F	R	C		
15H-CC, 21-26	136.70	142.49	F	M				A			C	F	C		
16H-CC, 9-14	149.24	156.66	A	M					F			F	C		
18H-1, 30-30	159.60	167.56	C	M								F	C		
18H-2, 30-30	161.10	169.06	C	M								F	F		
18H-2, 130-130	162.10	170.06	C	M								F	F		
18H-3, 130-130	163.60	171.56	C	M								F	C		
18H-4, 30-30	164.10	172.06	B												
18H-4, 130-130	165.10	173.06	B												
18H-5, 30-30	165.60	173.56	C	M									F		
18H-5, 70-70	166.00	173.96	C	M									C		
18H-CC, 21-26	166.22	174.18	A	M											Reworking
19H-1, 30-30	169.10	177.11	F	M									F		
19H-1, 120-120	170.00	178.01	C	M						F			C		
19H-2, 30-30	170.60	178.61	B												
19H-3, 30-30	172.10	180.11	C	M						C			A		
19H-4, 30-30	173.60	181.61	C	M						F			F		
19H-5, 30-30	175.10	183.11	B												
19H-5, 120-120	176.00	184.01	B												
19H-CC, 0-10	177.69	185.70	A	M						C			C		

Table T6 (continued).

Core, section, interval (cm)	Depth (mbsf)	Depth (mcd)	Abundance	Preservation	*Discoaster brouweri*	*Gephyrocapsa caribbeanica*	*Calcidiscus macintyrei*	*Gephyrocapsa* small	*Gephyrocapsa* medium (4-5.5 µm)	*Gephyrocapsa* large (>5.5 µm)	*Gephyrocapsa* sp. 3	*Reticulofenestra asanoi*	*Pseudoemiliania lacunosa*	*Emiliania huxleyi*	Comments
20H-CC, 13-23	187.53	195.35	A	M						C			C		
21H-CC, 21-26	195.09	208.71	F	M							C		A		
23H-1, 30-30	207.10	219.40	F	M					F				C		
23H-1, 120-120	208.00	220.30	B												
23H-2, 30-30	208.60	220.90	A	M			F		F				C		
23H-2, 120-120	209.50	221.80	C	M			F		F				C		
23H-3, 30-30	210.10	222.40	A	M			F		F				C		
23H-3, 120-120	211.00	223.30	A	M			R						C		
23H-4, 30-30	211.60	223.90	A	M			F		F				F		
23H-4, 120-120	212.50	224.80	A	M			F						A		
23H-5, 130-130	214.10	226.40	A	M			R						R		
23H-6, 20-20	214.50	226.80	A	M			F						F		
23H-6, 60-60	214.90	227.20	B												
23H-CC, 31-41	215.29	227.59	A	M			R						C		Empty (Pliocene reworking?)
177-1089B-															
2H-CC, 10-15	13.67	19.37	A	C					C		C			C	
3H-CC, 8-16	23.12	28.56	A	M				A	C		C			C	
4H-CC, 12-17	32.42	38.02	A	M		A		A	A		A			R	
5H-2, 30-30	35.10	39.56	A	M		F		C						F	
5H-2, 130-130	36.10	40.56	B												
5H-3, 30-30	36.60	41.06	F	M		A								?	
5H-3, 130-130	37.60	42.06	A	P		F								?	
5H-4, 30-30	38.10	42.56	C	M										?	
5H-4, 120-120	39.00	43.46	F	M										?	
5H-CC, 16-21	41.90	46.36	B												
6H-1, 30-30	43.10	49.30	A	M		A								?	
6H-1, 120-120	44.00	50.20	A	M				C							
6H-CC, 11-16	51.18	57.38	A	M		C		A	R						
7H-6, 80-80	60.60	68.02	A	M									R		
7H-CC, 8-14	60.73	68.15	A	M		D									
8H-1, 30-30	62.10	70.15	A	M									F		
8H-1, 120-120	63.00	71.05	A	M									R		
8H-2, 30-30	63.60	71.65	A	M									F		
8H-2, 120-120	64.50	72.55	A	M									F		
8H-CC, 20-25	70.02	78.07	A	M		A		D					F		
9H-CC, 15-20	80.24	89.61	A	P				D					C		
10H-CC, 15-20	88.25	99.51	A	M							C		C		
11H-CC, 9-14	99.09	110.35	A	M							A		C		
12H-6, 100-100	108.30	119.56	C	M											
12H-CC, 8-13	108.43	119.69	A	M				D			C		C		
13H-1, 30-30	109.60	120.86	F	M									F		
13H-1, 130-130	110.60	121.86	C	M								R	F		
13H-2, 30-30	111.10	122.36	F	P								R	R		
13H-2, 130-130	112.10	123.36	C	M								R	C		
13H-3, 30-30	112.60	123.86	C	M									F		
13H-3, 130-130	113.60	124.86	C	M								R	F		
13H-4, 30-30	114.10	125.36	C	M								R	C		
13H-4, 130-130	115.10	126.36	A	M					F			F	C		
13H-6, 108-108	117.88	129.14	A	M					F			F	C		
13H-CC, 0-8	117.90	129.16	A	M							C	C	C		
14H-CC, 14-19	127.14	138.40	A	M							C	C	C		
15H-1, 130-130	129.60	140.86	A	M					C			A	C		
15H-6, 30-30	136.10	147.36	A	M					C			C	A		
16H-1, 30-30	138.10	149.36	A	M					C				F		
16H-5, 130-130	145.10	156.36	A	M							C	C	C		
16H-6, 30-30	145.60	156.86	A	M								R	C		
16H-CC, 12-17	146.40	157.66	A	M								C	A		
17H-1, 30-30	147.60	158.86	A	M					R			R	C		
17H-1, 120-120	148.50	159.76	C	M					F			C	A		
17H-2, 30-30	149.10	160.36	C	M					F			R	A		
17H-2, 120-120	150.00	161.26	C	M								C	C		
17H-4, 30-30	152.10	163.36	A	G								R	C		

Table T6 (continued).

Core, section, interval (cm)	Depth (mbsf)	Depth (mcd)	Abundance	Preservation	*Discoaster brouweri*	*Gephyrocapsa caribbeanica*	*Calcidiscus macintyrei*	*Gephyrocapsa* small	*Gephyrocapsa* medium (4-5.5 µm)	*Gephyrocapsa* large (>5.5 µm)	*Gephyrocapsa* sp. 3	*Reticulofenestra asanoi*	*Pseudoemiliania lacunosa*	*Emiliania huxleyi*	Comments
17H-4, 120-120	153.00	164.26	A	G								C	C		
17H-5, 30-30	153.60	164.86	A	M									C		Reworking
17H-5, 120-120	154.50	165.76	C	P									C		
17H-CC, 18-23	155.28	166.54	A	M									A		
18H-1, 30-30	157.10	168.36	C	M									C		
18H-1, 120-120	158.00	169.26	F	P									F		
18H-2, 120-120	159.50	170.76	B												
18H-4, 120-120	162.50	173.76	B												
18H-CC, 13-18	165.39	176.65	A	M									C		
19H-5, 120-120	173.50	185.34	A	G		A			C	A			C		
20H-1, 120-120	177.00	189.68	A	G					A	A			C		
20H-4, 120-120	181.50	194.18	A	G		A			A	C			A		
20H-5, 20-20	182.00	194.68	A	G					A	C			C		
20H-6, 30-30	182.88	195.56	C	G		C			C	C			C		
20H-CC, 0-10	185.15	197.83	R	P									R		Almost barren
21H-5, 30-30	191.60	206.70	B												
21H-CC, 11-16	194.21	209.31	R	P		R			R				R		Almost barren
22H-2, 130-130	197.60	212.70	A	G		A			A				C		
22H-5, 130-130	202.10	217.20	A	G					C				C		
22H-CC, 0-5	204.30	219.40	B												
23H-1, 30-30	204.60	219.70	R	P					F				R		
23H-1, 130-130	205.60	220.70	B												
23H-2, 30-30	206.10	221.20	A	M			R						A		
23H-3, 30-30	207.60	222.70	C	M			R						C		
23H-3, 130-130	208.60	223.70	F	P									C		
23H-4, 30-30	209.10	224.20	A	M			F						C		
23H-4, 130-130	210.10	225.20	A	M			R						C		
24H-5, 30-30	220.10	235.20	B												
24H-6, 30-30	221.60	236.70	F	P			R								
24H-CC, 23-28	223.43	238.53	A	P	R								VA		Reworking (Pliocene?)
25H-3, 130-130	227.60	242.70	F	P	1								C		
25H-5, 130-130	230.60	245.70	C	P	F		F						C		
26H-4, 130-130	238.60	253.70	B												
26H-6, 130-130	241.60	256.70	R	P	R		R								
26H-CC, 11-16	242.01	257.11	B												
27H-CC, 45-53	250.79	265.89	B												
28H-CC, 25-30	257.84	272.94	B												
29H-CC, 62-67	264.91	280.01	B												

Notes: Abundance abbreviations: D = dominant, A = abundant, C = common, F = few, R = rare, B = barren. Preservation abbreviations: G = good, M = moderate, P = poor. For more specific definitions, refer to the **"Explanatory Notes"** chapter. Taxon distribution is mainly described in those stratigraphic intervals where events can be identified. This table is also available in ASCII format in the **TABLES** directory.

Table T7. Distribution of major planktic foraminifer species at Site 1089. (**See table note.** Continued on next page.)

Core, section, interval (cm)	Depth (mbsf)	Depth (mcd)	Abundance	Preservation	*Globigerina bulloides*	*Globigerina quinqueloba*	*Globigerina woodi*	*Globigerinella calida*	*Globigerinita glutinata*	*Globigerinita uvula*	*Globorotalia inflata*	*Globorotalia puncticuloides*	*Globorotalia scitula*	*Globorotalia truncatulinoides*	*Neogloboquadrina humerosa*	*Neogloboquadrina pachyderma* (sinistral)	*Neogloboquadrina pachyderma* (dextral)	*Orbulina universa*
177-1089A-																		
1H-CC, 17-22	7.27	7.03	A	M	D	A			F	R	A		R	R	R	A		
2H-CC, 16-21	16.90	16.48	A	M	D	A			F		A		R	R	R	F	R	
3H-CC, 13-18	21.18	24.02	A	M	D	A			A		F			R		A	R	R
4H-CC, 22-27	30.66	35.04	A	M	D	A			A		A			F				
5H-CC, 14-19	43.36	44.32	A	M	D	F			F		A			R	F			
6H-CC, 18-23	52.25	54.13	A	M	D	A	R		A		A	R		F	R	F		
7H-CC, 51-56	63.40	67.54	A	P	D				A		F					A	F	
8H-CC, 9-14	74.03	78.80	A	P	D	A			A		F	F		R		F		R
9H-CC, 10-15	75.24	81.42	A	M	D	F					A	A				F		R
11H-CC, 0-5	92.97	103.16	A	P	F	A			F	F	F			R		A		R
10H-CC, 53-58	97.90		C	P	F				F				R	A		D		
12H-CC, 0-5	111.59	117.38	F	P	R						R	R	R			R		
13H-CC, 0-5	111.80	111.80	C	P	R	R					F	F				F		
14H-CC, 11-16	130.07	135.86	A	M	A	R						R				D		R
15H-CC, 21-26	136.70	142.49	C	P	F	R			R							D		
16H-CC, 9-14	149.24	156.66	F	P	A	F			R		A	R	R			A		R
17H-CC, 0-8	149.80	149.80	C	P	A	F	R				F	A				D		
18H-CC, 21-26	166.22	174.18	F	P	F	F					F	A						
19H-CC, 0-10	177.69	185.70	C	P	A	A			F		A	D				A		
20H-CC, 13-23	187.53	195.35	C	P	F						A	A				F		
21H-CC, 21-26	195.09	208.71	T	P	P	P			P			P				P		
177-1089B-																		
2H-CC, 10-15	13.67	19.37	A	M	F	F	F									F		F
3H-CC, 8-16	23.12	28.56	A	M	A	F					A		R			F		
4H-CC, 12-17	32.42	38.02	A	M	D	F					A			R	R	A		
5H-CC, 16-21	41.90	46.36	A	M	D	F	F				A	F		R		A		
6H-CC, 11-16	51.18	57.38	A	M	D	A					A	F				A		
7H-CC, 8-14	60.73	68.15	A	M	A	A			F	F		F	R			D		F
8H-CC, 20-25	70.02	78.07	C	M	A	F	R		R		A			A		A		
9H-CC, 15-20	80.24	89.61	R	P	P										P	P	P	
10H-CC, 15-20	88.25	99.51	F	P	P						P					P	P	
11H-CC, 9-14	99.09	110.35	C	P	R						F	A				D	P	
12H-CC, 8-13	108.43	119.69	C	P	F	R					A	A				D		
13H-CC, 0-8	117.90	129.16	F	P	F						R	F				D	R	
14H-CC, 14-19	127.14	138.40	F	P	F	F			R		A	R			R	D	R	
15H-CC, 0-5	136.68	147.94	F	P	A						A	F				F		
16H-CC, 12-17	146.40	157.66	F	P	F						F	A				D		
17H-CC, 18-23	155.28	166.54	F	P	F				R		F	A	R			F	R	
18H-CC, 13-18	165.39	176.65	C	P		R			R		R	A				D		
19H-CC, 16-21	175.33	187.17	T	P														
20H-CC, 0-10	185.15	197.83	T	P							P							
21H-CC, 11-16	194.21	209.31	T	P														
22H-CC, 0-5	204.30	219.40	B															
23H-CC, 0-8	213.65	228.75	B															
24H-CC, 23-28	223.43	238.53	B															
25H-CC, 14-19	232.78	247.88	T	P														
26H-CC, 11-16	242.01	257.11	B															
27H-CC, 45-48	250.79	265.89	B															
28H-CC, 23-30	257.84	272.92	B															
29H-CC, 62-67	264.91	280.01	B															
177-1089C-																		
1H-CC, 8-13	2.38	2.08	A	M	P	A			F		A			F		R	F	R
2H-CC, 0-8	9.37	12.61	C	M	F	R	R				F	R			R	F	F	
3H-CC, 9-14	17.42	21.84	A	M	D		R		R		F	R		R		A	F	R
4H-CC, 10-15	31.78	35.36	A	M	D		F		F		A	R	R	F		F	R	R
5H-CC, 10-15	40.91	44.33	R	P	P						P						P	
6H-CC, 9-14	51.46	53.52	A	M	D	A			F				R	R	F	A	R	
7H-CC, 0-10	60.81	64.33	A	M	A						D	F						

Table T7 (continued).

Core, section, interval (cm)	Depth (mbsf)	Depth (mcd)	Abundance	Preservation	*Globigerina bulloides*	*Globigerina quinqueloba*	*Globigerina woodi*	*Globigerinella calida*	*Globigerinita glutinata*	*Globigerinita uvula*	*Globorotalia inflata*	*Globorotalia puncticuloides*	*Globorotalia scitula*	*Globorotalia truncatulinoides*	*Neogloboquadrina humerosa*	*Neogloboquadrina pachyderma* (sinistral)	*Neogloboquadrina pachyderma* (dextral)	*Orbulina universa*
8H-CC, 0-10	70.34	74.21	A	M	A	F			R		F			R		D	R	R
9H-CC, 7-12	80.10	84.48	A	M	A	F			F		F	A				D		
10H-CC, 18-23	88.08	94.57	R	P	P						P	P						
11H-CC, 13-18	99.16	108.05	F	P		F	R		R		F					A		
12H-CC, 10-15	107.43	116.32	R	P	R							R				F		
13H-CC, 0-10	117.42	126.31	R	P	R						R	R				F		
14H-CC, 9-14	126.55	135.44	R	P	P							P				P		
15H-CC, 21-26	135.76	144.65	F	P					R		F	A				A		R
16H-CC, 10-15	146.80	157.45	C	P	D			R			F	A				A		
17H-CC, 11-16	156.33	169.44	C	P	F						F	F						
18H-CC, 0-3	165.57	178.68	C	P							R	R				F		
19H-CC, 22-27	169.56	183.55	T	P												P		
20H-CC, 46-51	184.01	194.60	R	P	F				R		F					F	R	
21H-CC, 19-24	190.84	202.05	T	P	P				P		P	P				P		
177-1089D-																		
1H-CC, 5-13	6.62	5.98	F	M	A				R		F					A	F	
2H-CC, 8-13	15.29	12.41	A	M	D	R			F		A	F		R		A	F	
3H-CC, 7-12	22.51	22.33	C	P	A	A					A	R				D	A	
4H-CC, 0-10	32.56	31.66	F	P	F						A					F	R	
5H-CC, 0-5	42.07	38.97	C	P	F	F			R		R					D	R	
6H-CC, 24-29	51.42	49.80	A	M	A	A			A	F	F	R				D		
7H-CC, 0-10	61.06	60.00	A	M	A				R			F	R			D		
8H-CC, 5-10	70.72	70.69	C	P	A				F		A					D		
9H-CC, 0-10	79.70	83.43	A	M	D				F		A	F				A		
10H-CC, 0-5	89.72	97.24	C	P	D						A	R	R			A		
11H-CC, 0-10	98.00	105.52	R	P	P						P	P				P		

Notes: Abundance abbreviations: D = dominant, A = abundant, C = common, F = few, R = rare, T = trace, P = present, B = barren. Preservation abbreviations: M = moderate, P = poor. For more specific definitions, refer to the **"Explanatory Notes"** chapter . This table is also available in ASCII format in the **TABLES** directory.

Table T8. Distribution of benthic foraminifers in Holes 1089A and 1089B. (Continued on next page.)

Core, section, interval (cm)	Depth (mbsf)	Depth (mcd)	Abundance	Preservation	*Adercotryma glomeratum*	*Alabaminella weddellensis*	*Anomalinoides glazanensis*	*Bolivina* spp.	*Cassidulina obtusa*	*Cassidulina reniforme*	*Cassidulinoides* spp.	*Chilostomella oolina*	*Cibicidoides* spp.	*Cibicidoides wuellerstorfi*	*Dentalina* sp.	*Eggerella bradyi*	*Ehrenbergina* sp.	*Epistominella exigua*	*Fissurina* spp.	*Francesita* sp.	*Gyroidinoides soldanii*	*Gyroidinoides* spp.	Indeterminates (calc.)	*Islandiella* sp.	*Karreriella bradyi*	*Lagena* spp.	*Laticarinina pauperata*	*Lenticulina* sp.	*Melonis barleeanum*	*Melonis pompilioides*	*Miliolinella* sp.	*Nodosaria* spp.	*Nonionella iridea*	*Nonionella* sp.	*Oolina* spp.	*Ophthalmidium* spp.	*Oridorsalis* sp.	*Oridorsalis umbonatus*	*Parafissurina* sp.
177-1089A-																																							
1H-CC, 17-22	7.27	7.03	C	G		3								6				10	7	2	3			3		2			1		1		2			1		7	
2H-CC, 16-21	16.9	16.48	C	G		1		2						2				31	1		1		2	2		3					1				2			1	
3H-CC, 13-18	21.18	24.02	C	G		2				1				3		1		7	6		2		10			4		1	1	1	2	1	3	1	1	3		2	5
4H-CC, 22-27	30.66	35.04	C	G		2		1					1	7		1		52	10		2	2	2	2		1					15			1		3		8	2
5H-CC, 14-19	43.36	44.32	C	G		9								6		2		72	5		2		8	4		8				1			4			5	6	19	4
6H-CC, 18-23	52.25	54.13	C	M		3		3		1		1		3		2		35	11	7			4	5		4				9			1		1	8		10	5
7H-CC, 51-56	63.4	67.54	C	G		1		3		16								14	6	4	5		10			6				2			4			5	1	1	11
8H-CC, 9-14	74.03	78.80	F	M						3			1	2		1			1		1	2			3	2			3							3		1	
9H-CC, 10-15	75.24	81.42	C	G		3				3	1		5	1		6		56	1	3	4		1			2		1	2	5	1					1		17	3
10H-CC, 0-5	92.97	103.16	C	G		10		14		4				6				55	4	16		5	1			2		2		21	2	1			4	2		4	4
11H-CC, 53-58	97.90	103.69	A	G		11		2		4	1			3	1	5		81	5		2		23	12	1	2		1	8	4			1			2		17	8
12H-CC, 0-5	111.59	117.38	C	G	1	20								6		4		43	6	8		14	20	11	2	4			1	3		4			2	5		33	
13H-CC, 0-5	111.8	111.80	A	G		13		2	2		1			6		6		36	7	1		4	19	7		4			1	6		1				5		19	5
14H-CC, 11-16	130.07	135.86	A	G		5		3		12				3		2		5	9	12	1	5	11	3		5				16			7		1	5		51	1
15H-CC, 21-26	136.7	142.49	F	G		49				2				1	1	5		6	1				2	2						3	6							4	5
16H-CC, 9-14	149.24	156.66	C	G		6		1	17	8	4			9		9		116	6	2	1	13	7	13		1		3	1	6			1		2	3		21	5
17H-CC, 0-8	149.8	149.80	C	G		4			9	3	1			6		11		27	6	4			23	1	1	9		1	6	7	1		1		4	3		17	2
18H-CC, 21-26	166.22	174.18																																					
19H-CC, 0-10	177.69	185.70																																					
20H-CC, 13-23	187.53	195.35																																					
21H-CC, 21-26	195.09	208.71	R	M		1							1					1												1								1	1
23H-CC, 31-41	215.29	227.59	C	M		27								7		2		69	1		1	2	4	6	1	2		2	1	17		1		3	4	3		21	5
177-1089B-																																							
24H-CC, 23-28	223.43	238.53	C	M		C												A	R					R					R										
25H-CC, 14-19	232.78	247.88	C	P		C								C		R				R				R					R	C								C	
26H-CC, 11-16	242.01	257.11	B																																				
27H-CC, 45-53	250.79	265.89	B																																				
28H-CC, 25-30	257.84	272.92	B																																				
29H-CC, 62-67	264.91	280.01	B																																				

Notes: Abundance abbreviations: A = abundant, C = common, F = few, R = rare, B = barren. Preservation abbreviations: G = good, M = moderate, P = poor. For more specific definitions, refer to the **"Explanatory Notes"** chapter. This table is also available in ASCII format in the **TABLES** directory.

Table T8 (continued).

Core, section, interval (cm)	Depth (mbsf)	Depth (mcd)	Abundance	Preservation	*Pleurostomella* sp.	*Polymorphinid* spp.	*Pullenia bulloides*	*Pullenia quinqueloba*	*Pullenia subcarinata*	*Pullenia* sp.	*Pyrgo murrhina*	*Pyrgo* spp.	*Quinqueloculina* sp.	*Rhizammina* sp.	*Siphotextularia* sp.	*Sphaeroidina bulloides*	*Spirophthalmidium* sp.	*Stainforthia loeblichi*	*Stainforthia* sp.	*Stilostomella lepidula*	*Triloculina trihedra*	*Triloculina* sp.	*Uvigerina hispidicostata*	*Uvigerina proboscidea*	*Uvigerina* sp.	Sample sum	Number of species	Abundance (specimens/cm^3)
177-1089A-																												
1H-CC, 17-22	7.27	7.03	C	G				5	1		3		6		2		1						1			66	24	16.5
2H-CC, 16-21	16.9	16.48	C	G		1		12			2		1		1			1					1			68	21	17.0
3H-CC, 13-18	21.18	24.02	C	G				15			4	1	1		2			7					3			90	40	36.0
4H-CC, 22-27	30.66	35.04	C	G				10	4		2		1		6		1		1				1			138	32	34.5
5H-CC, 14-19	43.36	44.32	C	G				45	13						3	1			7				12			236	32	35.4
6H-CC, 18-23	52.25	54.13	C	M				7	1		6		3		6			11	6				1			154	37	30.8
7H-CC, 51-56	63.4	67.54	C	G		1		16	7		5		5					18	11				3			155	37	38.8
8H-CC, 9-14	74.03	78.80	F	M			1	15							1	1		4			1		6			52	21	13.0
9H-CC, 10-15	75.24	81.42	C	G				41	3				1		2	2		8						2		175	30	35.0
10H-CC, 0-5	92.97	103.16	C	G				33	20		1	2	2		1	2		15	9	1			3			246	38	46.1
11H-CC, 53-58	97.90	103.69	A	G			4	50	5		1		6	2	3	1							3			269	41	67.3
12H-CC, 0-5	111.59	117.38	C	G		2		52	2		1		4	1	1										1	251	37	37.7
13H-CC, 0-5	111.8	111.80	A	G				49	8		4			1	1			11	2				3			224	37	77.6
14H-CC, 11-16	130.07	135.86	A	G				40	10		3	1	3		1			17		2	1					235	40	70.5
15H-CC, 21-26	136.7	142.49	F	G				5	21		6				2	1		10				3				135	23	13.5
16H-CC, 9-14	149.24	156.66	C	G			1	22	4				5		5	2		11				1				306	38	95.6
17H-CC, 0-8	149.8	149.80	C	G	1		2	47	3		1		1		7	3		10								222	43	66.6
18H-CC, 21-26	166.22	174.18																								0		0.0
19H-CC, 0-10	177.69	185.70																								0		0.0
20H-CC, 13-23	187.53	195.35																								0		0.0
21H-CC, 21-26	195.09	208.71	R	M				3					2													11	9	0.6
23H-CC, 31-41	215.29	227.59	C	M			1	63	8	1			3		1	1		8								265	33	33.1
177-1089B-																												
24H-CC, 23-28	223.43	238.53	C	M			R																					
25H-CC, 14-19	232.78	247.88	C	P				A			R				R			R										
26H-CC, 11-16	242.01	257.11	B																									
27H-CC, 45-53	250.79	265.89	B																									
28H-CC, 25-30	257.84	272.92	B																									
29H-CC, 62-67	264.91	280.01	B																									

Table T9. Control points used to calculate sedimentation rates for Holes 1089A, 1089B, 1089C, and 1089D.

		Depth range of stratigraphic datums									
		Top			Bottom			Mean			Sedimetation rate (m/m.y.)
Code	Event/Zone/Chron	Core, section, interval (cm)	Depth (mbsf)	Depth (mcd)	Core, section, interval (cm)	Depth (mbsf)	Depth (mcd)	Depth (mbsf)	Depth (mcd)	Age (Ma)	
		177-			177-						
DIAT/REFL	MID MIS 5.3	1089B			1089B			17.56	23.00	0.099	
DIAT/REFL	MID MIS 5.5	1089B			1089B			23.50	27.08	0.122	
DIAT/REFL	MID MIS 6.5	1089C			1089C			26.50	30.08	0.171	
DIAT/REFL	MID MIS 7.1	1089B			1089B			31.10	35.50	0.194	
DIAT/REFL	MID MIS 7.5	1089B			1089B			35.45	39.20	0.240	
CN	FO E. huxleyi	1089B-5H-2, 30-30	35.10	39.56	1089B-5H-2, 130-130	36.10	40.56	35.60	40.06	0.260	~128
DIAT/REFL	MID MIS 9.3	1089B			1089B			46.00	52.20	0.331	
DIAT/REFL	MID MIS 11.1	1089B			1089B			52.40	55.90	0.368	
DIAT/REFL	MID MIS 11.3	1089B			1089B			58.35	63.50	0.405	
CN	LO P. lacunosa	1089A-7H-CC, 51-56	63.40	67.54	1089A-8H-1, 30-30	64.60	69.37	63.90	68.46	0.460	
DIAT	TOP *A. ingens* Subzone c, MIS 16.3	1089B-9H-CC, 15-20	80.20	89.61	1089C-10H-3, 60-60	84.00	90.49	82.10	90.05	0.640	
MAG	BOT C1n (Brunhes)	1089B-12H-4, 65-65	105.00	116.26	1089B-13H-4, 20-20	114.00	125.26	109.50	120.76	0.780	
CN	RE *Geph.* medium (4-5.5 µm)	1089B-17H-2, 130-130	149.10	160.36	1089B-17H-2, 120-120	150.00	161.26	149.55	160.81	0.960	
DIAT	TOP *A. ingens* Subzone b	1089B-16H-CC, 12-17	146.40	157.66	1089B-17H-CC, 18-23	155.30	166.54	86.65	162.10	1.070	
MAG	BOT C1r.1n (Jaramillo)	1089B-17H-3, 130-130	151.60	162.86	1089B-17H-5, 30-30	153.60	164.86	152.60	163.86	1.070	
CN	FO R. asanoi	1089A-18H-3, 130-130	163.60	171.56	1089A-18H-4, 30-30	164.10	172.05	163.85	171.80	1.080	~110
CN	LO *Gephyrocapsa* large (>5.5 µm)	1089B-18H-CC, 13-18	165.39	176.65	1089A-19H-1, 120-120	170.00	178.01	167.69	177.33	1.240	
DIAT	TOP *A. ingens* Subzone a*	1089C-21H-CC, 19-24	185.20	197.83	1089B-20H-CC, 0-10	190.80	202.05	95.40	199.94	1.300	
CN	FO *Gephyrocapsa* large (>5.5 µm)	1089B-20H-6, 30-30	182.88	195.56	1089B-20H-CC, 0-10	185.15	197.83	184.02	196.70	1.460	
CN	LO C. macintyrei	1089A-23H-1, 120-120	208.00	220.30	1089A-23H-2, 30-30	208.60	220.90	208.30	220.60	1.600	
CN	FO *Gephyrocapsa* medium (4-5 µm)	1089A-23H-4, 30-30	211.60	223.90	1089A-23H-4, 120-120	212.50	224.80	212.05	224.35	1.690	
MAG	TOP C2n (Olduvai)	1089B-23H-7, 50-50	213.80	228.90	1089B-24H-2, 50-50	215.80	230.90	214.80	229.90	1.770	
DIAT	TOP *P. barboi* Zone	1089B-23H-CC, 0-8	213.70	228.75	1089B-24H-CC, 23-28	223.40	238.53	123.20	233.64	1.800	~84
CN	LO D. brouweri	1089B-24H-6, 30-30	221.60	236.70	1089B-24H-CC, 23-28	223.43	238.53	222.52	237.62	1.950	
MAG	BOT C2n (Olduvai)	1089B-25H-2, 65-65	225.45	240.55	1089B-25H-3, 135-135	227.65	242.75	226.55	241.65	1.950	
DIAT	TOP *T. kolbei/F. matuyama* Zone	1089B-24H-CC, 23-28	223.40	238.53	1089B-25H-CC, 14-19	232.80	247.88	228.10	243.21	2.000	

Notes: Code abbreviations: DIAT = diatom, REFL = reflectance, CN = calcareous nannofossil, MAG = magnetic polarity. Event abbreviations: FO = first occurrence, LO = last occurrence, RE = reentrance, TOP = top of interval, MID = middle of interval, BOT = bottom of interval. Age assignment of marine isotope stages (MIS) according to Imbrie et al. (1984). * = datum not included in sedimentation rate calculations. Sedimentation rates at 1.07 Ma were calculated by averaging the mean depth range between the TOP of *A. ingens* and the BOT of C1r.1n (Jaramillo Subchron). Shaded area indicates a disturbed interval. This table is also available in ASCII format in the **TABLES** directory.

Table T10. Diatom, silicoflagellate, ebridian, *Actiniscus*, sponge spicule, and opaline phytolith occurrence in smear slides investigated at Site 1089. (**See table note.** Continued on next eight pages.)

Core, section, interval (cm)	Depth (mbsf)	Depth (mcd)	Diatom abundance	Diatom preservation	Silicoflagellate occurrence	Ebridian occurrence	*Actiniscus* occurrence	Sponge spicule occurrence	Opaline phytolith occurrence	*Actinocyclus actinochilus*	*Actinocyclus praeactinochilus*	*Actinocyclus curvatulus*	*Actinocyclus fasciculatus*	*Actinocyclus ingens*	*Actinoptychus senarius*	*Alveolus marinus*	*Asteromphalus hookeri*	*Azpeitia nodulifer*	*Azpeitia tabularis*	*Chaetoceros* spp.	*Coscinodiscus marginatus*	*Coscinodiscus radiatus*	*Ethmodiscus rex*	*Eucampia antarctica*	*Fragilariopsis barronii*	*Fragilariopsis curta*	*Fragilariopsis doliolus*	*Fragilariopsis donahuensis*	*Fragilariopsis fossilis*
177-1089A-																													
1H-CC, 17-22	7.27	7.03	C	M	T	B	B	X	B				R		T				F	R				T			C		
2H-CC, 16-21	16.90	16.48	C	M	T	B	B	X	B			T			T	R	R		F					T			F		
3H-CC, 13-18	21.18	24.02	C	M	T	B	B	X	B							R		R		F				R			F		
4H-CC, 22-27	30.66	35.04	A	M	R	X	X	X	B						R	R		T	R	R		R		R		R	T		
5H-CC, 14-19	43.36	44.32	A	M	T	B	B	X	B							R			R								R		
6H-CC, 18-23	52.25	54.13	A	M	R	X	B	X	B							T			R	R		R	X	R					
7H-CC, 51-56	63.43	67.57	C	M	T	X	B	X	X	T					T		T			T									
8H-CC, 9-14	74.03	78.80	C	M	T	B	X	X	B						T	T			R	T							T		
9H-CC, 10-15	75.24	81.42	C	M	T	B	B	X	B						T				R		T			R			T		
10H-CC, 0-5	92.97	97.50	C	M	T	B	B	X	B					R		R							X						
11H-CC, 53-58	97.90	103.69	C	M	T	B	B	X	B					F															
12H-CC, 0-5	111.59	117.38	C	M	T	B	B	X	B					F		R							X						F
13H-CC, 0-5	111.80	117.59	C	M	T	B	B	X	B					F					R										R
14H-CC, 11-16	130.07	135.86	A	M-G	T	B	B	X	B					R				R					X						R
15H-CC, 21-26	136.70	142.49	C	M	T	B	B	X	B					F		R		R		C			X						F
16H-CC, 9-14	149.24	156.66	C	M	T	B	B	X	B					R		R													F
18H-CC, 21-26	166.22	174.18	C	M	T	B	B	X	B			R		F	T	R			R										F
19H-CC, 0-10	177.69	185.70	F	M	T	B	B	X	B					F					R						T				R
20H-CC, 13-23	187.48	195.30	F	M	T	B	X	X	B		T			F				R					X						
21H-CC, 21-26	195.09	208.71	C	M	T	B	B	X	B					F															R
23H-CC, 31-41	215.29	227.59	C	M	R	B	B	X	B					F							T		X		R				T
177-1089B-																													
2H-CC, 10-15	13.67	19.37	C	M	T	B	B	X	B										F								F		
3H-CC, 8-16	23.12	28.56	A	G	T	B	B	X	B					T		R											R		
4H-CC, 12-17	32.42	38.02	C	M	T	B	B	X	B							R		R						R					
5H-CC, 16-21	41.90	46.36	A	G	T	B	B	X	B						T												R		
6H-CC, 11-16	51.18	57.38	F	M	T	B	B	X	B										R										
7H-CC, 8-14	60.73	68.15	F	M	T	B	B	X	B						T				R								R		
8H-CC, 20-25	70.02	78.07	C	M	T	B	B	X	B										R										
9H-CC, 15-20	80.24	89.61	C	M	T	B	B	X	B					R															T
10H-CC, 15-20	88.25	99.51	C-F	M	T	B	B	X	B					R				F				T		R					
11H-CC, 9-14	99.09	110.35	C-F	M	T	B	B	X	B					F	R	R			R										R
12H-CC, 8-13	108.43	119.69	F	M	T	B	B	X	B					R		R		R	R				X				R		
13H-CC, 0-8	117.90	129.16	C	M	T	B	B	X	B					F		R		R	R								R		
14H-CC, 14-19	127.14	138.40	F	M	T	X	B	X	B					R	T				T				X				R		F
15H-CC, 0-5	136.68	147.94	C	M	T	X	B	X	B					T	T	R		R	T				X	T	T		R		R
16H-CC, 12-17	146.40	157.66	F	M	T	X	B	X	X					R													R		R

Table T10 (continued).

Core, section, interval (cm)	Depth (mbsf)	Depth (mcd)	*Fragilariopsis interfrigidaria*	*Fragilariopsis kerguelensis*	*Fragilariopsis matuyamae*	*Fragilariopsis reinholdii*	*Fragilariopsis ritscherii*	*Fragilariopsis separanda*	*Fragilariopsis weaveri*	*Hemidiscus cuneiformis*	*Hemidiscus karstenii*	*Navicula directa*	*Nitzschia* aff. *januaria*	*Paralia sulcata*	*Proboscia barboi*	*Rhizosolenia bergonii*	*Rhizosolenia hebetata* fo. *semispina*	*Rhizosolenia praebergonii*	*Rhizosolenia styliformis*	*Roperia tesselata*	*Rouxia heteropolara*	*Rouxia isopolica*	*Rouxia naviculoides*	*Stephanopyxis turris*	*Thalassionema nitzschioides*	*Thalassionema nitzschioides* fo. 1	*Thalassionema nitzschioides* var. *parva*	*Thalassiosira eccentrica*	*Thalassiosira elliptopora*	*Thalassiosira fasciculata*	*Thalassiosira gracilis*	*Thalassiosira kolbei*
177-1089A-																																
1H-CC, 17-22	7.27	7.03		C													R								F							
2H-CC, 16-21	16.9	16.48								R															F		R	T				
3H-CC, 13-18	21.18	24.02		C																					R							
4H-CC, 22-27	30.66	35.04		C				T		R	R														R			T				
5H-CC, 14-19	43.36	44.32		A							F														R							
6H-CC, 18-23	52.25	54.13		F				T						T												T	T	R				
7H-CC, 51-56	63.43	67.57		R						T				T												T	T					
8H-CC, 9-14	74.03	78.80		C												T									T		T	T				
9H-CC, 10-15	75.24	81.42		C			T					T		T											R			T				
10H-CC, 0-5	92.97	97.50		C		F																										
11H-CC, 53-58	97.9	103.69				R																										
12H-CC, 0-5	111.59	117.38		C		R																							T			
13H-CC, 0-5	111.8	117.59		C		R																			R				T			
14H-CC, 11-16	130.07	135.86		F		F								T															R	R		
15H-CC, 21-26	136.7	142.49		F		F								T										R	F				R	R		
16H-CC, 9-14	149.24	156.66		F		F																						R	R	R		
18H-CC, 21-26	166.22	174.18		F																												
19H-CC, 0-10	177.69	185.70				F																										
20H-CC, 13-23	187.48	195.30		F		R																										
21H-CC, 21-26	195.09	208.71		F		F				T																						
23H-CC, 31-41	215.29	227.59		R		T															T				R							
177-1089B-																																
2H-CC, 10-15	13.67	19.37		C																												
3H-CC, 8-16	23.12	28.56		A																												
4H-CC, 12-17	32.42	38.02		C				R			R																					
5H-CC, 16-21	41.9	46.36		C							R			T											F							
6H-CC, 11-16	51.18	57.38		C							R																					
7H-CC, 8-14	60.73	68.15		C																					R		T					
8H-CC, 20-25	70.02	78.07		C																					R							
9H-CC, 15-20	80.24	89.61		C																T												
10H-CC, 15-20	88.25	99.51		C		R																			R							
11H-CC, 9-14	99.09	110.35		C																					R		R		R			
12H-CC, 8-13	108.43	119.69		C		R								R															R	F		
13H-CC, 0-8	117.9	129.16		F		R																							R			
14H-CC, 14-19	127.14	138.40		F		R																										
15H-CC, 0-5	136.68	147.94		R		R												T								T						
16H-CC, 12-17	146.4	157.66		R		R												T														

Table T10 (continued).

Core, section, interval (cm)	Depth (mbsf)	Depth (mcd)	*Thalassiosira lentiginosa*	*Thalassiosira* aff. *lineata*	*Thalassiosira oestrupii*	*Thalassiosira oliverana*	*Thalassiosira tetraoestrupii* var. *reimeri*	*Thalassiosira vulnifica*	*Thallassiothrix antarctica-longissima* group	Benthic diatoms, marine	Benthic diatoms, freshwater	Diatom zone	Diatom age (Ma)
177-1089A-													
1H-CC, 17-22	7.27	7.03	R		R				F		T	*T. lentiginosa* Subzone c	0-0.18
2H-CC, 16-21	16.9	16.48	R							T		*T. lentiginosa* Subzone c	0-0.18
3H-CC, 13-18	21.18	24.02								R		*T. lentiginosa* Subzone c	0-0.18
4H-CC, 22-27	30.66	35.04	F	R	R				R			*T. lentiginosa* Subzone b	0.18-0.42
5H-CC, 14-19	43.36	44.32	F			F				T		*T. lentiginosa* Subzone b	0.18-0.42
6H-CC, 18-23	52.25	54.13		R								*T. lentiginosa* Subzone b	0.18-0.42
7H-CC, 51-56	63.43	67.57	T	T					R	T		*T. lentiginosa* Subzone a	0.42-0.65
8H-CC, 9-14	74.03	78.80	R		R				R			*T. lentiginosa* Subzone a	0.42-0.65
9H-CC, 10-15	75.24	81.42	R	T		T			R			*T. lentiginosa* Subzone a	0.42-0.65
10H-CC, 0-5	92.97	97.50	F						F			*A. ingens* Subzone c	0.65-1.07
11H-CC, 53-58	97.9	103.69										*A. ingens* Subzone c	0.65-1.07
12H-CC, 0-5	111.59	117.38	R						F			*A. ingens* Subzone c	0.65-1.07
13H-CC, 0-5	111.8	117.59				R			F			*A. ingens* Subzone c	0.65-1.07
14H-CC, 11-16	130.07	135.86			R				C			*A. ingens* Subzone c	0.65-1.07
15H-CC, 21-26	136.7	142.49								T		*A. ingens* Subzone c	0.65-1.07
16H-CC, 9-14	149.24	156.66	R		R	R			F			*A. ingens* Subzone b	1.07-1.3
18H-CC, 21-26	166.22	174.18			R				F			*A. ingens* Subzone b	1.07-1.3
19H-CC, 0-10	177.69	185.70			R				F	T		*A. ingens* Subzone b	1.07-1.3
20H-CC, 13-23	187.48	195.30			R				F	T		*A. ingens* Subzone b	1.07-1.3
21H-CC, 21-26	195.09	208.71			R				F			*A. ingens* Subzone a	1.3-1.8
23H-CC, 31-41	215.29	227.59	T	T	T	R			R			*A. ingens* Subzone a	1.3-1.8
177-1089B-													
2H-CC, 10-15	13.67	19.37							F			*T. lentiginosa* Subzone c	0-0.18
3H-CC, 8-16	23.12	28.56	R		R				F			*T. lentiginosa* Subzone c	0-0.18
4H-CC, 12-17	32.42	38.02	F						F			*T. lentiginosa* Subzone b	0.18-0.42
5H-CC, 16-21	41.9	46.36	F						F	T		*T. lentiginosa* Subzone b	0.18-0.42
6H-CC, 11-16	51.18	57.38			R				F			*T. lentiginosa* Subzone b	0.18-0.42
7H-CC, 8-14	60.73	68.15										*T. lentiginosa* Subzone a	0.42-0.65
8H-CC, 20-25	70.02	78.07							F			*T. lentiginosa* Subzone a	0.42-0.65
9H-CC, 15-20	80.24	89.61							F			*T. lentiginosa* Subzone a	0.42-0.65
10H-CC, 15-20	88.25	99.51	F						F	T		*A. ingens* Subzone c	0.65-1.07
11H-CC, 9-14	99.09	110.35	F		R				F			*A. ingens* Subzone c	0.65-1.07
12H-CC, 8-13	108.43	119.69			R				F	T		*A. ingens* Subzone c	0.65-1.07
13H-CC, 0-8	117.9	129.16							F			*A. ingens* Subzone c	0.65-1.07
14H-CC, 14-19	127.14	138.40							F			*A. ingens* Subzone c	0.65-1.07
15H-CC, 0-5	136.68	147.94	R					T	F			*A. ingens* Subzone c	0.65-1.07
16H-CC, 12-17	146.4	157.66			T				R			*A. ingens* Subzone c	0.65-1.07

Table T10 (continued).

Core, section, interval (cm)	Depth (mbsf)	Depth (mcd)	Diatom abundance	Diatom preservation	Silicoflagellate occurrence	Ebridian occurrence	*Actiniscus* occurrence	Sponge spicule occurrence	Opaline phytolith occurrence	*Actinocyclus actinochilus*	*Actinocyclus praeactinochilus*	*Actinocyclus curvatulus*	*Actinocyclus fasciculatus*	*Actinocyclus ingens*	*Actinoptychus senarius*	*Alveolus marinus*	*Asteromphalus hookeri*	*Azpeitia nodulifer*	*Azpeitia tabularis*	*Chaetoceros* spp.	*Coscinodiscus marginatus*	*Coscinodiscus radiatus*	*Ethmodiscus rex*	*Eucampia antarctica*	*Fragilariopsis barronii*	*Fragilariopsis curta*	*Fragilariopsis doliolus*	*Fragilariopsis donahuensis*	*Fragilariopsis fossilis*
17H-CC, 18-23	155.28	166.54	F-R	M	T	B	B	X	B					R				R					X				R		R
18H-CC, 13-18	165.39	176.65	F	M	T	B	X	X	B					T		R		T	T				X		T		T		R
19H-CC, 16-21	175.33	187.17	C	M	T	B	B	X	B					R											T				
20H-CC, 0-10	185.15	197.83	C	M	T	X	B	X	B					F	T	T			T	T					R				
21H-CC, 11-16	194.21	209.31	C	M	T	B	B	X	B					F									X		R				R
22H-CC, 0-5	204.30	219.40	F	M	T	B	B	X	B					F		R					T		X		R				
23H-CC, 0-8	213.65	228.75	C	M	T	X	B	X	X					F	T				T				X		R				T
24H-CC, 23-28	223.43	238.53	C	M	T	X	X	X	B		R			F									X						
25H-CC, 14-19	232.78	247.88	F	M	T	B	B	X	B		T			F									X		F		T		
26H-CC, 11-16	242.01	257.11	F	M	T	B	X	X	B					R		R					T		X		F				
27H-CC, 45-53	250.79	265.89	R	P	T	B	B	X	B					T									X	T	T				
28H-CC, 25-30	257.84	272.94	R	M	T	B	B	X	B		R			T											R				
29H-CC, 62-67	264.91	280.01	F	M	T	B	B	X	X					F				R					X		T				R
177-1089C-																													
1H-CC, 8-13	2.38	2.08	A	M	T	B	B	X	X			T				T			T	R				T					
2H-CC, 0-8	9.37	12.61	A	M	T	X	B	X	B										R	R				T			R		
3H-1, 110-110	15	19.42	A	G	F	B	B	X	B			T			T	F			F				X	T			F		
3H-CC, 9-14	17.42	21.84	C-F	M	T	B	B	X	B			T			T	T		T	T	R			X	T			T		
4H-1, 10-10	23.5	27.08	C	G	T	B	B	X	B							R		R	R					R			F		
4H-3, 10-10	26.5	30.08	A	G	T	X	X	X	B	T						R		T	R	R			X	T		T	R		
4H-5, 90-90	30.3	33.88	C	M	B	X	B	X	B						T	R		T	R	R							R		
4H-CC, 10-15	31.78	35.36	C	M	T	X	X	X	B						T				T										
5H-1, 10-10	33	36.42	C	M	T	B	B	X	B							R			R	R-F			X	R			F		
5H-1, 90-90	33.8	37.22	C	M	B	X	B	X	B							R				F				T			F		
5H-3, 10-10	36	39.42	F	M	T	X	B	X	B							R			F	R			X	F			F		
5H-CC, 10-15	40.91	44.33	C	M	T	X	B	X	B										R				X				T		
6H-2, 10-10	44	46.06	F-C	M	B	B	X	X	B						T	R			F	F									R
6H-3, 60-60	46	48.06	F	M	B	B	B	X	B							F		T	R								R		R
6H-4, 10-10	47	49.06	C-F	M	T	B	B	X	B						T	R		R	R	R			X	T			F		R
6H-CC, 9-14	51.46	53.52	C	M	T	B	B	X	B	T					T	T			R		T		X				R		
7H-1, 10-10	52	55.52	C	M	R	B	B	X	B	T							T		C	F			X				F		
7H-2, 60-60	54	57.52	C	M	B	B	B	X	B							R		R	C	R					T		R		R
7H-3, 110-110	56	59.52	C-F	M	T	X	B	X	B			T		T	T	R		T	C				X				F		
7H-5, 10-10	58	61.52	F	M	B	B	B	X	B							R			C	R			X				R		R
7H-6, 60-60	60	63.52	R	P	T	X	B	X	B						T	F			C				X				R		
7H-CC, 0-10	60.81	64.33	C-F	M	T	B	B	X	B						T	T			R								R		
8H-CC, 0-10	70.34	74.21	C	M	T	B	X	X	B							T			R				X				T		T
9H-5, 121-121	78	82.38	C	M	T	B	B	X	B					T		F	T		C					R			R		
9H-7, 60-60	80	84.38	C	M-G	T	B	B	X	B										R				X						

Table T10 (continued).

Core, section, interval (cm)	Depth (mbsf)	Depth (mcd)	*Fragilariopsis interfrigidaria*	*Fragilariopsis kerguelensis*	*Fragilariopsis matuyamae*	*Fragilariopsis reinholdii*	*Fragilariopsis ritscherii*	*Fragilariopsis separanda*	*Fragilariopsis weaveri*	*Hemidiscus cuneiformis*	*Hemidiscus karstenii*	*Navicula directa*	*Nitzschia* aff. *januaria*	*Paralia sulcata*	*Proboscia barboi*	*Rhizosolenia bergonii*	*Rhizosolenia hebetata* fo. *semispina*	*Rhizosolenia praebergonii*	*Rhizosolenia styliformis*	*Roperia tesselata*	*Rouxia heteropolara*	*Rouxia isopolica*	*Rouxia naviculoides*	*Stephanopyxis turris*	*Thalassionema nitzschioides*	*Thalassionema nitzschioides* fo. 1	*Thalassionema nitzschioides* var. *parva*	*Thalassiosira eccentrica*	*Thalassiosira elliptopora*	*Thalassiosira fasciculata*	*Thalassiosira gracilis*	*Thalassiosira kolbei*
17H-CC, 18-23	155.28	166.54		R		R																										
18H-CC, 13-18	165.39	176.65				R				R				T											R							
19H-CC, 16-21	175.33	187.17				R				T							T							T		T					
20H-CC, 0-10	185.15	197.83		R		R				T				T												T			R		
21H-CC, 11-16	194.21	209.31		F		F				R					T	R																
22H-CC, 0-5	204.3	219.40		R		R				T				T											F				T	R		
23H-CC, 0-8	213.65	228.75		R		R				T	T			T			T								F				R			
24H-CC, 23-28	223.43	238.53		F		R				T	R				R											R			T			
25H-CC, 14-19	232.78	247.88		R	F	F			T					T	T		T		T											T	R	
26H-CC, 11-16	242.01	257.11			R	R				T					R																T	R
27H-CC, 45-53	250.79	265.89	T						T															T	R						T	T
28H-CC, 25-30	257.84	272.94	T		T	T									R									T		T						T
29H-CC, 62-67	264.91	280.01				F									T											R						
177-1089C-																																
1H-CC, 8-13	2.38	2.08		C						T																R			T			
2H-CC, 0-8	9.37	12.61		C															T													
3H-1, 110-110	15	19.42		F						R	T			T			T												R			
3H-CC, 9-14	17.42	21.84		F						R															T							
4H-1, 10-10	23.5	27.08		F						F				R						R									R			
4H-3, 10-10	26.5	30.08		F				T			R			T																		
4H-5, 90-90	30.3	33.88		F							F			T											R							
4H-CC, 10-15	31.78	35.36		C							R																					
5H-1, 10-10	33	36.42		C							F														R							
5H-1, 90-90	33.8	37.22		C							F			R											F	T						
5H-3, 10-10	36	39.42		F						T	F			T			T															
5H-CC, 10-15	40.91	44.33		C							R																					
6H-2, 10-10	44	46.06		C							R														T							
6H-3, 60-60	46	48.06		C							F			T			T								R							
6H-4, 10-10	47	49.06		F							R			R												R	R					
6H-CC, 9-14	51.46	53.52		C						T				T											T							
7H-1, 10-10	52	55.52		C							R			T											R							
7H-2, 60-60	54	57.52		C				R						R											R							
7H-3, 110-110	56	59.52		C				R		T	F														R				T			
7H-5, 10-10	58	61.52		C							F														R							
7H-6, 60-60	60	63.52		C							R																					
7H-CC, 0-10	60.81	64.33		F		T																				T						
8H-CC, 0-10	70.34	74.21		C				T		T															T							
9H-5, 121-121	78	82.38		C		T		R						R									T									
9H-7, 60-60	80	84.38		C										T									T		R			T				

Table T10 (continued).

Core, section, interval (cm)	Depth (mbsf)	Depth (mcd)	*Thalassiosira lentiginosa*	*Thalassiosira* aff. *lineata*	*Thalassiosira oestrupii*	*Thalassiosira oliverana*	*Thalassiosira tetraoestrupii* var. *reimeri*	*Thalassiosira vulnifica*	*Thallassiothrix antarctica-longissima* group	Benthic diatoms, marine	Benthic diatoms, freshwater	Diatom zone	Diatom age (Ma)
17H-CC, 18-23	155.28	166.54							F	T		*A. ingens* Subzone b	1.07-1.3
18H-CC, 13-18	165.39	176.65	T		T				R	T		*A. ingens* Subzone b	1.07-1.3
19H-CC, 16-21	175.33	187.17							F			*A. ingens* Subzone b	1.07-1.3
20H-CC, 0-10	185.15	197.83			R				F			*A. ingens* Subzone b	1.07-1.3
21H-CC, 11-16	194.21	209.31			R				F	T		*A. ingens* Subzone a	1.3-1.8
22H-CC, 0-5	204.3	219.40			F	F	R	T	F	R		early *A. ingens* Subzone a	1.5-1.8
23H-CC, 0-8	213.65	228.75					R		F			early *A. ingens* Subzone a	1.5-1.8
24H-CC, 23-28	223.43	238.53	R		R	R			F			*P. barboi*	1.8-2.0
25H-CC, 14-19	232.78	247.88	R		R	T	R		F	T		*T. kolbei/F. matuyama*	2.0-2.5
26H-CC, 11-16	242.01	257.11			R				F			*T. kolbei/F. matuyama*	2.0-2.5
27H-CC, 45-53	250.79	265.89				T			R	T		*T. kolbei/F. matuyama*	2.0-2.5
28H-CC, 25-30	257.84	272.94							F			*T. kolbei/F. matuyama*	2.0-2.5
29H-CC, 62-67	264.91	280.01			R				F			*T. kolbei/F. matuyama*	2.0-2.5
177-1089C-													
1H-CC, 8-13	2.38	2.08	R						C			*T. lentiginosa* Subzone c	0-0.18
2H-CC, 0-8	9.37	12.61	R						F			*T. lentiginosa* Subzone c	0-0.18
3H-1, 110-110	15	19.42	R	R	R				F			*T. lentiginosa* Subzone c	0-0.18
3H-CC, 9-14	17.42	21.84	T	T		T						*T. lentiginosa* Subzone c	0-0.18
4H-1, 10-10	23.5	27.08	R		F				F	R		*T. lentiginosa* Subzone c	0-0.18
4H-3, 10-10	26.5	30.08	F	R					F			*T. lentiginosa* Subzone b	0.18-0.42
4H-5, 90-90	30.3	33.88	F		R				F			*T. lentiginosa* Subzone b	0.18-0.42
4H-CC, 10-15	31.78	35.36				T			F			*T. lentiginosa* Subzone b	0.18-0.42
5H-1, 10-10	33	36.42	F		R				F			*T. lentiginosa* Subzone b	0.18-0.42
5H-1, 90-90	33.8	37.22	F		R				F			*T. lentiginosa* Subzone b	0.18-0.42
5H-3, 10-10	36	39.42	F	T	R				F			*T. lentiginosa* Subzone b	0.18-0.42
5H-CC, 10-15	40.91	44.33	R		T				R			*T. lentiginosa* Subzone b	0.18-0.42
6H-2, 10-10	44	46.06	F	T					F			*T. lentiginosa* Subzone b	0.18-0.42
6H-3, 60-60	46	48.06	F	R	R				F			*T. lentiginosa* Subzone b	0.18-0.42
6H-4, 10-10	47	49.06	F	R	R				F			*T. lentiginosa* Subzone b	0.18-0.42
6H-CC, 9-14	51.46	53.52	T		T				R			*T. lentiginosa* Subzone b	0.18-0.42
7H-1, 10-10	52	55.52	F						F			*T. lentiginosa* Subzone b	0.18-0.42
7H-2, 60-60	54	57.52	F		R	T			F			*T. lentiginosa* Subzone b	0.18-0.42
7H-3, 110-110	56	59.52	F			T			F	T		*T. lentiginosa* Subzone b	0.18-0.42
7H-5, 10-10	58	61.52	F		R							*T. lentiginosa* Subzone b	0.18-0.42
7H-6, 60-60	60	63.52	R						F			*T. lentiginosa* Subzone b	0.18-0.42
7H-CC, 0-10	60.81	64.33		T	T				F			*T. lentiginosa* Subzone a	0.42-0.65
8H-CC, 0-10	70.34	74.21	T		T				F			*T. lentiginosa* Subzone a	0.42-0.65
9H-5, 121-121	78	82.38	F		F	R			F		T	*T. lentiginosa* Subzone a	0.42-0.65
9H-7, 60-60	80	84.38	F		R				F			*T. lentiginosa* Subzone a	0.42-0.65

Table T10 (continued).

Core, section, interval (cm)	Depth (mbsf)	Depth (mcd)	Diatom abundance	Diatom preservation	Silicoflagellate occurrence	Ebridian occurrence	*Actiniscus* occurrence	Sponge spicule occurrence	Opaline phytolith occurrence	*Actinocyclus actinochilus*	*Actinocyclus praeactinochilus*	*Actinocyclus curvatulus*	*Actinocyclus fasciculatus*	*Actinocyclus ingens*	*Actinoptychus senarius*	*Alveolus marinus*	*Asteromphalus hookeri*	*Azpeitia nodulifer*	*Azpeitia tabularis*	*Chaetoceros* spp.	*Coscinodiscus marginatus*	*Coscinodiscus radiatus*	*Ethmodiscus rex*	*Eucampia antarctica*	*Fragilariopsis barronii*	*Fragilariopsis curta*	*Fragilariopsis doliolus*	*Fragilariopsis donahuensis*	*Fragilariopsis fossilis*
9H-CC, 7-12	80.1	84.48	C	M	T	B	B	X	B					T					R				X	T			T		
10H-2, 10-10	82	88.49	A	G	B	B	B	X	B															R					
10H-3, 60-60	84	90.49	A	G	T	B	B	X	B					R					R					R					
10H-4, 110-110	86	92.49	C	M	T	B	B	X	B					R		R			F				X				R		
10H-CC, 5-5	88.04	94.53	C	M	T	B	B	X	B					R				R	T								R		
10H-CC, 18-23	88.08	94.57	A	M	T	B	B	X	B					T	T	T		T	R				X				R		
11H-CC, 13-18	99.16	108.05	A	M	T	B	B	X	B					R				T					T				R		
12H-CC, 10-15	107.43	116.32	A	M	T	B	B	X	B					R					R				X	T			T		
13H-CC, 0-10	117.42	126.31	C	M	T	B	B	X	B			T		T		T			T	R			X						T
14H-CC, 9-14	126.55	135.44	C	M	B	X	B	X	B					R		T											T		T
15H-CC, 21-26	135.76	144.65	F	M	T	B	B	X	B			T		T		T		T	T			T							T
16H-CC, 10-15	146.8	157.45	F	M	T	B	B	X	B					T	T	T									T				
17H-CC, 11-16	156.33	169.44	C	M	T	X	B	X	B					R		R				T							T		R
18H-CC, 0-3	165.57	178.68	C	M	T	B	B	X	B					R	T	R		R		R			T				T		T
19H-CC, 22-27	169.56	183.55	F	M	R	X	B	X	B	T		T		F	T				T		T		X				T		R
20H-CC, 46-51	184.01	194.60	F	M	T	B	X	X	B		R			R				R	T	T			X				T		R
21H-CC, 19-24	190.84	202.05	F	M-P	T	B	B	X	B		R			F		R							X						R
177-1089D-																													
1H-CC, 5-13	6.62	5.98	F	M	T	B	B	X	B										T	R				T			R		
2H-CC, 8-13	15.29	12.41	C	M	T	B	X	X	B			T			T	R		T	T	F				T			R		
3H-CC, 7-12	22.51	22.33	F	M	T	X	B	X	B			T				T			T	R							R		
4H-CC, 0-10	32.56	31.66	C	M	B	X	B	X	X										R				T				T		
5H-CC, 0-5	42.07	38.97	F	M	T	X	B	X	B	T						T			T	R			X	T			T		
6H-CC, 24-29	51.42	49.80	F	P	T	X	B	X	B						T	T		T	T				X	T			T		
7H-CC, 0-10	61.06	60.00	C	M	T	X	B	X	X			T				T			R								T		
8H-CC, 5-10	70.72	70.69	F	M	T	X	B	X	B							T			R	R	T		X	T			R		T
9H-CC, 0-10	79.7	83.43	C-F	M	T	B	B	X	B						T	T		T	R	R							T		T
10H-CC, 0-5	89.72	97.24	C	M	T	B	B	X	B							T		T	T				X	T			T		T
11H-CC, 0-10	98	105.52	F-C	M	T	X	B	X	B					R				T	T	R			X	T	T		R		T
12H-CC, 13-18	108.44	115.96	C	M	T	X	X	X	B					T	T	R		T	R			T	X	T			T		T
13H-CC, 0-5	118.07	125.59	C	M	T	B	B	X	B					R		T			R				X				T		

Notes: Abundance abbreviations: C = common, F = few, R = rare, T = trace, B = barren. Preservation abbreviations: G = good, M = moderate, P = poor. For more specific definitions, refer to the **"Explanatory Notes"** chapter. This table is also available in ASCII format in the **TABLES** directory.

Table T10 (continued).

Core, section, interval (cm)	Depth (mbsf)	Depth (mcd)	*Fragilariopsis interfrigidaria*	*Fragilariopsis kerguelensis*	*Fragilariopsis matuyamae*	*Fragilariopsis reinholdii*	*Fragilariopsis ritscherii*	*Fragilariopsis separanda*	*Fragilariopsis weaveri*	*Hemidiscus cuneiformis*	*Hemidiscus karstenii*	*Navicula directa*	*Nitzschia* aff. *januaria*	*Paralia sulcata*	*Proboscia barboi*	*Rhizosolenia bergonii*	*Rhizosolenia hebetata* fo. *semispina*	*Rhizosolenia praebergonii*	*Rhizosolenia styliformis*	*Roperia tesselata*	*Rouxia heteropolara*	*Rouxia isopolica*	*Rouxia naviculoides*	*Stephanopyxis turris*	*Thalassionema nitzschioides*	*Thalassionema nitzschioides* fo. 1	*Thalassionema nitzschioides* var. *parva*	*Thalassiosira eccentrica*	*Thalassiosira elliptopora*	*Thalassiosira fasciculata*	*Thalassiosira gracilis*	*Thalassiosira kolbei*
9H-CC, 7-12	80.1	84.48		C		T		T												T					T				T			
10H-2, 10-10	82	88.49		A									R									R										
10H-3, 60-60	84	90.49		A																								R				
10H-4, 110-110	86	92.49		C		R				R			R																			
10H-CC, 5-5	88.04	94.53		C		R								R																		
10H-CC, 18-23	88.08	94.57		C		R		T																								
11H-CC, 13-18	99.16	108.05		C		T		T		T																				T		
12H-CC, 10-15	107.43	116.32		C		R								T																		
13H-CC, 0-10	117.42	126.31		R		R								T																R		
14H-CC, 9-14	126.55	135.44		F		R								T															R			
15H-CC, 21-26	135.76	144.65		R		T											T												T			
16H-CC, 10-15	146.8	157.45		F		R								T			T								T				T	T		
17H-CC, 11-16	156.33	169.44				T								T						T												
18H-CC, 0-3	165.57	178.68		F		R								T															T			
19H-CC, 22-27	169.56	183.55		R		F				T																T						
20H-CC, 46-51	184.01	194.60		R		R				T				T			T												T			
21H-CC, 19-24	190.84	202.05		R		R																										
177-1089D-																																
1H-CC, 5-13	6.62	5.98		F						R																T						
2H-CC, 8-13	15.29	12.41		F										T			R								T							
3H-CC, 7-12	22.51	22.33		F						T																						
4H-CC, 0-10	32.56	31.66		C				T			R														T							
5H-CC, 0-5	42.07	38.97		F						T	R														T							
6H-CC, 24-29	51.42	49.80		F										T											T				T			
7H-CC, 0-10	61.06	60.00		C				T		T	T			T							T				T							
8H-CC, 5-10	70.72	70.69		R		T								T											T							
9H-CC, 0-10	79.7	83.43		F		T								T											T	T						
10H-CC, 0-5	89.72	97.24		C		R								T											T					T		
11H-CC, 0-10	98	105.52		F		R								T			T									T			T	T		
12H-CC, 13-18	108.44	115.96		F		R				T				T										T		T				T		
13H-CC, 0-5	118.07	125.59		F		R				T				T															T			

Table T10 (continued).

Core, section, interval (cm)	Depth (mbsf)	Depth (mcd)	*Thalassiosira lentiginosa*	*Thalassiosira* aff. *lineata*	*Thalassiosira oestrupii*	*Thalassiosira oliverana*	*Thalassiosira tetraoestrupii* var. *reimeri*	*Thalassiosira vulnifica*	*Thallassiothrix antarctica-longissima* group	Benthic diatoms, marine	Benthic diatoms, freshwater	Diatom zone	Diatom age (Ma)
9H-CC, 7-12	80.1	84.48	R		T				F	T		*T. lentiginosa* Subzone a	0.42-0.65
10H-2, 10-10	82	88.49	F		R				R			*T. lentiginosa* Subzone a	0.42-0.65
10H-3, 60-60	84	90.49	R		R				F			*A. ingens* Subzone c	0.65-1.07
10H-4, 110-110	86	92.49	R		F				F			*A. ingens* Subzone c	0.65-1.07
10H-CC, 5-5	88.04	94.53	F		F				F			*A. ingens* Subzone c	0.65-1.07
10H-CC, 18-23	88.08	94.57	R		T				F			*A. ingens* Subzone c	0.65-1.07
11H-CC, 13-18	99.16	108.05	R						R			*A. ingens* Subzone c	0.65-1.07
12H-CC, 10-15	107.43	116.32	R						F			*A. ingens* Subzone c	0.65-1.07
13H-CC, 0-10	117.42	126.31			T				C			*A. ingens* Subzone c	0.65-1.07
14H-CC, 9-14	126.55	135.44							C			*A. ingens* Subzone c	0.65-1.07
15H-CC, 21-26	135.76	144.65				T			F			*A. ingens* Subzone c	0.65-1.07
16H-CC, 10-15	146.8	157.45	T			T		T	R			*A. ingens* Subzone c	0.65-1.07
17H-CC, 11-16	156.33	169.44	T			T			R	T		*A. ingens* Subzone b	1.07-1.3
18H-CC, 0-3	165.57	178.68	T			T			F-C			*A. ingens* Subzone b	1.07-1.3
19H-CC, 22-27	169.56	183.55	R		R	R			F	T		*A. ingens* Subzone b	1.07-1.3
20H-CC, 46-51	184.01	194.60			T				R			*A. ingens* Subzone b	1.07-1.3
21H-CC, 19-24	190.84	202.05			R				F			*A. ingens* Subzone a	1.3-1.8
177-1089D-													
1H-CC, 5-13	6.62	5.98	T	T	T				F			*T. lentiginosa* Subzone c	0-0.18
2H-CC, 8-13	15.29	12.41	R		T				F			*T. lentiginosa* Subzone c	0-0.18
3H-CC, 7-12	22.51	22.33	R	T	T				F	R		*T. lentiginosa* Subzone c	0-0.18
4H-CC, 0-10	32.56	31.66	R						C			*T. lentiginosa* Subzone b	0.18-0.42
5H-CC, 0-5	42.07	38.97	R						F			*T. lentiginosa* Subzone b	0.18-0.42
6H-CC, 24-29	51.42	49.80	R						F	T		*T. lentiginosa* Subzone b	0.18-0.42
7H-CC, 0-10	61.06	60.00	R		T	T			F			*T. lentiginosa* Subzone a	0.42-0.65
8H-CC, 5-10	70.72	70.69	T		T				F	T		*T. lentiginosa* Subzone a	0.42-0.65
9H-CC, 0-10	79.7	83.43	R		R				F			*T. lentiginosa* Subzone a	0.42-0.65
10H-CC, 0-5	89.72	97.24	R	T						T		*A. ingens* Subzone c	0.65-1.07
11H-CC, 0-10	98	105.52	R			T			F			*A. ingens* Subzone c	0.65-1.07
12H-CC, 13-18	108.44	115.96	R	T	T				C			*A. ingens* Subzone c	0.65-1.07
13H-CC, 0-5	118.07	125.59	R			T			F			*A. ingens* Subzone c	0.65-1.07

Table T11. Summary of biostratigraphic age assignments for Holes 1089A, 1089B, 1089C, and 1089D. (**See table note.** Continued on next two pages.)

Core, section, interval (cm)	Depth (mbsf)	Depth (mcd)	Calcareous nannofossil zone	Calcareous nannofossil age (Ma)	Diatom zone	Diatom age (Ma)	Radiolaria zone	Radiolaria age (Ma)	Comment
177-1089A-									
1H-CC, 17-22	7.27	7.27	NN21	0-0.26	*T. lentiginosa* Subzone c	0-0.18			
2H-CC, 16-21	16.90	16.90	NN21	0-0.26	*T. lentiginosa* Subzone c	0-0.18			
3H-CC, 13-18	21.18	21.18	NN21	0-0.26	*T. lentiginosa* Subzone c	0-0.18			
4H-CC, 22-27	30.66	30.66	NN21	0-0.26	*T. lentiginosa* Subzone b	0.18-0.42	Omega/*B. aquilonalis*	0-0.46	
5H-2, 100-100	38.30	38.30	NN21	0-0.26					
5H-2, 130-130	38.60	38.60	NN21	0-0.26					
5H-CC, 14-19	43.36	43.36	NN20	<0.46 dissolved	*T. lentiginosa* Subzone b	0.18-0.42	Omega/*B. aquilonalis*	0-0.46	
6H-CC, 18-23	52.25	52.25	NN20	0.26-0.46	*T. lentiginosa* Subzone b	0.18-0.42	Omega/*B. aquilonalis*	0-0.46	
7H-CC, 51-56	63.43	63.43	NN20	0.26-0.46	*T. lentiginosa* Subzone a	0.42-0.65	?	>0.46	
8H-1, 120-120	65.50	65.50	NN19	>0.46					
8H-3, 30-30	70.60	70.60	NN19	>0.46					
8H-CC, 9-14	74.03	74.03	NN19	0.46-0.88	*T. lentiginosa* Subzone a	0.42-0.65	?	>0.46	
9H-CC, 10-15	75.24	75.24	NN19	0.46-0.88	*T. lentiginosa* Subzone a	0.42-0.65			
10H-CC, 0-5	92.97	92.97	NN19	0.46-0.88	*A. ingens* Subzone c	0.65-1.07			
11H-CC, 53-58	97.90	97.90	NN19	0.46-0.88	*A. ingens* Subzone c	0.65-1.07			
12H-4, 120-120	109.00	109.00	NN19	<0.88					
12H-6, 30-30	110.10	110.10	NN19	>0.88?					
12H-7, 30-30	111.50	111.50	NN19	>0.88?					
12H-CC, 0-5	111.59	111.59	NN19	0.88-0.96	*A. ingens* Subzone c	0.65-1.07	?	>0.46	
13H-CC, 0-5	111.80	111.80	NN19	0.88-0.96	*A. ingens* Subzone c	0.65-1.07			
14H-CC, 11-16	130.07	130.07	NN19	0.88-0.96	*A. ingens* Subzone c	0.65-1.07			
15H-CC, 21-26	136.70	136.70	NN19	0.88-0.96	*A. ingens* Subzone c	0.65-1.07			
16H-CC, 9-14	149.24	149.24	NN19	Dissolved	*A. ingens* Subzone b	1.07-1.3	?	>0.46	
18H-1, 30-30	159.60	159.60	NN19	>1.08					
18H-CC, 21-26	166.22	166.22	NN19	1.08-1.24	*A. ingens* Subzone b	1.07-1.3			
19H-1, 120-120	170.00	178.01	NN19	>1.24					
19H-CC, 0-10	177.69	177.69	NN19	1.24-1.46	*A. ingens* Subzone b	1.07-1.3			
20H-CC, 13-23	187.48	187.48	NN19	1.24-1.46	*A. ingens* Subzone b	1.07-1.3	?	>0.46	
21H-CC, 21-26	195.09	195.09	NN19	>1.46	*A. ingens* Subzone a	1.3-1.8			
23H-1, 30-30	207.10	207.10	NN19	<1.69					
23H-1, 120-120	207.60	207.60	NN19	<1.69					
23H-3, 120-120	209.50	209.50	NN19	<1.69					
23H-4, 120-120	212.50	224.80	NN19	>1069					
23H-CC, 31-41	215.29	215.29	?	RWK-Pliocene?	*A. ingens* Subzone a	1.3-1.8			
177-1089B-									
2H-CC, 10-15	13.67	13.67	NN21	0-0.26	*T. lentiginosa* Subzone c	0-0.18	Omega/*B. aquilonalis*	0-0.46	
3H-CC, 8-16	23.12	23.12	NN21	0-0.26	*T. lentiginosa* Subzone c	0-0.18			
4H-CC, 12-17	32.42	32.42	NN21	0-0.26	*T. lentiginosa* Subzone b	0.18-0.42			
5H-3, 30-30	36.60	36.60	?	?					
5H-3, 130-130	37.10	37.10	NN20	>0.26? dissolved					
5H-CC, 16-21	41.90	41.90	NN20	0.26-0.46	*T. lentiginosa* Subzone b	0.18-0.42			
6H-CC, 11-16	51.18	51.18	NN20	0.26-0.46	*T. lentiginosa* Subzone b	0.18-0.42	Omega/*B. aquilonalis*	0-0.46	
7H-CC, 8-14	60.73	60.73	NN20	0.26-0.46	*T. lentiginosa* Subzone a	0.42-0.65	?	>0.46	
8H-1, 120-120	63.00	63.00	NN20	>0.46 reworking					
8H-2, 30-30	63.60	63.60	NN19	>0.46 reworking					
8H-CC, 20-25	70.02	70.02	NN19	0.46-0.88	*T. lentiginosa* Subzone a	0.42-0.65			
9H-CC, 15-20	80.24	80.24	NN19	0.46-0.88	*T. lentiginosa* Subzone a	0.42-0.65			
10H-CC, 15-20	88.25	88.25	NN19	0.46-0.88	*A. ingens* Subzone c	0.65-1.07	?	>0.46	
11H-CC, 9-14	99.09	99.09	NN19	0.46-0.88	*A. ingens* Subzone c	0.65-1.07			
12H-CC, 8-13	108.43	108.43	NN19	0.46-0.88?	*A. ingens* Subzone c	0.65-1.07			

Table T11 (continued).

Core, section, interval (cm)	Depth (mbsf)	Depth (mcd)	Calcareous nannofossil zone	Calcareous nannofossil age (Ma)	Diatom zone	Diatom age (Ma)	Radiolaria zone	Radiolaria age (Ma)	Comment
13H-4, 30-30	114.40	114.40	NN19	>0.88					
13H-4, 130-130	115.10	115.10	NN19	>0.88					
13H-CC, 0-8	117.90	117.90	NN19	0.88-0.96	*A. ingens* Subzone c	0.65-1.07			
14H-CC, 14-19	127.14	127.14	NN19	0.88-0.96	*A. ingens* Subzone c	0.65-1.07	?	>0.46	
15H-CC, 0-5	136.68	136.68	NN19	<0.96	*A. ingens* Subzone c	0.65-1.07			
16H-5, 130-130	145.10	145.10	NN19	<0.96					
16H-6, 30-30	145.60	145.60	NN19	<0.96					
16H-CC, 12-17	146.40	146.40	NN19	<0.96	*A. ingens* Subzone c	0.65-1.07			
17H-2, 120-120	150.00	161.26	NN19	0.96-1.08					
17H-4, 120-120	153.00	153.00	NN19	<1.08					
17H-5, 30-30	153.60	153.60	NN19	>1.08					
17H-CC, 18-23	155.28	155.28	NN19	>1.08	*A. ingens* Subzone b	1.07-1.3			
18H-CC, 13-18	165.39	165.39	NN19	1.08-1.24	*A. ingens* Subzone b	1.07-1.3	?	>0.46	
19H-5, 120-120	173.50	185.34	NN19	>1.24					
19H-CC, 16-21	175.33	175.33		Barren	*A. ingens* Subzone b	1.07-1.3			
20H-6, 30-30	183.60	183.60	NN19	<1.46					
20H-CC, 0-10	185.15	185.15		Barren	*A. ingens* Subzone b	1.07-1.3			
21H-CC, 11-16	194.21	194.21	NN19	>1.46? (~barren)	*A. ingens* Subzone a	1.3-1.8			
22H-2, 130-130	197.60	197.60	NN19	>1.46					
22H-CC, 0-5	204.30	204.30	NN19	Barren	early *A. ingens* Subzone a	1.5-1.8	?	>0.46	
23H-1, 30-30	204.60	204.60	NN19	<1.69					
23H-2, 30-30	206.10	206.10	NN19	>1.69					
23H-CC, 0-8	213.65	213.65		Barren	early *A. ingens* Subzone a	1.5-1.8			
24H-CC, 23-28	223.43	223.43	NN18	>1.95	*P. barboi*	1.8-2.0			
25H-CC, 14-19	232.78	232.78	NN18	>1.95	*T. kolbei/F.matuyama*	2.0-2.5			
26H-CC, 11-16	242.01	242.01		Barren	*T. kolbei/F.matuyama*	2.0-2.5	?	>0.46	
27H-CC, 45-53	250.79	250.79		Barren	*T. kolbei/F.matuyama*	2.0-2.5			
28H-CC, 25-30	257.84	257.84		Barren	?*T. kolbei/F.matuyama*	2.0-2.5			No age-indicative diatom taxa
29H-CC, 62-67	264.91	264.91		Barren	?*T. kolbei/F.matuyama*	2.0-2.5	?	close to 2.61	No age-indicative diatom taxa
177-1089C-									
1H-CC, 8-13	2.38	2.38	NN21	0-0.26	*T. lentiginosa* Subzone c	0-0.18			
2H-CC, 0-8	9.37	9.37	NN21	0-0.26	*T. lentiginosa* Subzone c	0-0.18			
3H-1, 110-110	15.00	15.00	NN21		*T. lentiginosa* Subzone c	0-0.18			Warm-water diatom assemblage: MIS 5.1
3H-CC, 9-14	17.42	17.42	NN21	0-0.26	*T. lentiginosa* Subzone c	0-0.18	Omega/*B. aquilonalis*	0-0.46	
4H-1, 10-10	23.50	23.50	NN21		*T. lentiginosa* Subzone c	0-0.18			Warm-water diatom assemblage: MIS 5.5
4H-3, 10-10	26.50	26.50	NN21		*T. lentiginosa* Subzone b	0.18-0.42			Cold-water diatom assemblage: MIS 6
4H-5, 90-90	30.30	30.30	NN21		*T. lentiginosa* Subzone b	0.18-0.42			Warm-water diatom assemblage: MIS 7
4H-CC, 10-15	31.78	31.78	NN21	<0.26?	*T. lentiginosa* Subzone b	0.18-0.42			
5H-1, 10-10	33.00	33.00	?		*T. lentiginosa* Subzone b	0.18-0.42			Warm-water diatom assemblage: MIS 7
5H-1, 90-90	33.80	33.80			*T. lentiginosa* Subzone b	0.18-0.42			Warm-water diatom assemblage: MIS 7
5H-3, 10-10	36.00	36.00			*T. lentiginosa* Subzone b	0.18-0.42			Warm-water diatom assemblage: MIS 7
5H-CC, 10-15	40.91	40.91	NN20	0.26-0.46	*T. lentiginosa* Subzone b	0.18-0.42	Omega/*B. aquilonalis*	0-0.46	
6H-2, 10-10	44.00	44.00	NN20		*T. lentiginosa* Subzone b	0.18-0.42			Warm-water diatom assemblage: MIS 9
6H-3, 60-60	46.00	46.00	NN20		*T. lentiginosa* Subzone b	0.18-0.42			Warm-water diatom assemblage: MIS 9
6H-4, 10-10	47.00	47.00	NN20		*T. lentiginosa* Subzone b	0.18-0.42			Warm-water diatom assemblage: MIS 9
6H-CC, 9-14	51.46	51.46	NN20	0.26-0.46	*T. lentiginosa* Subzone b	0.18-0.42	?	>0.46	
7H-1, 10-10	52.00	52.00	NN20		*T. lentiginosa* Subzone b	0.18-0.42			Warm-water diatom assemblage: MIS 11
7H-2, 60-60	54.00	54.00	NN20		*T. lentiginosa* Subzone b	0.18-0.42			Warm-water diatom assemblage: MIS 11
7H-3, 110-110	56.00	56.00	NN20		*T. lentiginosa* Subzone b	0.18-0.42			Warm-water diatom assemblage: MIS 11
7H-5, 10-10	58.00	58.00	NN20		*T. lentiginosa* Subzone b	0.18-0.42			Warm-water diatom assemblage: MIS 11
7H-6, 60-60	60.00	60.00	NN20		*T. lentiginosa* Subzone b	0.18-0.42			Warm-water diatom assemblage: MIS 11

Table T11 (continued).

Core, section, interval (cm)	Depth (mbsf)	Depth (mcd)	Calcareous nannofossil zone	Calcareous nannofossil age (Ma)	Diatom zone	Diatom age (Ma)	Radiolaria zone	Radiolaria age (Ma)	Comment
7H-CC, 0-10	60.81	60.81	NN20	0.26-0.46	*T. lentiginosa* Subzone a	0.42-0.65	?	>0.46	
8H-CC, 0-10	70.34	70.34	NN19	0.46-0.88	*T. lentiginosa* Subzone a	0.42-0.65			
9H-5, 121-121	78.00	78.00	NN19		*T. lentiginosa* Subzone a	0.42-0.65			Warm-water diatom assemblage
9H-7, 60-60	80.00	80.00	NN19		*T. lentiginosa* Subzone a	0.42-0.65			
9H-CC, 7-12	80.10	80.10	NN19	0.46-0.88	*T. lentiginosa* Subzone a	0.42-0.65			
10H-2, 10-10	82.00	82.00	NN19		*T. lentiginosa* Subzone a	0.42-0.65			Cold-water diatom assemblage: MIS 16
10H-3, 60-60	84.00	84.00	NN19		*A. ingens* Subzone c	0.65-1.07			Cold-water diatom assemblage: MIS 16
10H-4, 110-110	86.00	86.00	NN19		*A. ingens* Subzone c	0.65-1.07			Warm-water diatom assemblage: MIS 17
10H-CC, 5-5	88.04	88.04	NN19		*A. ingens* Subzone c	0.65-1.07			Warm-water diatom assemblage: MIS 17
10H-CC, 18-23	88.08	88.08	NN19	0.46-0.88	*A. ingens* Subzone c	0.65-1.07			
11H-CC, 13-18	99.16	99.16	NN19	0.46-0.88	*A. ingens* Subzone c	0.65-1.07	?	>0.46	
12H-CC, 10-15	107.43	107.43	NN19	<0.88	*A. ingens* Subzone c	0.65-1.07			
13H-CC, 0-10	117.42	117.42	NN19	0.88-0.96	*A. ingens* Subzone c	0.65-1.07			
14H-CC, 9-14	126.55	126.55	NN19	0.88-0.96	*A. ingens* Subzone c	0.65-1.07			
15H-CC, 21-26	135.76	135.76	NN19	0.88-0.96	*A. ingens* Subzone c	0.65-1.07	?	>0.46	
16H-CC, 10-15	146.80	146.80	NN19	0.96-1.08	*A. ingens* Subzone c	0.65-1.07			
17H-CC, 11-16	156.33	156.33	NN19	1.08-1.24	*A. ingens* Subzone b	1.07-1.3			
18H-CC, 0-3	165.57	165.57	NN19	1.08-1.24	*A. ingens* Subzone b	1.07-1.3			
19H-CC, 22-27	169.56	169.56	NN19	Barren	*A. ingens* Subzone b	1.07-1.3	?	>0.46	
20H-CC, 46-51	184.01	184.01	NN19	1.24-1.46	*A. ingens* Subzone b	1.07-1.3			
21H-CC, 19-24	190.84	190.84	NN19	1.24-1.46	*A. ingens* Subzone b	1.3-1.8	?	>0.46	
20H-CC, 46-51	184.01	184.01	NN19	1.24-1.46	*A. ingens* Subzone b	1.07-1.3			
21H-CC, 19-24	190.84	190.84	NN19	1.24-1.46	*A. ingens* Subzone a	1.3-1.8	?	>0.46	
177-1089D-									
1H-CC, 5-13	6.62	6.62	NN21	0-0.26	*T. lentiginosa* Subzone c	0-0.18	Omega/*B. aquilonalis*	0-0.46	
2H-CC, 8-13	15.29	15.29	NN21	0-0.26	*T. lentiginosa* Subzone c	0-0.18			
3H-CC, 7-12	22.51	22.51	NN21	0-0.26	*T. lentiginosa* Subzone c	0-0.18			
4H-CC, 0-10	32.56	32.56		Barren	*T. lentiginosa* Subzone b	0.18-0.42			
5H-CC, 0-5	42.07	42.07	NN20	0.26-046	*T. lentiginosa* Subzone b	0.18-0.42	Omega/*B. aquilonalis*	0-0.46	
6H-CC, 24-29	51.42	51.42	NN20	0.26-046?	*T. lentiginosa* Subzone b	0.18-0.42	Omega/*B. aquilonalis*	0-0.46	
7H-CC, 0-10	61.06	61.06	NN20	0.26-046?	*T. lentiginosa* Subzone a	0.42-0.65		>0.46	
8H-CC, 5-10	70.72	70.72	NN19	0.46-0.88	*T. lentiginosa* Subzone a	0.42-0.65			
9H-CC, 0-10	79.70	79.70	NN19	0.46-0.88	*T. lentiginosa* Subzone a	0.42-0.65	?	>0.46	
10H-CC, 0-5	89.72	89.72	NN19	0.46-0.88	*A. ingens* Subzone c	0.65-1.07			
11H-CC, 0-10	98.00	98.00	NN19	0.46-0.88	*A. ingens* Subzone c	0.65-1.07			
12H-CC, 13-18	108.44	108.44	NN19	disolved	*A. ingens* Subzone c	0.65-1.07			
13H-CC, 0-5	118.07	118.07	NN19	0.88-0.96	*A. ingens* Subzone c	0.65-1.07	?	>0.46	

Notes: MIS = marine isotopic stage; RWK = reworking. This table is also available in ASCII format in the **TABLES** directory.

Table T12. Distribution of the main components of the radiolarian assemblage at Site 1089. (See table note. Continued on next two pages.)

Core, section, interval (cm)	Depth (mbsf)	Depth (mcd)	Abundance	Preservation	*Acanthodesmia vinculata*	*Actinomma glownini*	*Actinomma leptodermum*	*Amphyrhopalum ypsilon*	*Antarctissa denticulata*	*Antarctissa strelkovi*	*Antarctissa* sp.	*Anthocyrtidium* spp.	*Axoprunum bispiculum*	*Ceratocyrtis* spp.	*Cycladophora bicornis*	*Cycladophora davisiana*	*Cycladophora davisiana cornutoides*	*Cycladophora pliocenica*	*Cyrtocapsella longithorax*	*Dictyocoryne truncatum*	*Dictyomitrella* sp.	*Dictyophimus crisiae*	*Didymocyrtis tetrathalamus*	*Euchitonia elegans*	*Eucyrtidium calvertense*	*Eucyrtidium teuscheri*	*Gondwanaria dogieli*	*Lamprocyclas aegles*	*Lamprocyrtis heteroporos*	*Lamprocyrtis neoheteroporos*	*Lamprocyrtis nigriniae*	*Lithelius nautiloides*	*Lithocampe* spp.	*Lithopera bacca*	*Lophophaena hispida*	*Prunopyle antarctica*	*Prunopyle titan*	*Pterocanium praetextum*	*Pterocanium trilobum*	*Pterocorys* spp.	*Saccospyris antarctica*	*Saturnalis circularis*	*Spongaster tetras*	*Spongodiscus osculosus*	*Spongoplegma antarcticum*	*Spongotrochus glacialis*	*Spongurus pylomaticus*	*Stichocorys peregrina*	*Stylatractus universus*	*Tetrapyle octacantha*	*Theocorythium trachelium dianae*	*Theocorythium trachelium trachelium*
177-1089A-																																																	
1H-CC, 17-22	7.27	7.03																																																
2H-CC, 16-21	16.9	16.48																																															
3H-CC, 13-18	21.18	24.02																																															
4H-CC, 22-27	30.66	35.04	A	E				F	F			C	F			C		C				C	F	F				F			C			F		F		C				C	F	C
5H-CC, 14-19	43.36	44.32	A	E				F	F			C	F			C		F				F	F	F				F			C			F		F	F	C	F	F		C	F	C
6H-CC, 18-23	52.25	54.13	A	E				F	F			C	F		F	C	F	F		F		F	F	F				F			C	F		F		F	R	C	F	F		C	F	C
7H-CC, 51-56	63.4	67.54	A	E				F	F			C	F		F	C		F				F	F	F				F			C	F		F		F		C	F	F	R	C	F	C
8H-CC, 9-14	74.03	78.8	A	E	F			F	F			C		F	R	C		F		F		F	F		F		R	F	F		C			F		F	F	C			F	F	C		F
9H-CC, 10-15	75.24	81.42																																														
10H-CC, 0-5	92.97	97.5																																														
11H-CC, 53-58	97.9	103.69																																														
12H-CC, 0-5	111.59	117.38	A	E				F	F			C	F			C		F		F		F	F		F			F					F			F	F	C			F	F	F			F	F	F
13H-CC, 0-5	111.8	111.8																																														
14H-CC, 11-16	130.07	135.86																																														
15H-CC, 21-26	136.7	142.49																																														
16H-CC, 9-14	149.24	156.66	A	E				F	F	R		F		R	F	C		F		F		F	F		F			F					C			R		F	F	C	F	F			F		F
17H-CC, 0-8	149.8	149.8																																														
18H-CC, 21-26	166.22	174.18																																														
19H-CC, 0-10	177.69	185.7																																														
20H-CC, 13-23	187.53	195.35	A	E	F			F	R			F				C		F		F		F						F					F		F			C		F			R			C	F	
21H-CC, 21-26	195.09	208.71																																														
23H-CC, 31-41	215.29	227.59																																														
177-1089B-																																																
2H-CC, 10-15	13.67	19.37	A	E	R			F	F					R	F	C		F		F		F	F				F	F			F						F		C		F	F	F			F		F
3H-CC, 8-16	23.12	28.56																																														
4H-CC, 12-17	32.42	38.02																																														
5H-CC, 16-21	41.9	46.36																																														
6H-CC, 11-16	51.18	57.38	A	E	F				F			C	F		F	C		F		F		F	F		F	F			F	R			C	F			F	C	F	F	R	F			F	F	C
7H-CC, 8-14	60.73	68.15	A	E					F			F	F		R	C		F				F	F		F								F			F	C	F	F		F	R		R	F	F	C
8H-CC, 20-25	70.02	78.07																																														
9H-CC, 15-20	80.24	89.61																																														
10H-CC, 15-20	88.25	99.51	A	E	F							F	F			C		F				F	F		F								F			F	C	F	F	R	F		R		R	C	F	C
11H-CC, 9-14	99.09	110.35																																														
12H-CC, 8-13	108.43	119.69																																														
13H-CC, 0-8	117.9	129.16																																														
14H-CC, 14-19	127.14	138.4	A	E					R			F				C		F			R	F	F						F								F	C	F	F		F			F	R	C	F	F
15H-CC, 0-5	136.68	147.94																																														
16H-CC, 12-17	146.4	157.66																																														

Table T12 (continued).

Core, section, interval (cm)	Depth (mbsf)	Depth (mcd)	Abundance	Preservation	*Acanthodesmia vinculata*	*Actinomma glownini*	*Actinomma leptodermum*	*Amphyrhopalum ypsilon*	*Antarctissa denticulata*	*Antarctissa strelkovi*	*Antarctissa* sp.	*Anthocyrtidium* spp.	*Axoprunum bispiculum*	*Ceratocyrtis* spp.	*Cycladophora bicornis*	*Cycladophora davisiana*	*Cycladophora davisiana cornutoides*	*Cycladophora pliocenica*	*Cyrtocapsella longithorax*	*Dictyocoryne truncatum*	*Dictyomitrella* sp.	*Dictyophimus crisiae*	*Didymocyrtis tetrathalamus*	*Euchitonia elegans*	*Eucyrtidium calvertense*	*Eucyrtidium teuscheri*	*Gondwanaria dogieli*	*Lamprocyclas aegles*	*Lamprocyrtis heteroporos*	*Lamprocyrtis neoheteroporos*	*Lamprocyrtis nigriniae*	*Lithelius nautiloides*	*Lithocampe* spp.	*Lithopera bacca*	*Lophophaena hispida*	*Prunopyle antarctica*	*Prunopyle titan*	*Pterocanium praetextum*	*Pterocanium trilobum*	*Pterocorys* spp.	*Saccospyris antarctica*	*Saturnalis circularis*	*Spongaster tetras*	*Spongodiscus osculosus*	*Spongoplegma antarcticum*	*Spongotrochus glacialis*	*Spongurus pylomaticus*	*Stichocorys peregrina*	*Stylatractus universus*	*Tetrapyle octacantha*	*Theocorythium trachelium dianae*	*Theocorythium trachelium trachelium*
17H-CC, 18-23	155.28	166.54																																															
18H-CC, 13-18	165.39	176.65	A	E			F		R			F			F	C		F				F	F			F						F	C				F					F			F	F	C
19H-CC, 16-21	175.33	187.17																																															
20H-CC, 0-10	185.15	197.83																																															
21H-CC, 11-16	194.21	209.31																																															
22H-CC, 0-5	204.3	219.4	A	E			F		F			F				C		F		F		F	F		F															C		F			F	F	F
23H-CC, 0-8	213.65	228.75																																														
24H-CC, 23-28	223.43	238.53																																															
25H-CC, 14-19	232.78	247.88																																															
26H-CC, 11-16	242.01	257.11	A	E												C	F	F					F		F	F		F				F	F												F	F	F
27H-CC, 45-53	250.79	265.89																																															
28H-CC, 25-30	257.84	272.94																																															
29H-CC, 62-67	264.91	279.65	A	E								F	F			R	F	F					F		F				F	R		F	F			C				F		F						
177-1089C-																																																	
1H-CC, 8-13	2.38	2.08																																															
2H-CC, 0-8	9.37	12.61																																															
3H-CC, 9-14	17.42	21.84	A	E	F				F			F			F	C		F					F	F	F				F					F	F		F	F	C	F	F	F			C	F	C
4H-CC, 10-15	31.78	35.36																																														
5H-CC, 10-15	40.91	44.33	A	E								F	F			C							F						F	F						F	F	C	F	F						F
6H-CC, 9-14	51.46	53.52	A	E					F			F	F		F	C	F	F		F		F	F	F				F					F	F	F	C		F			F			F		F
7H-CC, 0-10	60.81	64.33	A	E								F	F			C	F	R					F											F			C		F			F	F	F		F	F
8H-CC, 0-10	70.34	74.21																																														
9H-CC, 7-12	80.1	84.48																																															
10H-CC, 18-23	88.08	94.57																																															
11H-CC, 13-18	99.16	108.05	A	E					F			F				C	F	F					F	F	F								F			C	F	F			F					F
12H-CC, 10-15	107.43	116.32																																														
13H-CC, 0-10	117.42	126.31																																															
14H-CC, 9-14	126.55	135.44																																															
15H-CC, 21-26	135.76	144.65	A	E					F			F	F			C		F		F			F	F											F			C	F	F	F			F		F
16H-CC, 10-15	146.8	157.45																																															
17H-CC, 11-16	156.33	169.44																																															
18H-CC, 0-3	165.57	178.68																																															
19H-CC, 22-27	169.56	183.55	A	E						F		F	F			C		F			R															F	F					F			F		
20H-CC, 46-51	184.01	194.6																																															
21H-CC, 19-24	190.84	202.05	A	E									F			C	F	F					F	F	F			F	F		R		F			F		F							C		F
177-1089D-																																																
1H-CC, 5-13	6.62	5.98	A	E		R		F	F			F	F	F		C	F	F					F	F					F	F								F			C				F	F	C
2H-CC, 8-13	15.29	12.41																																														
3H-CC, 7-12	22.51	22.33																																															
4H-CC, 0-10	32.56	31.66																																															
5H-CC, 0-5	42.07	38.97	A	E					F				F	F	F	C	F	F					F			F	F	F										C	F		F		F		F		C

Table T12 (continued).

Core, section, interval (cm)	Depth (mbsf)	Depth (mcd)	Abundance	Preservation	*Acanthodesmia vinculata*	*Actinomma glownini*	*Actinomma leptodermum*	*Amphyrhopalum ypsilon*	*Antarctissa denticulata*	*Antarctissa strelkovi*	*Antarctissa* sp.	*Anthocyrtidium* spp.	*Axoprunum bispiculum*	*Ceratocyrtis* spp.	*Cycladophora bicornis*	*Cycladophora davisiana*	*Cycladophora davisiana cornutoides*	*Cycladophora pliocenica*	*Cyrtocapsella longithorax*	*Dictyocoryne truncatum*	*Dictyomitrella* sp.	*Dictyophimus crisiae*	*Didymocyrtis tetrathalamus*	*Euchitonia elegans*	*Eucyrtidium calvertense*	*Eucyrtidium teuscheri*	*Gondwanaria dogieli*	*Lamprocyclas aegles*	*Lamprocyrtis heteroporos*	*Lamprocyrtis neoheteroporos*	*Lamprocyrtis nigriniae*	*Lithelius nautiloides*	*Lithocampe* spp.	*Lithopera bacca*	*Lophophaena hispida*	*Prunopyle antarctica*	*Prunopyle titan*	*Pterocanium praetextum*	*Pterocanium trilobum*	*Pterocorys* spp.	*Saccospyris antarctica*	*Saturnalis circularis*	*Spongaster tetras*	*Spongodiscus osculosus*	*Spongoplegma antarcticum*	*Spongotrochus glacialis*	*Spongurus pylomaticus*	*Stichocorys peregrina*	*Stylatractus universus*	*Tetrapyle octacantha*	*Theocorythium trachelium dianae*	*Theocorythium trachelium trachelium*
6H-CC, 24-29	51.42	49.8	A	E					F				F		F	C		F					F							F			F					C	F		F		F					F		C
7H-CC, 0-10	61.06	60	A	E					F				F		F	C		F					F										F			F	F	F				C	F	F				C	F	F
8H-CC, 5-10	70.72	70.69																																																		
9H-CC, 0-10	79.7	83.43	A	E					F			F	F			C	F	F	R			F	F		F			F					F	F			F	F			C			F	F					F		F
10H-CC, 0-5	89.72	97.24																																																		
11H-CC, 0-10	98	105.52																																																		
12H-CC, 13-18	108.44	115.96																																																		
13H-CC, 0-5	118.07	125.59	A	E					F			F	F			C		F		F			F									F	F					F			C				F	F				F		F

Notes: Abundance abbreviations: A = abundant, C = common, F = few, R = rare. Preservation abbreviation: E = excellent. For more specific definitions, refer to the **"Explanatory Notes"** chapter. This table is also available in ASCII format in the **TABLES** directory.

Table T13. Preliminary positions of polarity chron boundaries at Site 1089.

Interpreted boundary	Sample Top (cm)	Sample Bottom (cm)	Depth Top (mbsf)	Depth Bottom (mbsf)	Depth Mean (mbsf)	Depth Top (mbsf)	Depth Bottom (mbsf)	Depth Mean (mbsf)	Age (Ma)	Comment
	177-1089B-	177-1089B-								
C1n (Brunhes)	12H-4, 65	13H-4, 20	105	114	110	116.26	125.26	121.26	0.78	No clear transition
C1r.1n (Jaramillo) bottom	17H-3, 130	17H-5, 30	151.6	153.6	152.6	162.86	154.86	153.86	1.07	
C2n (Olduvai) top	23H-7, 50	24H-2, 50	213.8	215.8	214.8	228.9	230.9	229.9	1.77	
C2n (Olduvai) bottom	25H-2, 65	25H-3, 135	225.45	227.65	226.5	240.55	242.75	241.6	1.95	

Table T14. Concentrations of methane, ethane, and propane obtained by the headspace technique at Site 1089.

Core, section, interval (cm)	Depth (mbsf)	C_1 (ppmv)	C_2 (ppmv)	C_3 (ppmv)	C_1/C_2
177-1089A-					
1H-4, 0-5	4.53	6		1	
2H-5, 0-5	13.32	6			
3H-3, 0-5	19.82	11			
4H-2, 0-5	27.82	30			
5H-4, 0-5	40.33	40			
6H-4, 0-5	49.82	1740			
8H-5, 0-5	70.32	19,434			
10H-5, 0-5	89.32	23,858			
12H-5, 0-5	108.32	30,443			
14H-5, 0-5	127.32	25,493			
15H-3, 0-5	133.82	27,403			
16H-5, 0-5	146.33	24,053			
18H-4, 0-5	163.83	37,026	1		37,026
19H-5, 0-5	174.82	27,050	1		27,050
20H-5, 0-5	184.32	18,635			
21H-4, 0-5	192.32	23,318	1		23,318
23H-5, 0-5	212.82	20,248			
177-1089B-					
22H-5, 0-5	200.82	19,241	1		19,241
23H-4, 0-5	208.82	26,943	1		26,943
24H-5, 0-5	219.82	27,819	1		27,819
25H-5, 0-5	229.32	17,698	1		17,698
26H-5, 0-5	238.82	12,650	1		12,650
27H-5, 0-5	248.32	8,991			
28H-4, 0-5	256.30	10,746			
29H-2, 0-5	259.40	7,579			

Note: C_1 = methane, C_2 = ethane, C_3 = propane.

Table T15. Interstitial water chemistry from shipboard measurements at Site 1089. (Continued on next page).

Core, section, interval (cm)	Depth (mbsf)	pH	Method	Alkalinity (mM)	Method	Salinity	Method	Cl (mM)	Method	SO_4 (mM)	Method	Na (mM)	Method	Mg (mM)	Method	Ca (mM)	Method
177-1089A-																	
1H-3, 145-150	4.45	8.01	ISE	10.314	T	34.5	R	555	T	22.7	I	481	CB	51.1	I	7.9	I
2H-4, 145-150	13.25	7.80	ISE	18.916	T	34.5	R	555	T	14.5	I	481	CB	49.8	I	5.3	I
3H-2, 145-150	19.75	8.04	ISE	26.541	T	34.5	R	558	T	9.8	I	484	CB	50.2	I	3.8	I
4H-1, 140-150	27.70	8.06	ISE	33.701	T	34.5	R	562	T	5.6	I	488	CB	50.0	I	3.5	I
5H-3, 145-150	40.25	7.95	ISE	39.958	T	34.5	R	560	T	1.8	I	490	CB	48.4	I	2.8	I
6H-3, 145-150	49.75	8.13	ISE	42.062	T	34.5	R	561	T	0.4	I	491	CB	48.9	I	1.9	I
8H-4, 140-150	70.20	7.77	ISE	46.710	T	34.5	R	558	T	0.2	I	488	CB	50.3	I	2.7	I
10H-4, 140-150	89.20	7.70	ISE	46.734	T	34.5	R	558	T	0.0	I	488	CB	50.3	I	2.7	I
12H-4, 140-150	108.20	7.66	ISE	46.477	T	34.5	R	561	T	0.0	I	492	CB	48.6	I	3.3	I
14H-4, 140-150	127.20	7.64	ISE	45.436	T	34.0	R	560	T	0.3	I	498	CB	44.3	I	3.7	I
15H-2, 140-150	133.70	7.83	ISE	44.145	T	34.0	R	560	T	0.2	I	495	CB	45.7	I	3.6	I
16H-4, 140-150	146.20	7.40	ISE	42.839	T	34.0	R	560	T	0.1	I	494	CB	45.2	I	3.7	I
18H-3, 140-150	163.70	7.41	ISE	40.618	T	34.0	R	563	T	0.2	I	495	CB	44.4	I	4.5	I
19H-4, 140-150	174.70	7.85	ISE	41.634	T	34.0	R	560	T	0.0	I	496	CB	42.4	I	4.6	I
20H-4, 140-150	184.20	7.76	ISE	40.695	T	34.0	R	560	T	0.0	I	493	CB	42.7	I	5.3	I
21H-3, 140-150	192.20	7.84	ISE	40.030	T	34.0	R	560	T	0.3	I	498	CB	40.8	I	5.2	I
23H-4, 140-150	212.70	7.30	ISE	36.357	T	34.0	R	562	T	0.1	I	493	CB	41.5	I	5.7	I
177-1089B-																	
22H-4, 140-150	200.70	7.65	ISE	39.320	T	34.0	R	559	T	0.0	I	492	CB	41.7	I	6.1	I
23H-4, 140-150	210.20	7.59	ISE	36.541	T	34.0	R	562	T	0.3	I	493	CB	41.8	I	6.2	I
24H-4, 140-150	219.70	7.76	ISE	36.303	T	34.0	R	559	T	0.1	I	490	CB	40.8	I	6.6	I
25H-4, 140-150	229.20	7.56	ISE	37.264	T	34.0	R	560	T	0.0	I	492	CB	40.1	I	6.9	I
26H-4, 140-150	238.70	7.30	ISE	37.191	T	34.0	R	559	T	0.2	I	489	CB	41.1	I	7.8	I
27H-4, 140-150	248.20	7.77	ISE	36.980	T	34.0	R	562	T	0.0	I	495	CB	38.8	I	7.7	I
28H-3, 140-150	256.20	7.49	ISE	36.125	T	34.0	R	561	T	0.0	I	492	CB	39.3	I	8.8	I
29H-1, 140-150	259.30	7.59	ISE	34.931	T	33.0	R	560	T	0.7	I	492	CB	38.7	I	8.6	I

Note: Method abbreviations: ISE = ion selective electrode, T = titration, R = refractometer, I = ion chromatography, CB = charge balance calculation, S = spectrophotometry, AAS = atomic absorption spectrometry, AES = atomic emission spectrometry.

Table T15 (continued).

Core, section, interval (cm)	Depth (mbsf)	K (mM)	Method	H_4SiO_4 (mM)	Method	NH_4 (µM)	Method	HPO_4 (µM)	Method	Sr (µM)	Method	Fe (µM)	Method	Mn (µM)	Method	Li (µM)	Method
177-1089A-																	
1H-3, 145-150	4.45	12.2	I	752	S	667	S	67	S	81	AAS	6.4	AAS	69.0	AAS	23	AES
2H-4, 145-150	13.25	12.1	I	752	S	1308	S	95	S	76	AAS	7.6	AAS	46.0	AAS	24	AES
3H-2, 145-150	19.75	12.1	I	828	S	1705	S	119	S	75	AAS	8.2	AAS	24.5	AAS	24	AES
4H-1, 140-150	27.70	11.9	I	816	S	2021	S	146	S	90	AAS	7.4	AAS	21.0	AAS	24	AES
5H-3, 145-150	40.25	11.4	I	871	S	2492	S	184	S	111	AAS	6.2	AAS	19.0	AAS	24	AES
6H-3, 145-150	49.75	11.3	I	897	S	2508	S	190	S	133	AAS	4.8	AAS	9.0	AAS	24	AES
8H-4, 140-150	70.20	10.7	I	905	S	2922	S	172	S	157	AAS	3.6	AAS	21.0	AAS	32	AES
10H-4, 140-150	89.20	10.6	I	907	S	3238	S	146	S	169	AAS	14.0	AAS	15.5	AAS	39	AES
12H-4, 140-150	108.20	10.5	I	971	S	3449	S	121	S	180	AAS	16.9	AAS	14.5	AAS	50	AES
14H-4, 140-150	127.20	11.2	I	1005	S	3595	S	106	S	189	AAS	15.4	AAS	5.5	AAS	63	AES
15H-2, 140-150	133.70	10.5	I	998	S	3555	S	108	S	188	AAS	13.9	AAS	4.0	AAS	70	AES
16H-4, 140-150	146.20	10.7	I	1024	S	3636	S	95	S	188	AAS	19.9	AAS	6.0	AAS	84	AES
18H-3, 140-150	163.70	11.2	I	1148	S	3303	S	72	S	195	AAS	22.2	AAS	5.5	AAS	99	AES
19H-4, 140-150	174.70	11.0	I	1084	S	3546	S	64	S	198	AAS	11.4	AAS	5.5	AAS	117	AES
20H-4, 140-150	184.20	11.1	I	1139	S	3279	S	57	S	201	AAS	11.4	AAS	5.0	AAS	128	AES
21H-3, 140-150	192.20	10.5	I	1217	S	3133	S	49	S	203	AAS	14.3	AAS	6.0	AAS	142	AES
23H-4, 140-150	212.70	10.7	I	1084	S	3100	S	23	S	192	AAS	31.5	AAS	8.0	AAS	165	AES
177-1089B-																	
22H-4, 140-150	200.70	10.5	I	1131	S	3003	S	39	S	204	AAS	15.0	AAS	6.5	AAS	158	AES
23H-4, 140-150	210.20	10.2	I	1093	S	3108	S	28	S	195	AAS	12.6	AAS	7.5	AAS	171	AES
24H-4, 140-150	219.70	10.5	I	1198	S	2938	S	48	S	201	AAS	26.2	AAS	6.0	AAS	186	AES
25H-4, 140-150	229.20	10.7	I	1227	S	2857	S	44	S	204	AAS	20.3	AAS	6.5	AAS	201	AES
26H-4, 140-150	238.70	9.7	I	1301	S	2760	S	36	S	207	AAS	19.4	AAS	7.5	AAS	213	AES
27H-4, 140-150	248.20	10.5	I	1253	S	2962	S	46	S	201	AAS	28.9	AAS	7.5	AAS	232	AES
28H-3, 140-150	256.20	9.1	I	1229	S	2435	S	39	S	209	AAS	8.0	AAS	14.0	AAS	255	AES
29H-1, 140-150	259.30	9.6	I	1026	S	2532	S	35	S	189	AAS	15.0	AAS	17.0	AAS	245	AES

Table T16. Concentrations of inorganic carbon, calculated calcium carbonate, total carbon, total organic carbon, total nitrogen, total sulfur, and TOC/TN at Site 1089. (Continued on next three pages.)

Core, section, interval (cm)	Depth (mbsf)	IC (wt%)	$CaCO_3$ (wt%)	TC (wt%)	TOC (wt%)	TN (wt%)	TS (wt%)	TOC/TN
177-1089A-								
1H-1, 76-77	0.76	5.43	45.2					
1H-2, 71-72	2.21	6.07	50.6					
1H-3, 74-75	3.74	4.33	36.0					
1H-4, 72-73	5.22	3.70	30.8					
1H-5, 54-55	6.54	5.07	42.2					
2H-2, 109-110	9.89	5.56	46.3					
2H-3, 122-123	11.52	2.47	20.6					
2H-4, 70-71	12.50	2.41	20.1					
2H-5, 121-123	14.51	5.52	46.0					
2H-6, 69-70	15.49	2.67	22.2					
2H-7, 22-23	16.52	3.31	27.6					
3H-1, 120-121	18.00	7.31	60.9					
3H-2, 72-73	19.02	6.35	52.9					
3H-3, 69-70	20.49	5.96	49.6					
4H-1, 80-81	27.10	1.73	14.4					
4H-2, 22-23	28.02	4.88	40.6					
4H-3, 73-74	29.78	0.99	8.2					
5H-1, 66-67	36.46	5.68	47.3					
5H-2, 70-71	38.00	0.67	5.6					
5H-3, 70-71	39.50	0.23	1.9					
5H-4, 74-75	41.04	4.78	39.9					
5H-5, 70-71	42.50	0.96	8.0					
6H-3, 69-70	48.99	3.79	31.6					
6H-4, 68-69	50.48	5.14	42.9					
7H-1, 60-61	55.40	0.70	5.8					
7H-2, 60-61	56.90	2.19	18.3					
7H-3, 60-61	58.40	4.38	36.5					
7H-4, 60-61	59.66	8.33	69.3					
7H-5, 60-61	61.16	5.62	46.8					
7H-6, 60-61	62.37	4.15	34.6					
8H-1, 72-73	65.02	6.60	55.0					
8H-2, 72-73	66.52	2.52	21.0					
8H-3, 18-19	67.48	5.79	48.3					
8H-4, 72-73	69.52	3.90	32.5					
8H-5, 12-13	70.42	3.91	32.6					
8H-6, 122-123	73.02	1.82	15.2					
8H-7, 15-16	73.45	3.06	25.5					
9H-1, 60-61	74.40	1.78	14.8					
10H-1, 102-103	84.32	2.90	24.1					
10H-2, 100-101	85.80	2.27	18.9					
10H-3, 122-123	87.52	0.69	5.7					
10H-4, 122-123	89.02	6.38	53.1					
10H-5, 76-77	90.06	7.64	63.6					
10H-6, 72-73	91.52	5.68	47.3					
11H-1, 62-63	93.42	6.31	52.6					
11H-2, 76-77	94.82	3.08	25.7					
11H-3, 72-73	96.28	1.62	13.5					
12H-1, 73-74	103.03	0.95	7.9					
14H-2, 90-91	123.70	0.07	0.6					
14H-3, 110-111	125.40	5.97	49.7					
14H-4, 122-123	127.02	0.56	4.7					
14H-5, 71-72	128.01	5.95	49.5					
14H-6, 80-81	129.60	3.61	30.0					
15H-1, 98-99	131.78	2.34	19.5					
15H-2, 70-71	133.00	1.69	14.0					
15H-3, 71-72	134.51	6.64	55.3					
15H-4, 71-72	136.01	0.68	5.7					
16H-1, 76-77	141.06	4.52	37.6					
16H-5, 22-23	146.52	5.60	46.6					
16H-6, 64-65	148.44	1.63	13.6					
18H-1, 82-83	160.12	0.68	5.7					
18H-2, 72-73	161.52	0.73	6.1					
18H-3, 72-73	163.02	0.23	1.9					
18H-4, 130-131	165.10	0.95	7.9					
18H-5, 42-43	165.72	1.15	9.6					
19H-1, 124-125	170.04	3.63	30.2					
19H-2, 70-71	171.00	0.12	1.0					
19H-3, 72-73	172.52	6.33	52.7					
19H-4, 71-72	174.01	0.99	8.2					
19H-5, 76-77	175.56	2.33	19.4					
19H-6, 76-77	177.06	6.24	52.0					
20H-1, 76-77	179.06	0.98	8.2					

Table T16 (continued).

Core, section, interval (cm)	Depth (mbsf)	IC (wt%)	$CaCO_3$ (wt%)	TC (wt%)	TOC (wt%)	TN (wt%)	TS (wt%)	TOC/TN
20H-2, 140-141	181.20	4.23	35.3					
20H-3, 122-123	182.52	0.13	1.1					
20H-4, 76-77	183.56	0.12	1.0					
20H-5, 76-77	185.06	0.10	0.9					
20H-6, 52-53	186.32	4.92	40.9					
21H-1, 102-103	188.82	0.24	2.0					
21H-2, 76-77	190.06	4.78	39.8					
21H-3, 76-77	191.56	0.18	1.5					
21H-4, 76-77	193.06	0.32	2.7					
23H-1, 72-73	207.52	0.39	3.2					
23H-2, 72-73	209.02	4.64	38.6					
23H-3, 72-73	210.52	2.04	17.0					
23H-4, 72-73	212.02	4.82	40.1					
23H-5, 72-73	213.52	0.94	7.8					
177-1089B-								
1H-1, 74-75	0.74	6.20	51.6	6.45	0.25	0.12	0.14	2.1
1H-2, 74-75	2.24	2.93	24.4					
1H-3, 121-122	3.83	3.89	32.4					
2H-1, 91-92	5.71	2.24	18.7					
2H-2, 76-77	7.06	1.47	12.2	1.73	0.26	0.14	0.11	1.9
2H-3, 71-72	8.51	5.28	44.0					
2H-4, 71-72	10.01	3.03	25.2					
2H-5, 71-72	11.51	3.60	30.0					
2H-6, 71-72	13.01	1.62	13.5	1.68	0.06	0.12	0.00	0.5
3H-1, 121-122	15.51	6.30	52.5					
3H-2, 70-71	16.50	5.59	46.6					
3H-3, 70-71	18.00	5.86	48.8	6.14	0.28	0.10	0.00	2.7
3H-4, 70-71	19.50	4.12	34.3					
3H-5, 70-71	21.00	5.66	47.1					
3H-6, 70-71	22.50	5.10	42.5					
4H-1, 70-71	24.50	0.07	0.5	0.58	0.51	0.12	0.17	4.3
4H-2, 70-71	26.00	2.42	20.2					
4H-3, 70-71	27.50	1.20	10.0	1.83	0.64	0.14	0.66	4.6
4H-4, 70-71	29.00	1.30	10.8					
4H-5, 70-71	30.50	6.49	54.0					
4H-6, 70-71	32.00	6.12	51.0					
5H-2, 70-71	35.50	0.64	5.4	1.46	0.82	0.15	0.37	5.4
5H-3, 70-71	37.00	1.65	13.8					
5H-4, 70-71	38.50	2.02	16.8	2.75	0.73	0.13	0.66	5.7
5H-5, 70-71	40.00	0.08	0.6					
5H-6, 70-71	41.50	0.06	0.5					
6H-1, 98-99	43.78	4.44	37.0					
6H-2, 72-73	45.02	5.06	42.2					
6H-3, 72-73	46.52	5.41	45.1	5.48	0.07	0.11	0.09	0.6
6H-4, 119-120	48.49	3.29	27.4	4.00	0.71	0.15	0.08	4.9
6H-5, 72-73	49.52	4.81	40.1					
6H-6, 33-34	50.63	1.97	16.4					
7H-1, 75-76	53.05	0.97	8.1					
7H-2, 75-76	54.55	1.92	16.0	2.29	0.37	0.12	0.00	3.2
7H-3, 75-76	56.05	7.69	64.1					
7H-4, 75-76	57.55	6.11	50.9					
7H-5, 75-76	59.05	3.31	27.6					
7H-6, 42-43	60.22	4.09	34.1	4.74	0.65	0.14	0.98	4.7
8H-1, 121-122	63.01	3.85	32.1					
8H-2, 76-77	64.06	4.35	36.2					
8H-3, 73-74	65.53	3.23	26.9					
8H-4, 76-77	67.06	3.83	31.9					
8H-5, 76-77	68.56	0.50	4.1	1.16	0.66	0.15	0.25	4.5
8H-6, 30-31	69.60	2.87	23.9					
9H-1, 76-77	72.06	3.62	30.1					
9H-2, 76-77	73.56	7.04	58.7					
9H-3, 76-77	75.06	4.89	40.8					
9H-4, 76-77	76.56	1.36	11.3					
9H-5, 76-77	78.06	0.09	0.7	0.54	0.46	0.13	0.26	3.6
9H-6, 76-77	79.56	2.60	21.7					
10H-1, 75-76	81.55	0.68	5.7	0.90	0.22	0.13	0.44	1.7
10H-2, 75-76	83.05	3.75	31.2					
10H-3, 75-76	84.55	7.45	62.1					
10H-4, 75-76	86.05	5.38	44.8	5.69	0.31	0.11	0.44	2.8
10H-5, 75-76	87.55	5.49	45.8					
11H-1, 76-77	91.06	1.91	15.9					
11H-2, 76-77	92.56	0.18	1.5	0.79	0.61	0.14	0.74	4.4
11H-3, 76-77	94.06	5.77	48.1					
11H-4, 72-73	95.52	6.54	54.5					
11H-5, 70-71	97.00	1.14	9.5					
11H-6, 60-61	98.40	1.80	15.0					
12H-1, 70-71	100.50	2.30	19.2					
12H-2, 70-71	102.00	0.65	5.4	1.42	0.77	0.16	0.73	4.8

Table T16 (continued).

Core, section, interval (cm)	Depth (mbsf)	IC (wt%)	$CaCO_3$ (wt%)	TC (wt%)	TOC (wt%)	TN (wt%)	TS (wt%)	TOC/TN
12H-3, 71-72	103.51	2.31	19.3					
12H-4, 72-73	105.02	0.79	6.6	1.36	0.57	0.14	0.17	4.2
12H-5, 78-79	106.58	6.03	50.2					
12H-6, 72-73	108.02	4.60	38.3					
13H-1, 59-60	109.89	2.44	20.3					
13H-2, 73-74	111.53	2.49	20.8	2.85	0.36	0.13	0.66	2.8
13H-3, 73-74	113.03	0.07	0.6					
13H-4, 73-74	114.53	4.29	35.7					
13H-5, 70-71	116.00	4.15	34.6					
13H-6, 72-73	117.52	4.32	36.0					
14H-1, 72-73	119.52	2.24	18.6					
14H-2, 72-73	121.02	0.72	6.0	1.54	0.82	0.17	0.71	4.8
14H-3, 72-73	122.52	6.04	50.4					
14H-4, 72-73	124.02	0.27	2.2					
14H-5, 72-73	125.52	0.07	0.6					
15H-1, 73-74	129.03	0.83	6.9	1.41	0.58	0.14	0.69	4.1
15H-2, 73-74	130.53	2.92	24.3					
15H-3, 73-74	132.03	2.95	24.6					
15H-4, 73-74	133.53	3.46	28.8					
15H-5, 73-74	135.03	0.57	4.8	1.23	0.66	0.14	0.67	4.6
15H-6, 73-74	136.53	0.14	1.2					
16H-1, 120-121	139.00	6.38	53.1					
16H-2, 120-121	140.50	1.04	8.7	1.74	0.69	0.15	0.68	4.7
16H-3, 120-121	142.00	1.00	8.3					
16H-4, 120-121	143.50	5.30	44.2					
16H-5, 120-121	145.00	1.54	12.8					
16H-6, 72-73	146.02	2.50	20.8					
17H-1, 76-77	148.06	3.27	27.3	3.60	0.33	0.11	0.51	2.9
17H-2, 76-77	149.56	2.21	18.4					
17H-5, 76-77	154.06	1.29	10.8					
18H-1, 76-77	157.56	1.79	14.9					
18H-2, 76-77	159.06	2.96	24.7					
18H-3, 73-74	160.53	0.12	1.0	0.59	0.47	0.14	0.78	3.5
19H-3, 76-77	170.06	0.75	6.3					
19H-4, 76-77	171.56	0.61	5.0	1.13	0.53	0.14	0.43	3.9
19H-5, 76-77	173.06	3.60	30.0	3.43	0.00	0.12	0.60	
19H-6, 76-77	174.56	1.33	11.1					
20H-1, 76-77	176.56	4.67	38.9					
20H-2, 76-77	178.06	0.22	1.8	0.79	0.57	0.14	0.70	4.1
20H-3, 76-77	179.56	0.09	0.8					
20H-4, 76-77	181.06	2.87	23.9					
20H-5, 71-72	182.51	4.96	41.4					
20H-6, 76-77	183.34	1.57	13.1	1.52	0.00	0.13	1.25	
20H-7, 70-71	184.78	0.10	0.8					
21H-1, 75-76	186.05	1.22	10.2					
21H-2, 75-76	187.55	0.09	0.8	0.50	0.40	0.13	0.75	3.1
21H-3, 122-123	189.52	0.16	1.3					
21H-4, 75-76	190.55	0.13	1.1					
21H-5, 75-76	192.05	0.18	1.5					
21H-6, 75-76	193.55	2.38	19.8					
22H-1, 76-77	195.56	1.00	8.3	1.35	0.35	0.12	0.04	2.9
22H-2, 76-77	197.06	6.51	54.2	6.42	0.00	0.08	0.35	
22H-3, 76-77	198.56	0.32	2.6					
22H-4, 76-77	200.06	0.28	2.3					
22H-5, 76-77	201.56	4.77	39.8					
22H-6, 76-77	203.06	0.78	6.5					
23H-1, 72-73	205.02	1.66	13.8	1.85	0.19	0.11	0.71	1.7
23H-2, 72-73	206.52	5.53	46.1					
23H-3, 72-73	208.02	1.89	15.8					
23H-4, 78-79	209.58	4.59	38.2					
23H-5, 66-67	210.96	0.56	4.7	1.17	0.61	0.13	1.82	4.7
23H-6, 72-73	212.52	5.30	44.1					
24H-3, 72-73	217.52	0.07	0.6	0.68	0.61	0.14	0.65	4.4
24H-4, 72-73	219.02	3.04	25.4					
24H-5, 72-73	220.52	0.08	0.7					
24H-6, 72-73	222.02	0.12	1.0	0.65	0.52	0.12	0.22	4.4
25H-1, 131-132	224.61	0.87	7.2	0.98	0.11	0.12	0.72	0.9
25H-4, 17-18	227.97	2.28	19.0					
25H-5, 72-73	230.02	1.30	10.9					
25H-6, 72-73	231.52	3.94	32.8					
26H-3, 72-73	236.52	1.03	8.6	1.59	0.56	0.13	0.62	4.4
26H-4, 72-73	238.02	0.08	0.6					
26H-5, 66-67	239.46	1.72	14.3					
26H-6, 84-85	241.14	0.66	5.5					
27H-1, 72-73	243.02	4.35	36.2	4.58	0.23	0.10	0.54	2.2
27H-2, 132-133	245.12	0.13	1.1					
27H-3, 120-121	246.50	0.10	0.9					
27H-4, 120-121	248.00	0.29	2.4					

Table T16 (continued).

Core, section, interval (cm)	Depth (mbsf)	IC (wt%)	$CaCO_3$ (wt%)	TC (wt%)	TOC (wt%)	TN (wt%)	TS (wt%)	TOC/TN
27H-5, 120-121	249.50	0.07	0.6					
28H-1, 120-121	253.00	0.06	0.5	0.45	0.39	0.12	0.71	3.3
28H-2, 72-73	254.02	0.07	0.6					
28H-3, 72-73	255.52	0.08	0.6					
28H-4, 72-73	257.02	0.08	0.6					
29H-1, 80-81	258.70	0.05	0.4	0.39	0.34	0.12	0.69	2.9
29H-2, 80-81	260.20	0.05	0.4					
29H-3, 52-53	261.32	0.05	0.4					
29H-4, 80-81	262.78	0.08	0.6					
29H-5, 42-43	263.90	0.07	0.6					

Note: IC = inorganic carbon, $CaCO_3$ = calcium carbonate, TC = total carbon, TOC = total organic carbon, TN = total nitrogen, TS = total sulfur.

Table T17. Summary of physical properties measurements conducted at Site 1089.

Measurement	Core 177-1089A	Core 177-1089B	Core 177-1089C	Core 177-1089D
GRA sample spacing	1H-12H, 14H-16H, 18H-21H, 23H: 2 cm	1H-29H: 2 cm	1H-21H: 2 cm	1H-13H: 2 cm
MS sample spacing	1H-12H, 14H-16H, 18H-21H, 23H: 2 cm	1H-29H: 2 cm	1H-21H: 2 cm	1H-13H: 2 cm
NGR sample spacing	1H-12H, 14H-16H, 18H-21H, 23H: 2 cm	1H-15H, 2 cm	1H-2H: 2 cm	—
PWL sample spacing	1H-12H, 14H-16H, 18H-21H, 23H: 2 cm	1H-15H, 2 cm	18H-21H: 2 cm	—
OSU-SCAT sample spacing	1H-8H, 10H-12H, 14H-16H,18H-21H, 23H: 4 cm	1H-11H: 4 cm; 12H-29H: 6 cm	1H, 4H, 6H-8H: 4 cm; 2H-3H, 5H-6H, 9H: 6 cm	2H, 6H, 8H-9H:4 cm; 10H-11H: 6 cm
CM-2002 sample spacing	1H: 5 cm	1H-12H: 5 cm	—	—
PWS3	*N* = 192	*N* = 384	—	—
MAD	*N* = 94	*N* = 142	—	—
TC	*N* = 12	*N* = 28	*N* = 15	—

Notes: GRA = gamma-ray attenuation, MS = magnetic susceptibility, NGR = natural gamma radiation, PWL = *P*-wave logger, OSU-SCAT = Oregon State University Split Core Analysis Track, CM-2002 = Minolta spectrophotometer, PWS3 = *P*-wave velocity sensor 3 for split cores, MAD = moisture and density, TC = thermal conductivity.

Table T18. Thermal conductivity measurements at Site 1089. (See table note. Continued on next page.)

Core, section, interval (cm)	Depth (mbsf)	Depth (mcd)	TC (W/[m·K])	Start (s)	Length (s)	End (s)
177-1089A-						
2H-3, 75	11.1	10.6	0.81	107	25	132
4H-3, 75	29.8	34.2	0.87	79.5	28	108
4H-3, 75	29.8	34.2	0.86	107	25.5	133
6H-3, 75	49.1	50.9	0.87	102	25	127
6H-3, 75	49.1	50.9	0.86	89	25.5	115
8H-3, 75	68.1	72.8	0.91	58	26.5	84.5
8H-3, 75	68.1	72.8	0.87	111	25	136
10H-3, 75	87.1	91.6	0.87	31	25	56
12H-3, 75	106	112	0.97	70	25	95
12H-3, 75	106	112	0.99	37.5	25.5	63
15H-3, 75	135	140	0.95	122	26	148
15H-3, 75	135	140	1.01	32	27.5	59.5
16H-3, 75	144	151	0.91	66.5	25	91.5
16H-3, 75	144	151	0.93	41	25.5	66.5
19H-3, 75	173	181	1.01	60	25	85
19H-3, 75	173	181	1.01	37	27	64
21H-3, 75	192	205	0.96	61.5	26	87.5
21H-3, 75	192	205	0.91	110	25.5	136
23H-3, 75	211	223	0.9	112	26	138
23H-3, 75	211	223	0.93	66	25	91
177-1089B-						
2H-3, 75	8.55	14.3	0.84	119	26.5	145
2H-3, 75	8.55	14.3	0.86	51	25	76
3H-3, 75	18.1	23.5	0.89	32	25	57
3H-3, 75	18.1	23.5	0.87	60	27	87
4H-3, 75	27.6	33.2	0.9	37	27	64
5H-3, 75	37.1	41.5	0.79	124	25.5	150
5H-3, 75	37.1	41.5	0.83	41	25	66
6H-3, 75	46.6	52.8	0.94	44	25	69
6H-3, 75	46.6	52.8	0.88	96	30	126
7H-3, 75	56.1	63.5	1.01	64.5	27.5	92
7H-3, 75	56.1	63.5	1.02	29	25	54
8H-3, 75	65.6	73.6	0.9	89.5	26	116
8H-3, 75	65.6	73.6	0.86	121	25	146
9H-3, 75	75.1	84.4	0.91	46	26	72
9H-3, 75	75.1	84.4	0.91	56.5	25	81.5
10H-3, 75	84.6	95.8	0.96	89	25	114
10H-3, 75	84.6	95.8	0.97	66	27	93
11H-3, 75	94.1	105	0.92	73.5	28.5	102
11H-3, 75	94.1	105	0.91	92	25	117
12H-3, 75	104	115	0.88	104	27.5	132
12H-3, 75	104	115	0.89	32.5	25	57.5
13H-3, 75	113	124	0.83	124	25	149
13H-3, 75	113	124	0.84	67.5	27	94.5
15H-3, 75	132	143	0.92	115	28.5	144
15H-3, 75	132	143	0.93	77	25	102
16H-3, 75	142	153	0.92	74.5	25	99.5
16H-3, 75	142	153	0.89	120	25	145
17H-4, 75	153	164	0.99	62.5	25	87.5
17H-4, 75	153	164	0.98	68	25.5	93.5
18H-3, 75	161	172	0.9	85.5	25	111
18H-3, 75	161	172	0.9	56	28.5	84.5
19H-3, 75	170	182	0.83	124	25.5	150
19H-3, 75	170	182	0.81	112	26	138
20H-3, 75	180	192	0.85	94.5	25	120
21H-3, 75	189	204	0.98	124	25.5	150
21H-3, 75	189	204	0.98	95	25	120
22H-3, 75	199	214	0.93	85.5	25	111
22H-3, 75	199	214	0.89	123	25.5	148
23H-3, 75	208	223	0.95	50.5	25.5	76
23H-3, 75	208	223	0.9	112	25	137
24H-3, 75	218	233	0.86	124	25	149
24H-3, 75	218	233	0.84	116	25.5	142
25H-3, 75	227	242	0.97	121	29	150
25H-3, 75	227	242	0.96	80	25	105
26H-3, 75	237	252	1	61	25	86
26H-3, 75	237	252	0.98	101	25	126
27H-3, 75	246	261	0.97	72.5	25	97.5
27H-3, 75	246	261	0.94	118	32	150
28H-3, 75	256	271	1.01	122	25	147
28H-3, 75	256	271	1.02	94.5	28	123
29H-3, 75	262	277	0.94	107	25	132
29H-3, 75	262	277	0.93	113	25	138

Table T18 (continued).

Core, section, interval (cm)	Depth (mbsf)	Depth (mcd)	TC (W/[m·K])	Start (s)	Length (s)	End (s)
177-1089C-						
1H-2, 50	2	1.7	0.86	115	27	142
1H-2, 50	2	1.7	0.89	32.5	27.5	60
3H-2, 75	16.2	20.6	1	51	25	76
3H-2, 75	16.2	20.6	1	62.5	25	87.5
4H-3, 75	27.2	30.7	0.82	122	26	148
4H-3, 75	27.2	30.7	0.87	38.5	25	63.5
5H-3, 75	36.7	40.1	0.86	117	25	142
5H-3, 75	36.7	40.1	0.88	45.5	27	72.5
6H-3, 75	46.2	48.2	0.96	115	26	141
6H-3, 75	46.2	48.2	1.01	25	25	50
8H-3, 75	65.2	69	0.92	44	25	69
9H-3, 75	74.7	79	0.84	79	25	104
10H-3, 75	84.2	90.6	0.86	63	28.5	91.5
10H-3, 75	84.2	90.6	0.86	49.5	28	77.5
11H-3, 75	93.7	103	0.87	72.5	28	101
11H-3, 75	93.7	103	0.86	71.5	25	96.5
13H-3, 75	113	122	0.9	57.5	25	82.5
13H-3, 75	113	122	0.89	72.5	25	97.5
14H-3, 75	122	131	0.86	31.5	25	56.5
15H-3, 75	132	141	0.91	101	25	126
15H-3, 75	132	141	0.96	89	26.5	116
16H-3, 75	141	152	0.93	97.5	25	123
16H-3, 75	141	152	0.92	99	26.5	126
17H-3, 75	151	164	1.05	26.5	25.5	52
17H-3, 75	151	164	1.05	33	25	58
18H-3, 75	160	173	0.89	40	25	65
18H-3, 75	160	173	0.88	78.5	28	107

Notes: TC = thermal conductivity. Start, Length, and End refer to the interval of the time-temperature series used for the determination of thermal conductivity. This table is also available in ASCII format in the **TABLES** directory.

Table T19. Temperature measurement attempts at Site 1089.

Core	Depth (mbsf)	Comments
177-1089A-		
1H	Bottom water	1.1° ± 0.1°C
4H	35.8	Noisy data
7H	64.3	Noisy data